POLITECNICO DI MILANO

I Facoltà di Ingegneria

Master of Science in Civil Engineering

Grid model for the non-linear behavior of R/C flat-slab subjected to gravity and lateral loads

Relatore: Prof. Dario Coronelli

Guglielmo Corti 725186

ANNO ACCADEMICO 2009-2010

Contents

List of Tables

List of Figures

Abstract

Use of flat plate floor systems consisting of conventional reinforced concrete slab-column system is becoming increasingly popular for non-participating systems in medium and high seismic zones, as Italy is. Thus, it is of great interest to develop models able to represent their non-linear behavior under horizontal loads, both for the verification and design of this structural typology.
The aim of his dissertation is to apply a grid model, designed for the non-linear behavior of flat slab-column connections, on a real study case in order to test its performance in representing the experimental observed behavior.
The considered experimental study is the one carried out by Hwang and Moehle at the University of California at Berkeley (1993), consisting on a flat slab structure with sixteen slab-column joints, subjected to gravity and biaxial cyclic lateral loading.
The geometry of the grid has been designed in order to model in the best way the real geometry of the structure with its asymmetries; plastic hinges properties have been computed accordingly to the aforementioned grid model; loads applied are the same of the real slab.
A force controlled non-linear analysis under gravity loads and non-linear static (*pushover*) analyses under horizontal loading in the two principal directions of the structure, are performed on the model slab.
The software used for all the analyses is SAP 2000 v.10.
The numerical global structural behavior and the joints behavior have been compared with the experimental ones; the influence of column rectangularity has been also investigated in relation of experimental studies on this topic.
Analyses show a good correspondence between the numerical and experimental global structural behavior; interior connections are absolutely well modeled, whereas edge and corner connections show departures from experimental behavior, because the latter are strongly influenced by degradation of mechanical properties due to biaxial cyclic loading. All the results obtained may be interpreted taking into account for this fact.
Rectangularity of columns influence both the numerical global and connection response; this is less evident in the experimental case because of slab degradation due to biaxial cyclic loading.

Chapter 1

General Introduction

Reinforced concrete slabs are among the most common bearing structural elements. What is defined slab is a flat element with two dimensions, which identify a mean plane, much greater than the third one which represents the thickness of the element. The structural scope of a flat slab is to bear loads acting orthogonally to its mean plane thanks to its predominant flexural behavior which is particularly effective when the shape and constraints allow the slab to redistribute the loads along two or more preferential directions; this behavior is called "bidirectional" or "two way". In the case only one preferential direction exists, then we are dealing with "unidirectional " or "one way" slabs.
This is only a first subdivision based on the mechanical behavior of plates; a further distinction is accordingly to the type of constraints, which can be point or continuous:

- slab with constant thickness supported by columns with or without capitals (Fig. 1.1);
- with variable thickness with a local thickening at columns (Fig. 1.2);
- slab on border beams or bearing walls (Fig. 1.3).

Notice that the behavior of plates is bidirectional if the constraints set-up is mesh like, while is unidirectional if they are aligned in parallel.
Finally, another subdivision distinguishes between constant thickness slabs and lightened slabs (waffle slabs), suited for medium-big spans (Fig. 1.4). The latters consist on in very thin plates sustained by nerves intersecting in two principal directions (panelled slab) or in holes disposed inside the thickness (alveolar slab).
In this thesis the case study will be the reinforced concrete constant thickness slabs. The advantages of these particular structural elements are the very high constructive simplicity, the reduction of the construction time and an easy disposition of systems; the disadvantages are the greater amount of

construction materials, the necessity of displacements and cracks control and the critical verification against punching shear. The last issue will be one of the topics that will be discussed in this work.

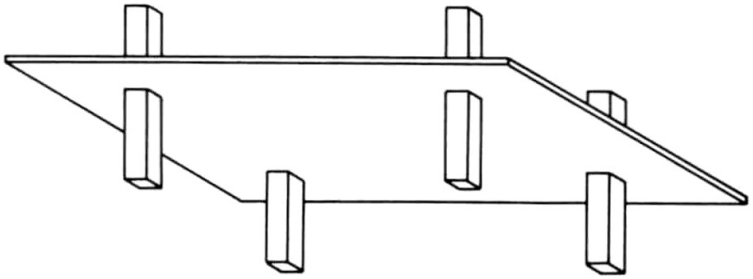

Figure 1.1: Example of constant thickness slab

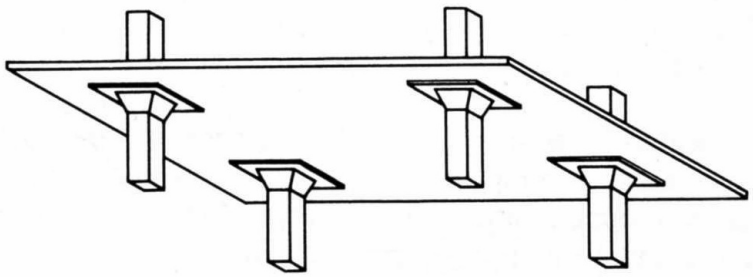

Figure 1.2: Example of variable thickness slab

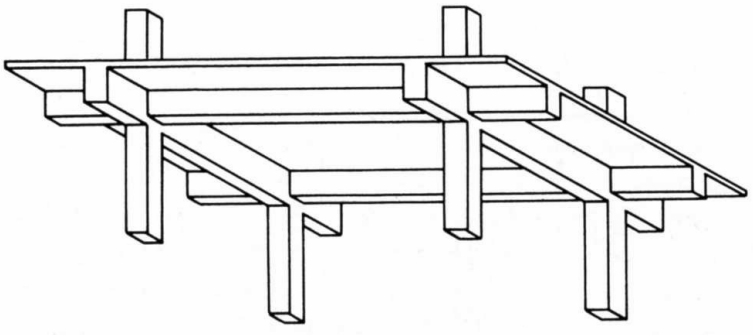

Figure 1.3: Example of slab sustained by beams

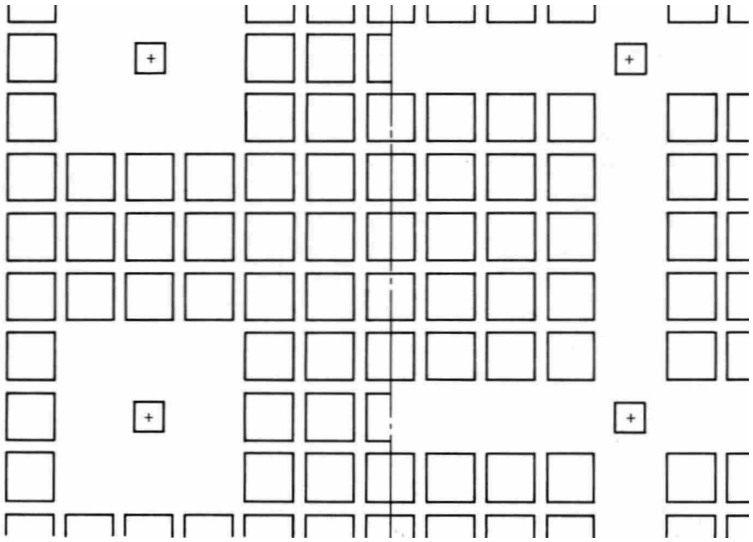

Figure 1.4: View of waffle slab in plan

1.1 Non-linear behaviour of slabs under vertical and horizontal loads

It is well known that the first cause of the concrete cracking is its very low tensile resistance and ductility; then it cracks when the principal tensile stresses has reached locally the maximum tensile strength of the material. Thus, taking into account an elastic-brittle behavior for tensioned concrete, it derives that the traces on the mean surface of the principal planes of the flexure in the plates (Fig. 1.5(a)) are indications given by elastic analysis, about the possible formation and direction of the cracks. With the increasing of the loads, the orientation of cracks become more and more different from the indications given by elastic analysis since the structural stiffness is influenced by both the proceeding of the cracks regime itself and the reinforcing bars direction with their reinforcing geometrical ratio (Fig. 1.5(b)). The collapse of reinforced concrete slabs occurs after that a series of cracked strips has formed, both in the positive and negative side, along which the deformations are concentrated, while the adjacent "fields" are nearly flat. The deformations along the cracked strips are in the form of micro and macro fractures of tensioned concrete and elongations of reinforcement bars beyond their elastic limit. Thus, the slab at the ultimate condition is a group of rigid plates linked together by means of linear constraints along the cracked strips and with yielded rebars. This behavior at the ultimate state is well modeled by the "yield line theory" of the Limit Analysis.

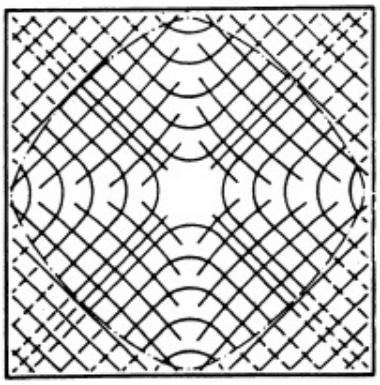

(a) Traces on the mean plane of the principal bending moments in elastic phase

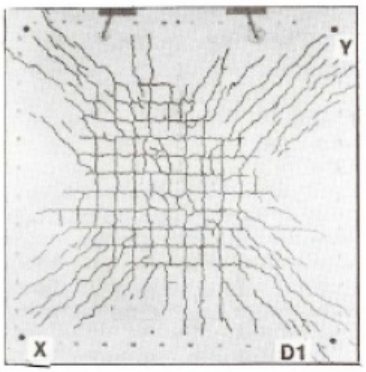

(b) Flexural cracks

Figure 1.5: Example of a plate in flexural regime

This method consider the slab being at the limit situation of equilibrium, just before the collapse, when the structure is no more redundant, since a number of internal and external constraints have been lost by means of cracking and yielding of reinforcement. The ultimate load of the slab system is estimated by postulating a collapse mechanism that is compatible with the boundary conditions. Bending moments at the plastic hinge lines (cracked strips) are the ultimate moments of resistance of the sections, and the ultimate load is determined using the virtual work principle or the equations of equilibrium. It's worth to remember that this is an upper bound approach based on the kinematic theorem, then it gives an ultimate load for a given slab which is either correct or too high, then unsafe; for this reason is necessary to examine all the possible collapse mechanisms in order to ensure that the load-carrying capacity of the slab is not overestimated. Finally notice that the yield line theory assumes a flexural collapse mode, that is, that the slab has sufficient shear strength to prevent a shear failure.
The non-linear behavior and the method for analysis and design of flat slabs described above refer to the application of vertical loads to the structure, for which usually this type of structural elements are designed. Anyway, the study of their structural behavior in seismic zones is becoming more and more important and of topical interest nowadays; for this reason, it is fundamental to study the behavior of structural bearing plates subjected also to lateral loads. An analytical simplified method proposed by ACI Building Code used for the analysis and design of slab systems loaded by both horizontal and uniformly distributed gravity loads is the so called *equivalent frame method*.

1.1.1 Equivalent Frame Method

This method represents a three-dimensional slab-column structure by a series of plane frames (equivalent frames) constructed along the axis mid-lines of the columns. Referring to Fig. 1.6 each equivalent frame consists of either a row of interior columns plus the slab extending to the panel center-lines on each side of the column line, or a row of columns at the edge of the structure plus the slab extending from the edge to the panel centreline. The division lines extend through the full height of the structure. Then, the complete analysis of the slab system consist on the analysis of a series of interior and edge equivalent frames, which extend longitudinally and transversally along the structure.
The code permits to consider either the entire frame or a single floor when only gravity loads act. The entire frame clearly should be considered if horizontal loads act and must be resisted bending of the columns rather than by shear walls or other bracing. Considering a single floor, the columns above and below the strip run up to the slabs of the upper and lower plane and at the extremities are fixed (Fig.1.7). The top and bottom stories may have other support conditions.
As a further simplification, in a structure of several spans, the joints two or more spans away from the one being considered may be taken as fixed if the structure extends beyond that joint.

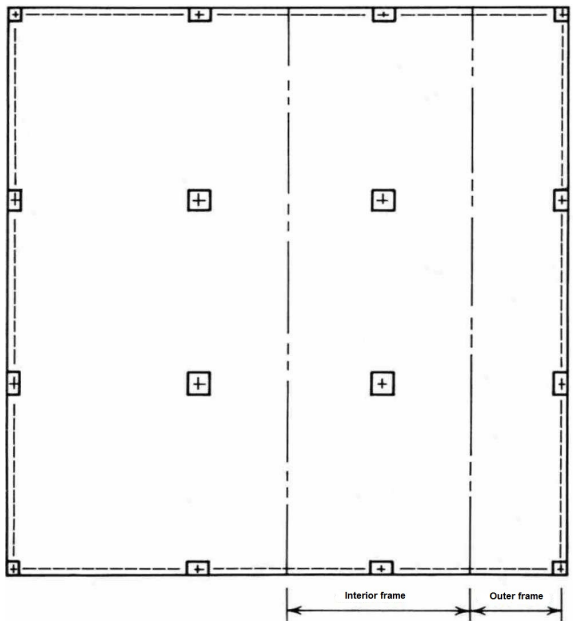

Figure 1.6: Example in plan of subdivision in equivalent frames

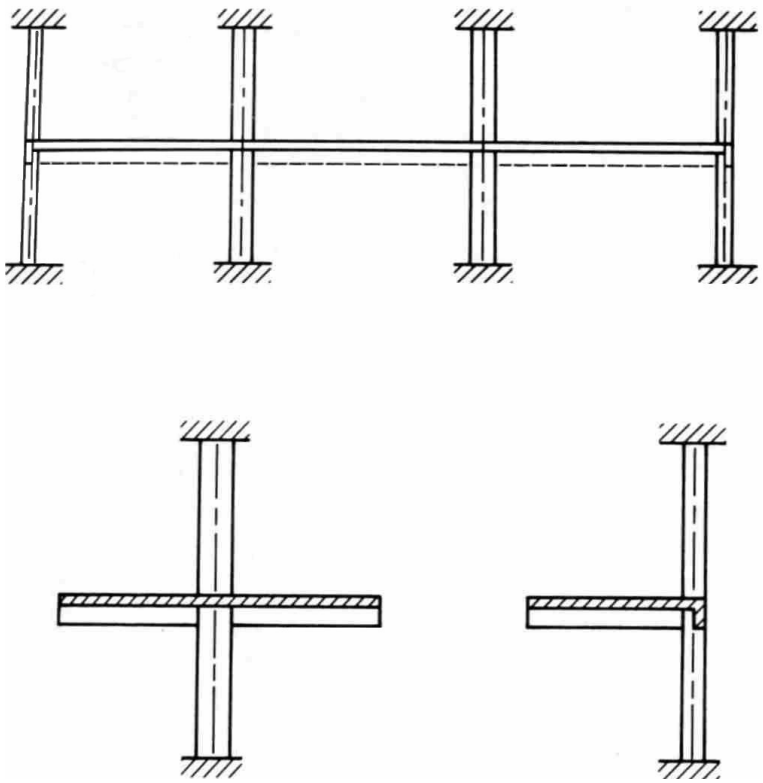

Figure 1.7: Elevation and sections of equivalent frames: at the top elevation of frame cut from slab structure, at the bottom on the left cross section of interior frame and on the rigth cross section of edge frame

Determination of the relative stiffnesses of the sections may be carried out considering the gross cross, uncracked cross sections. All variations in concrete cross section along a member that occur outside the joint regions should be taken into account. Therefore, a slab-beam (slab forming the beam of the equivalent frame) which has drop panels, has a larger moment of inertia near the ends than in the central part of the span. Then it is necessary to subdivide the slab-beam in different elements in correspondence of the changing of section area.
It's worth to notice that the parts of the slab-beam lying between the column centreline and column face are effectively stiffer than the clear span portion of the member. The code approximation consists on dividing the moment of inertia of the slab-beam just outside the column by the quantity $[1 - c_2/l_2]^2$, where c_2 and l_2 are respectively the dimension of the column and the width of the slab-beam orthogonally to the direction of the span for which the bending moment will be determined.
For the columns, the stiffness is computed along its length from the middle

of the thickness of the upper slab to the middle of the thickness of the slab below and its moment of inertia is computed according to its section. In the connection region instead, the moment of inertia is assumed to have an infinite value throughout the joint region. It's thus necessary that stiffness and carryover factors take into account for the rigid portions of the members; these can be computed with a number of methods among which the column analogy method[14]. Alternatively, factors can be derived from tables published by various agencies and authors, for example the Portland Cement Association[15] and Cross and Morgan[16]; several graphs and approximations for stiffness factors are published by Hoffman et al.[17] and Rice[18].
Once the stiffness of the columns have been determined, the stiffness of the equivalent columns K_{eq} can be found as:

$$\frac{1}{K_{eq}} = \frac{1}{\sum K_c} + \frac{1}{K_t} \tag{1.1}$$

where ΣK_c is the sum of the flexural stiffnesses of the columns above and below the slab which frame into the joint being considered and K_t is the torsional stiffness.
According to the ACI Code formulation, the singular torsional member stiffness is expressed as:

$$K_t = \sum \frac{9E_cC}{l_2(1 - c_2/l_2)} \tag{1.2}$$

In this summation where E_c is the Young's modulus of concrete and C is the torsional constant, the summation essentially refers to the torsional elements on either side of the column, and at a corner column there is obviously only one member to be considered. At columns with two members, the cross sections and spans may be different on the two sides of the column, so the $mathitK_t$ values are calculated separately for each and then summed.
The torsional constant is expressed as:

$$C = \sum \left(1 - 0.63\frac{x}{y}\right) \frac{x^3y}{3} = \sum x^4 \left(\frac{y}{3x} - 0.21\right) \tag{1.3}$$

where x is the shorter side of a rectangular area and y is the longer one of the same area.
The K_{eq} value found is then used in the frame analysis; K_{eq} refers to the combination of two columns (one above and one below), and if it is used to find a moment distribution factor, the factor applies to the total moment in the two columns. This is not usually satisfactory, since the individual column moments must be found for design purposes. The distribution factors to the two columns may be found by subdividing the total equivalent column factor K_{eq} in direct proportion to the individual Kc values.
An important factor that influences the stiffness of the structural members is their state of cracking; considering that the increasing of cracking means

decreasing of stiffness, this induces the increasing of the lateral flexibility of the whole structure when subjected to lateral loads. In flat-slab structures, slabs would usually be cracked more extensively than the columns, and lightly reinforced slabs would be expected to lose a significant amount of stiffness. Thus, in order to take into account for this effects, usually reduction of uncracked flexural stiffness are used, ranging between 25% and 50% for not pre-stressed flat slabs.

1.1.2 Punching phenomenon of slabs transferring uniform shear

A typical inelastic response of flat slabs under vertical and/or lateral loading is the punching of connections. This is by definition a phenomenon of rupture of the plane element in the zone around the point of application of a point load given by an external action or a constraint reaction, that could transmit also bending moment. This concentrate force provokes high shear solicitations orthogonally to the mean plane of the plate in the zone around the slab-column connection where also negative bending moments act; these produce a complex state of stress inside the material that could lead to the penetration of the column in the slab.
This type of failure is very dangerous because of its brittle nature and for this fact it is not preceded by premonitory signs; in addiction the collapse of a slab-column connection obviously leads to an increasing of the load acting on the adjacent columns and this could provoke their subsequent punching and then the sudden fall of slab portions over the inferior one. These phenomena, if not properly taken into account in the design stage, could lead the progressive collapse of a part or of the entire structure.
As already mentioned, in the zone of the plate around the slab-column joint, a very complex state of stress exists, not only due to bending moment and shear but also to torsion; in addiction these internal actions act with comparable magnitudes in two orthogonal directions ("two-way" system), differently to the other portions of the plate in which "one-way" actions principally act; this is principal difference in the behavior of beams and plates.
A further fact to underline is the confinement that the portions of plate around the loaded zone provide to the connection; this obviously increases the strength of concrete.
Thus, this complex state of stress and the presence of cracks due to the three combined actions make difficult to study theoretically the punching strength, whose quantification is based principally on results of experimental tests.
The punching phenomenon is preceded by the opening of circular cracks around the top part of the column due to radial negative bending moments; then radial cracks start to open from the pillar due to tangential bending moments (Fig. 1.8). From this situation, since bending moments decrease

very rapidly going away from the column, a great increase of load should be necessary in order to permit the formation of radial and circular cracks in the outer zones. Thus, next cracks that form will be diagonal and start to propagate at 2/3 of the ultimate load, from the level of the mean plane and then spreading within the whole thickness of the slab. The shape of the punching surface of rupture is typically conical. The causes of the phe-

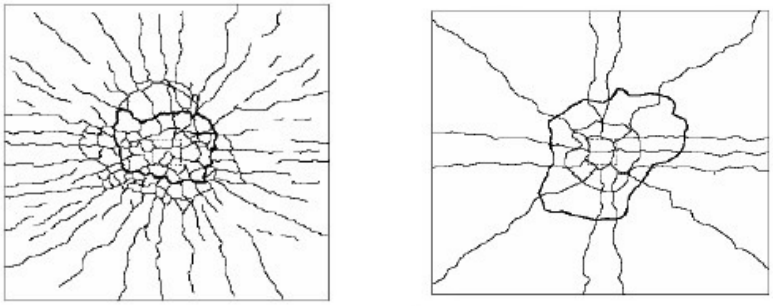

(a) Top part of the slab (b) Bottom part of the slab

Figure 1.8: Example of punching cracking at a slab-beam connection

nomenon are still now unknown and are topics of study. Two causes are the most probable: the tensile failure of the concrete in correspondence of the surface of rupture; the concrete crushing in radial direction at the base of the cone.
Several parameters have been identified as important for the resistance of slab-column connections subjected to concentric loading; the most important are the concrete strength (f'_c), longitudinal reinforcement ratio (ρ_s), the aspect ratio of the supporting column (β), perimeter to thickness ratio and size effect.

The influence of f'_c is quite obvious, since increasing it an increasing in the punching strength is obtained with the trend proposed in Fig. 1.9.

With respect to the flexural reinforcement, results of tests (Mokhatar et al., Elstner and Hognestad[1], Base, Manterola, Cristwell, Pectu et al., Ghali et al., Van der Voet et al.) in which the reinforcement ratio ρ_s was the main variable are plotted in Fig. 1.10 in terms of $v_u/(f_{cm})^{1/3}$ together with the function $0.7(100\rho)^{1/3}$. This type of function has been proposed by many researchers and forms the basis of several major building codes.
Tests of slabs in which the yield strength of the reinforcement was the main variable[19] indicated that if the flexural reinforcement yield significantly before the shear strength has been reached, the shear strength is reduced. However, a plot of the shear function of the yield strength, does not indicate

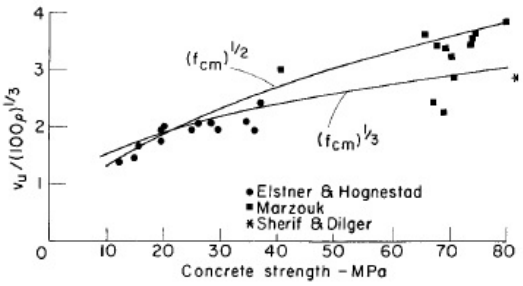

Figure 1.9: Effect of concrete strength f'_c on shear strength[1]

a clear trend[3].
Results of slab tests[20, 21, 22] with concentration of the reinforcement near the column showed that such concentration of reinforcement may be detrimental if too much steel is concentrated near the column. This harmful effect is probably due to a loss of bond[22].

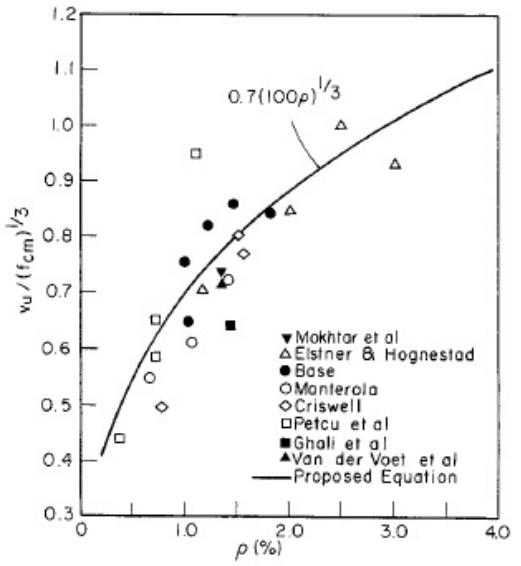

Figure 1.10: Effect of flexural reinforcement ratio ρ_s on shear strength[2]

The shape of the column section has been proved to influence the shear strength of connections. Experimental studies[23] indicate that the concentration of concrete strains near the corner of rectangular columns increases with the increasing aspect ratio β (ratio of long side to short side of a column)

and that circular columns give higher shear strength than rectangular ones, presumably due to absence of stress concentrations.

The influence of perimeter-to-thickness ratio (b_0/d) on the punching shear strength has been investigated[3] collecting and studying results form different experimental tests (Elstner and Hognestad[1], Taylor and Hayes, Manterola, Cristwell, Mokhatar et al., Ghali et al. Van der Voet et al.). It has been noticed its strong influence (Fig. 1.11).

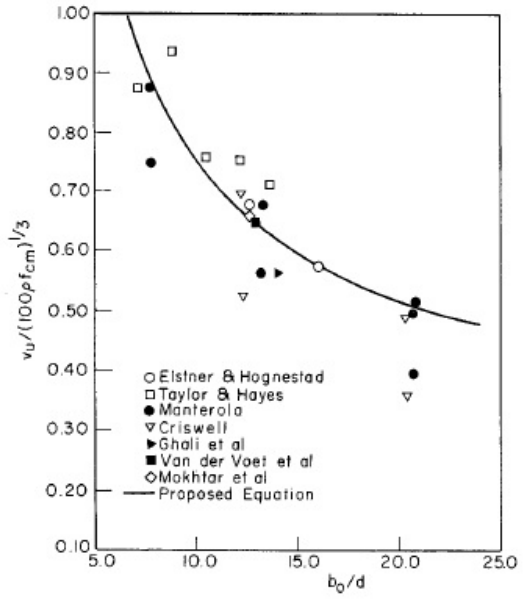

Figure 1.11: Effect of perimeter-to-thickness ratio on shear strength[3]

The effect of the slab effective depth d (*size effect*) is to reduce the shear strength with its increasing. The trend is appropriately given by function $f(d) = 1/(d)^{1/3}$[2].

1.1.2.1 Resistance mechanisms

The presence of flexural reinforcements at the bottom and top part of the slab partly oppose to the development of punching phenomenon, then is necessary to design them taking into account this; in addiction, in order to ensure a better level of safety against this shear failure, often shear reinforcement are added.
In general, it is possible to schematize punching phenomenon in two way:

- considering the equilibrium between the compression at the base of the cone and the tensile force of the top longitudinal reinforcements, at collapse conditions (Fig. 1.12);
- by means of a struts and ties system, with struts for compressed concrete and ties for the contribution of the tensioned concrete and reinforcements (Fig. 1.13).

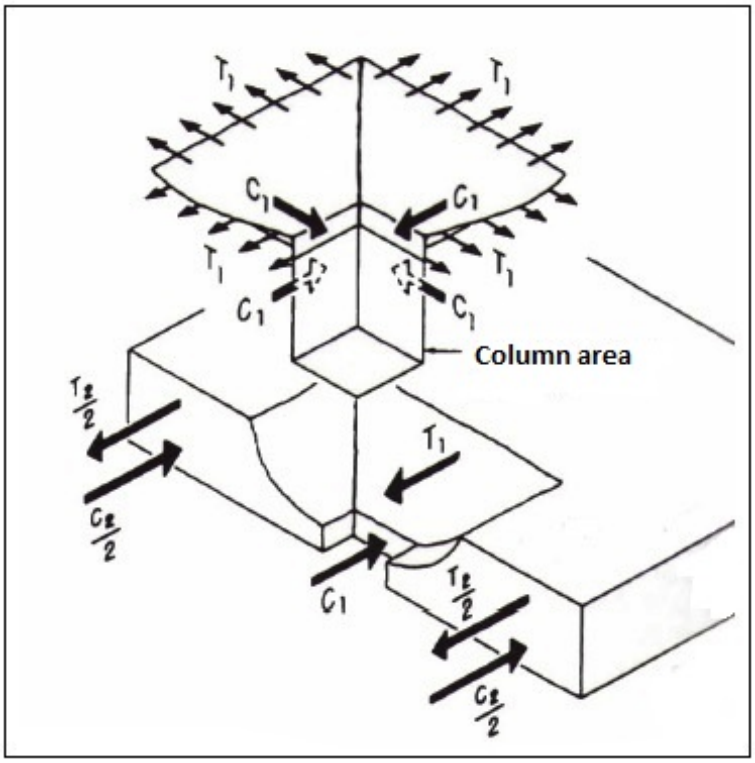

Figure 1.12: Horizontal forces acting on sections near critical diagonal tension cracks of a reinforced concrete slab-column connection

These models permit to take into account the different resistant contributions of concrete and reinforcements and then to simplify and understand a phenomenon which is actually complicated; anyway these approaches are not used in usual design but only in the research field.
A simplified and conventional method, common to different design codes, consists on redistributing the concentrated force along a surface within the thickness of the slab (*critical surface*) orthogonal to the mean plane. This area could have different shapes according to the code considered and is conventionally located at a defined distance from the column faces (Fig. 1.14); the resistance criterion consists on the limitation of the magnitude of shear

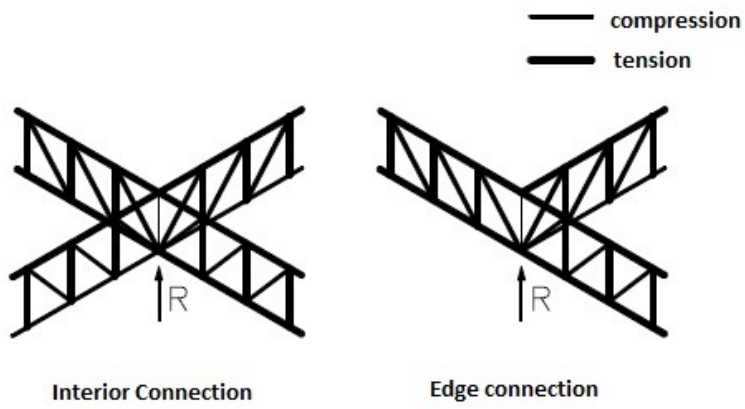

Figure 1.13: Strut and tie model for computing the strength with the presence of punching reinforcements

stresses on this surface below a certain value of stress (*shear strength*) which is determined on experimental basis.

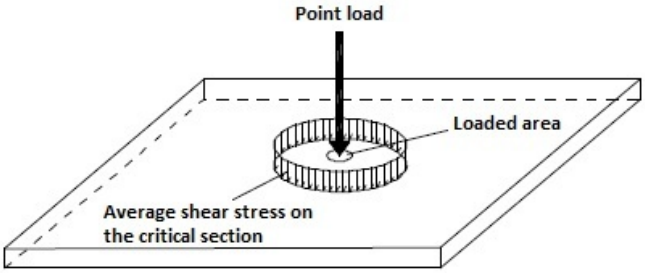

Figure 1.14: General schematization of the simplified method

Notice that the strength value is influenced, as already mentioned, by the confinement effect given by the surrounding portions of the plate, increasing the resistance, differently to what happens in beams.
Referring to figure 1.12, the compressive (C) and tensile (T) forces transmitted between the cone and the surrounding outer parts are statically undetermined; in fact the equilibrium $C_1 + C_2 = T_1 + T_2$ holds but not necessarily $C_1 = T_1$. Thus force C_1 can be redistributed in the surrounding concrete accordingly to the distribution of stiffness. In this way, displacements due to cracks opening are counteracted and compressive stresses arise in the slab.

This is confinement and increase both shear and flexural resistance. These tensile and compression forces are partly taken by longitudinal reinforcement, then it is possible to understand that the connection shear resistance depends also from longitudinal reinforcement ratio.

1.1.3 Punching phenomenon of slab-column connections transferring shear and unbalanced moment

A topic issue to analyze is the shear strength of slabs with nonuniform shear around the critical section. That is, both axial load and unbalanced bending moment are transferred at the slab-column connection. The term *unbalanced bending moment* is used to emphasized that this is the moment being transferred between slab and column at the connection. This can be compared with the situation at an interior column of a symmetrically loaded floor where the slab has a negative moment at the column, but that moment on one side of the column is balanced by the negative moment in the slab on the other side of the column and hence no unbalanced slab moment remains to be transferred to the column.
In a flat slab floor carrying gravity loading there will generally be transfer of both shear and unbalanced bending moments at edge columns and some interior column; anyway this design aspect becomes particularly important when horizontal loading on the building (wind or earthquake) causes a substantial unbalanced bending moment to be transferred within slab-column connections. Its transfer provokes a nonuniform distribution of shear stress in the slab around column and reduces the shear strength of the connection. The shear force and unbalanced bending moment are transferred by combined bending, torsion and shear at the faces of the critical section (Fig. 1.16).
If the shear strength of the slab is reached , the slab will fail in diagonal tension on the side of the column where the vertical shear stress is highest, which often corresponds to the side about which the higher negative bending acts, since it is the most damaged.
In addition to the parameters that affect the capacity of concentrically loaded connections, the shear resistance of eccentrically loaded slab-column connections also depends on the eccentricity of the load e, expressed by the ratio $e = M/V$[2].
Stamenkovic and Chapman[4] have tested interior, edge and corner connections, for which the eccentricity was varied systematically; their results are reported graphically in Fig. 1.15 and are explained in the following.
The results on interior joints show the same linear variation as the edge columns with moment transfer in the direction parallel to the free edge. If the moment at the edge column is applied normal to the free edge, experimental results suggest an interaction curve of the form $(V_u/V_0)^2 + (M_u/M_0)^2 = 1$,

where V_0 is the shear resistance when $M = 0$, and M_0 the moment resistance when $V = 0$. Results for corner connections subjected to moments applied normal to one edge, suggest that there is a little interaction between moment and shear force. However, tests with moment transfer in the diagonal direction show an increase in moment and shear resistance when V and M are applied simultaneously. For seismic situation is necessary to take also into

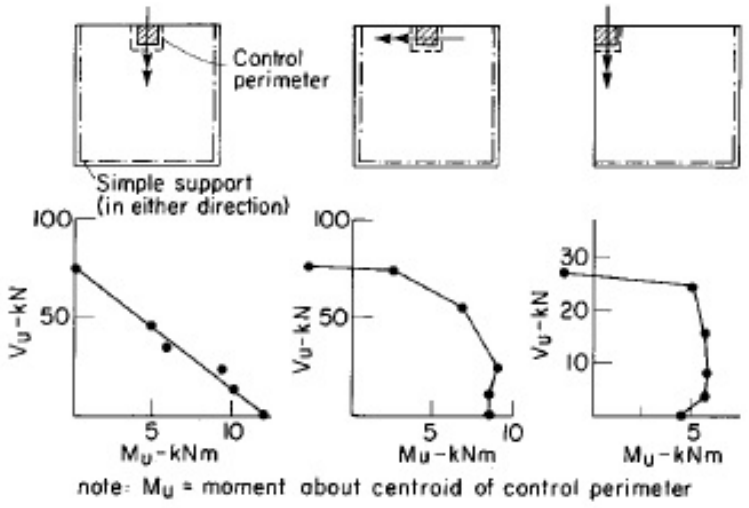

Figure 1.15: Interaction diagrams for eccentrically loaded slab-column connections[4]

account that slab-column connections of flat slab structures are subjected to repeated reversals of unbalanced bending moment, which may lead to failure in the slab around the column due to degradation of shear strength. In these cases, it's fundamental to guarantee both a sufficient strength and an adequately connections ductility, in order to guarantee a proper energy dissipation. In order to assure certain strength and ductility levels, the using of transversal reinforcement is needed.

1.1.3.1 Analysis methods

Several analytical methods have been evaluated for the evaluation of the solicitation and strength od a slab-column connection transferring shear and unbalanced moment. Two of these are presented in the following:

Analysis based on a linear variation in Shear stress
The method specified by 1995 ACI Code[24] is based on this type of analysis. The analysis assumes that shear stresses on a critical perimeter vary linearly

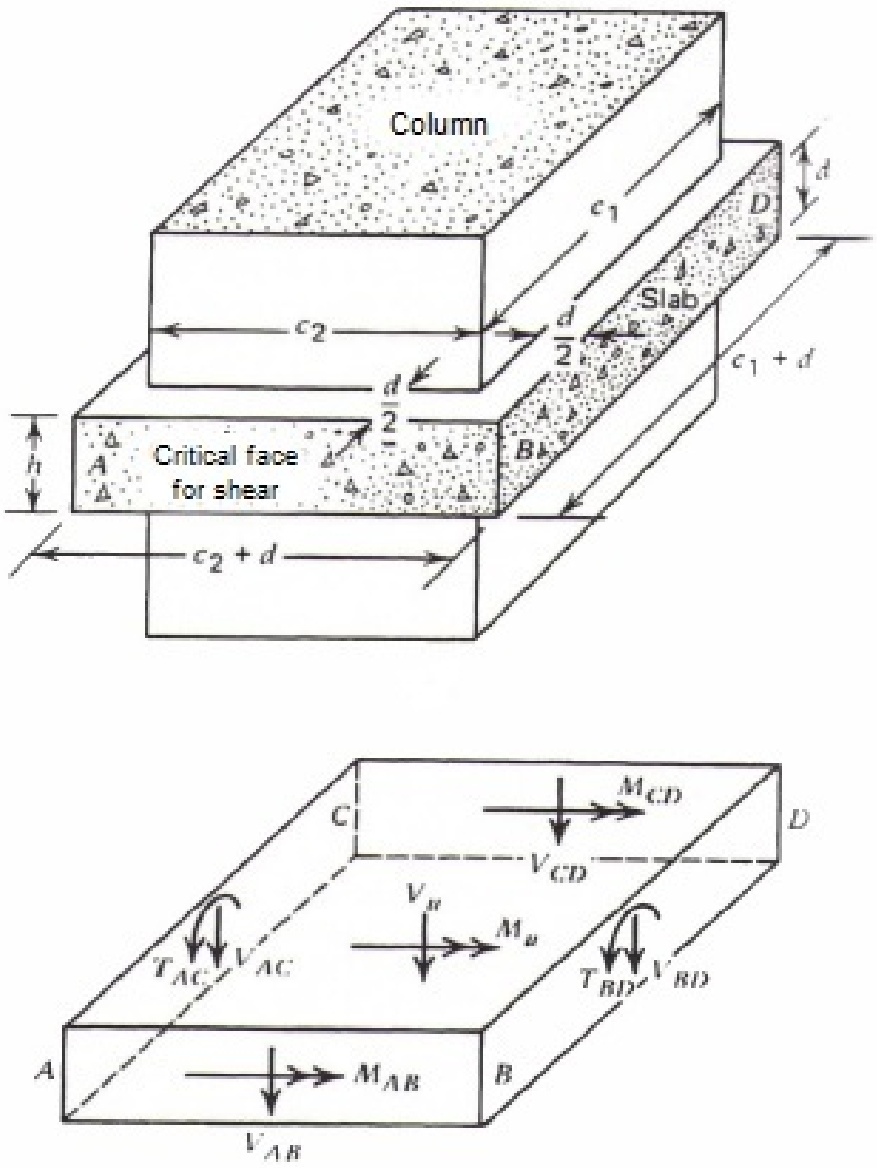

Figure 1.16: Critical section and actions at interior slab-column connection

with the distance from the centroidal axis of the perimeter (Fig. 1.17) and are induced by shear force V_u and by the part of the unbalanced bending moment $\gamma_v M_u$ ($\gamma_v = 1 - \gamma_f$) which is not transmitted by flexure ($\gamma_f M_u$). The method is semi-empirical, but the approach usually results in a conservative estimate of the measured strength. This method has been developed for slabs without shear reinforcement.

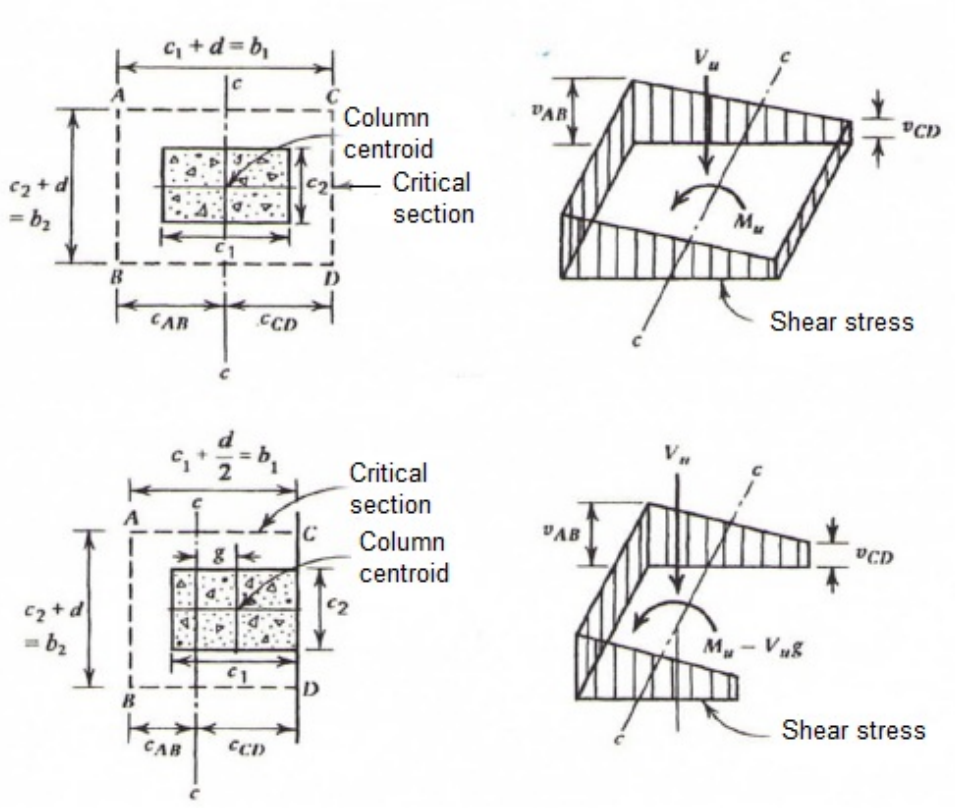

Figure 1.17: Assumed critical section and linear distribution of slab shear stress for connection transferring shear and unbalanced moment

Analysis based on constant shear stress distribution

This method considers a constant non-linear distribution of shear stresses around the column, with a change of sign at the columns mid-side. This a typical distribution of plasticized section (Fig. 1.18).

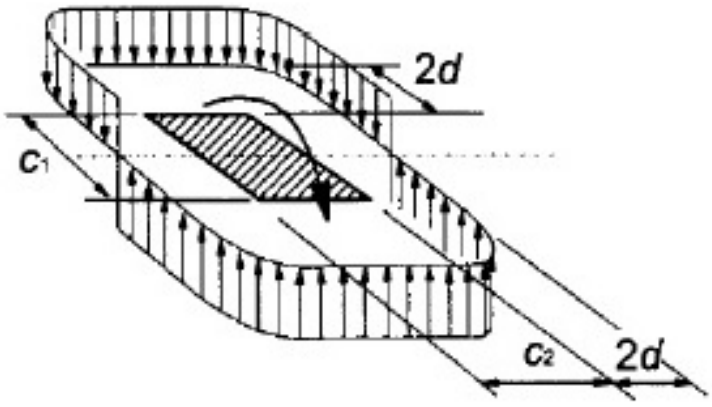

Figure 1.18: Assumed critical section and constant shear stress distribution for connection transferring shear and unbalanced moment

1.1.4 Lateral displacement ductility

A punching shear failure of a slab-column connection without well-designed shear reinforcement is usually a brittle failure and can have disastrous consequences, as aforementioned. Hence, attention should be given to the ductility associated with shear strength of connections to avoid a brittle condition if possible. Ideally, the connection should contain reinforcement that holds the connection together after punching shear failure of the slab and prevents the slab from slipping down the column. For slabs without shear reinforcement, some post-failure connection resistance can be obtained from the presence of sufficient quantities of bottom steel in the slab passing through the column, which acts as suspension steel, arresting movement of the slab down the column after punching shear failure and allowing redistribution of the gravity load to elsewhere in the floor.
In seismic design the ductility of structure in the post-elastic range is a very important consideration, since the structure, subjected to high magnitude earthquake, may have sufficient ductility to absorb and dissipate energy, given by repeated loading reversals, by post-elastic flexural deformation without collapse.
Slab-column connection ductility at failure μ cannot be defined uniquely because the force-displacement relation has no distinct yield point (because the yield spreads gradually across the slab transverse width).
To overcome the uncertainty in defining the yield displacement, an arbitrary procedure[5] is considered. The procedure was first to construct the envelope relation between lateral displacement and lateral load (Fig. 1.19). The envelope relation was then idealized by an elastoplastic relation. The initial slope of the idealized relation is a secant through the measured relation at

load equal to two-thirds of the measured strength. The plastic portion of the idealized relation passes through the maximum load and the maximum deformation at failure. The intersection between these two lines defines an effective yield displacement.
Displacement ductility is then calculated as the ratio between the ultimate displacement and yield displacement ($\mu = D_u/D_y$) of the idealized relation (Fig. 1.19). Notice that this formulation of ductility will be used to analyze and interpret results of the numerical analysis in section 4.2.4.

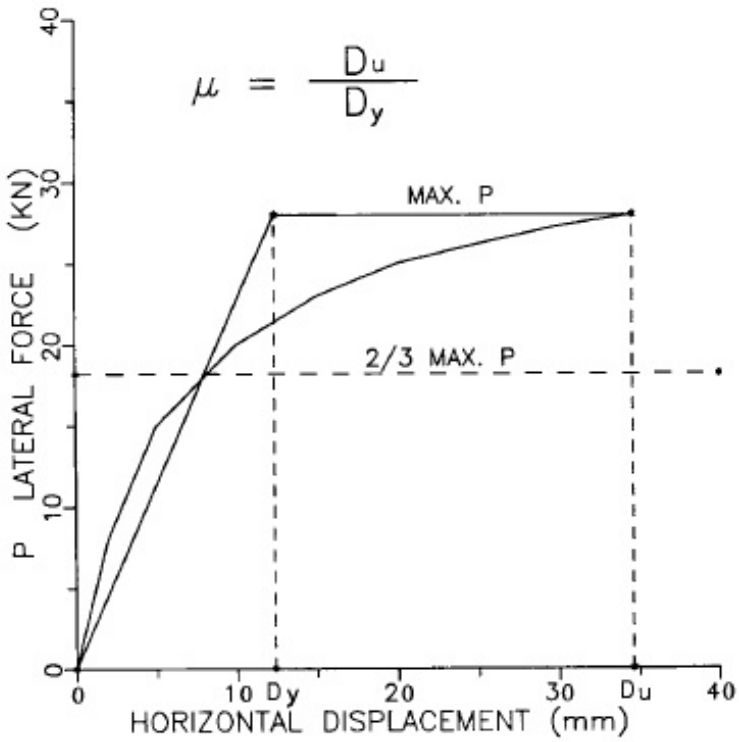

Figure 1.19: Definition of displacement ductility[5]

Effect of gravity load on lateral displacement ductility
The level of gravity load carried by the slab is a primary variable affecting the apparent lateral ductility[5]. This phenomenon has been identified in earlier tests by Kanoh and Yoshizaki[25].
To generalized the conclusion that gravity load affects lateral displacement capacity of the connection, lateral displacement ductility μ was plotted versus the normalized gravity shear ratio V_g/V_0 for test on interior connections, without shear reinforcement, subjected to shear and unbalanced bending moment[5] (Fig. 1.20). The value V_g is the vertical shear acting at the fail-

ure on the slab critical section; the quantity V_0 is the theoretical punching shear strength in the absence of moment transfer, as given by the following equation[9]:

Inch-pound units

$$V_0 = 4\sqrt{f'_c}b_0 d \tag{1.4}$$

SI units

$$V_0 = \frac{1}{3}\sqrt{f'_c}b_0 d \tag{1.5}$$

where b_0 is the perimeter length of the slab critical section and d is the critical depth.

As it is possible to notice from Fig. 1.20, for values of the gravity shear ratio V_g/V_0 exceeding approximately 0.4, there is virtually no lateral displacement ductility ($\mu = 1$); this means that connection fails by punching before any yield in the load-displacement relation is detected. As V_g/V_0 decreases, there is an increase in the available ductility.

The effect of gravity shear on lateral drift at failure shows, as for ductility, a reduction in available drift with increasing gravity shear ratio (Fig. 1.21).

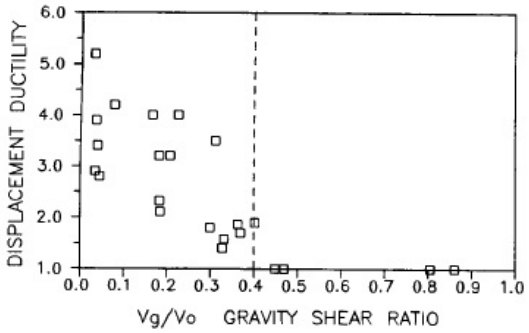

Figure 1.20: Effect of gravity load on ductility[5]

According to ACI Building Code[9], the shear strength for square interior columns is defined by Eq. 1.4 and 1.5; this limiting value has been established from tests of slab-column connections for which shear failure occurred before widespread yielding of the slab reinforcement[19].

Under this loading condition, the surrounding slab confines the connection region; this confinement is believed to be the reason why observed nominal shear stresses at failure are larger for slab-column connections than for linear elements such as beams[26].

Effect of biaxial lateral loading on lateral displacement ductility

During wind or earthquake loading, the slab-columns connection is subjected

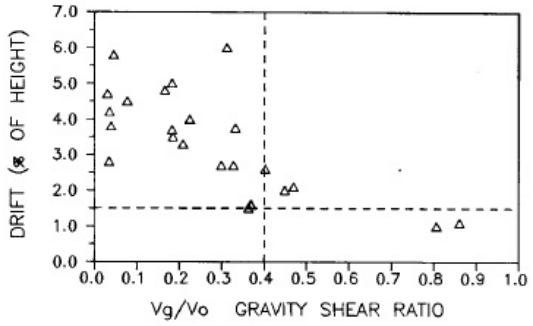

Figure 1.21: Effect of gravity load on drift[5]

to lateral loads acting in multiple directions; this is the rule and not the exception. For this reason it is important to investigate the influence of biaxial lateral loading on slab-column joints.
A little literature exists about this topic; Pan and Moehle[5] have shown results obtained by testing four specimens, two by uniaxial displacement history and two with biaxial lateral load histories (Fig. 1.22), representing interior connections without shear reinforcement.
Results show that biaxially loaded specimens failed at an earlier stage of testing in comparison with the uniaxially loaded specimens. Both stiffness and strength were less for the biaxially loaded specimens than for the equivalent uniaxially loaded ones.
Authors[5] conclude that biaxial lateral loading, as might occur during an earthquake or wind loading, reduces the available strength, stiffness and overall lateral displacement capacity of slab-column connections.

Effect of shear reinforcement on lateral displacement ductility
Test of slab-column connections with shear reinforcement demonstrate that shear reinforcement not only considerably increases the shear strength but also the ductility (Fig. 1.23). The using of closed stirrups, confining the longitudinal reinforcement passing through the joint, leads to good values of ductility; this beneficial effect it is not only due to the increment of torsional and flexural strength , but also to the fact that stirrups avoid movements and buckling of longitudinal reinforcement in the nearby of the column. This action avoid the spalling of superior concrete cover, then allowing also to the top longitudinal reinforcement to contribute to the slab suspension, differently to what happens without shear reinforcement.
Despite this fact, the increase of ductility depends also on many other factors; the most important are the type, the amount and detailing of shear reinforcement. For example, it has been proved that shear studs are very

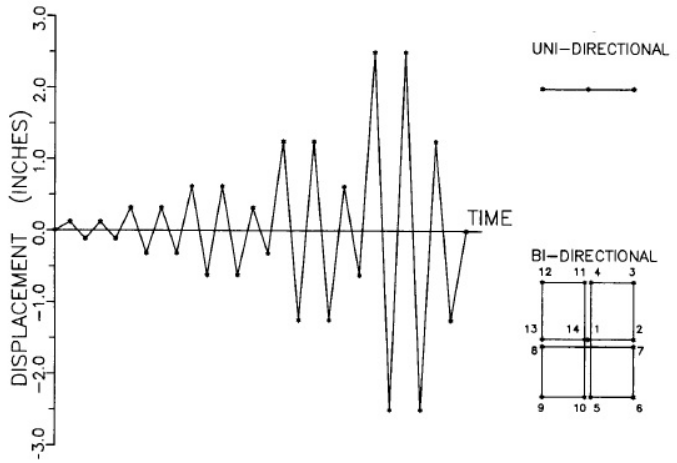

Figure 1.22: Lateral displacement history and loading patterns [5]

effective in the increasing of ductility since their particular shape provides a very good anchorage, which plays a major role for the efficiency of the shear reinforcement [2].

Data in Fig. 1.20 and 1.21 indicate that the available lateral displacement ductility of reinforcement concrete flat-plate connections without shear reinforcement is low by comparison with values often considered marginally acceptable in seismic design. Hence, in seismic zones it is not recommended to only rely on the flat slab-column connections in order to resist earthquake solicitation, without also the presence of shear walls or other stiffening systems.
Anyway, despite the fact of low ductility performance of slab-column joints, this does not actually mean that they provide poor performance during a strong earthquake loading.
Fig. 1.24 presents idealized load displacement envelopes of a typical slab-column connection [27] and a slender shearwall [28] that might be used to stiffen a flat-plate building. If the wall is sufficiently stiff to restrain lateral interstory drifts to approximately 1.5% (value usually indicated as a reasonable upper bound for severe seismic loading [29]), the required displacement ductility of the wall will be approximately 6. The required ductility of the slab-column connection will be less than 2.
According to the data presented in Fig. 1.20 and 1.21, a slab-column connection can be expected to possess some minimal ductility and a drift capacity of at least 1.5% drift only if $V_g/V_0 \leq 0.4$; expressed in terms of shear stresses, the nominal shear stress due to vertical loads should be limited to $0.4\frac{1}{3}\sqrt{f'_c}$

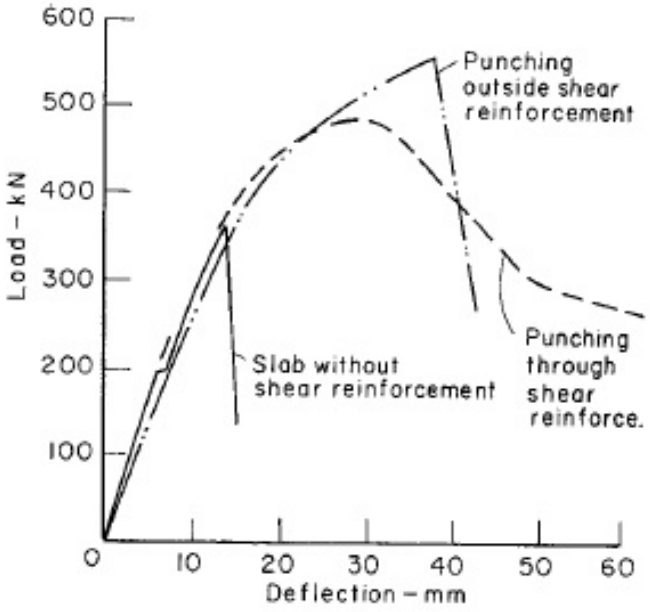

Figure 1.23: Influence of shear reinforcement on ductility[2]

MPa on the slab critical section. Notice that the vertical load should be taken at least equal to the design gravity load shear.
For lateral interstory drifts exceeding 1.5%, adequate performance of the flat plate cannot be assured. For this reason, a suitable structural system should be provided to limit lateral drifts.

1.2 Building codes

The present building codes regarding punching failure of slabs, considered the complexity of this phenomenon, adopt simplified procedures for verification, defining a control surface (*critical surface*), orthogonal to the mean plain, delimited by a critical perimeter at a certain distance to the column and with a depth equal to the slab effective depth. The fundamental criterion for verification is that the magnitude of shear stresses acting on the critical surface must be lesser than a particular value of strength of concrete, defined by experimental data. In general, the acting stress can be evaluated distributing the point load on the critical surface; anyway, in order to do this in the proper way, it is necessary to distinguish between cases of internal columns and edge columns as well as between vertical and lateral acting loads. As a matter of fact, the distribution of stresses will be uniformly distributed along the critical perimeter in the case of internal column or ver-

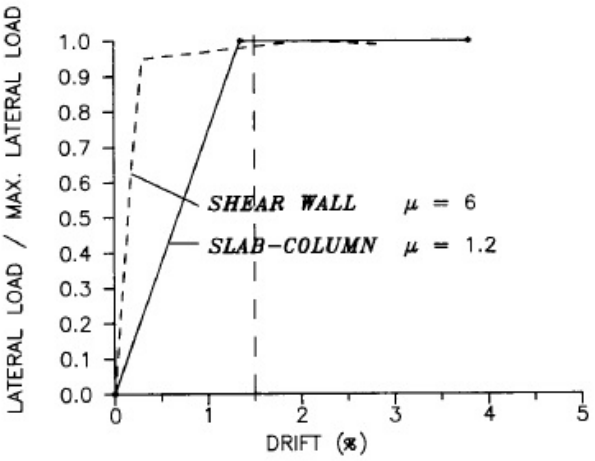

Figure 1.24: Comparison of ductility requirements at 1.5% drift[5]

tical load acting only, whereas lateral loads or, more generally, the transfer of bending moment in connections, produce a non-uniform distribution of stresses.
The definition of the critical surface according to all the different codes is actually not much correspondent to what observed experimentally; in addiction the different provisions lead to very different control surface. For a detailed information regarding these topics, refer to the national code provisions.
In the following section provisions related to the seismic design of punching shear reinforcement in flat plates, according to the american code, will be examined in the perspective of a future use of the grid model for the seismic design and verification of structures.

1.2.1 ACI 421.2R-07: Seismic design of punching shear reinforcement in flat plates

During an earthquake, significant horizontal displacement of a flat plate-column connection may occur, resulting in unbalanced moments that induce additional slab shear; connections must be designed in order to prevent brittle punching shear failure.
Even when an independent lateral-force-resisting system is provided, flat slab-column connections must be designed to accommodate the moments and shear forces with the displacements during earthquakes. This demand may be effectively addresses by changes in dimensions of certain members and/or their material strengths and/or provision of shear reinforcement.
The objective of ACI 421.2R-07[8] is to give recommendations for the design of flat plate-column connections with sufficient ductility to accommodate lat-

eral drift given by the selected lateral-force-resisting system, without punching shear failure or loss of moment transfer capacity.
The term "ductility" is the ratio of the displacement at ultimate strength to the displacement at which yielding of the flexural reinforcement occurs. For flat plate-column connections, there is no unique definition for these two displacements; however definition adopted by Pan and Moehle (1989)[5] is used.
ACI 318-05[9] allows the analysis of flat plate-column frames as equivalent plane frames. When the frame is not designated as part of the lateral-force-resisting system and is subjected to horizontal displacements, the width of slab strip to be included in the frame model and how to account for cracking are modeling parameters that significantly affect the resulting computed values of the moments transferred between slabs and columns. ACI 421.2R-07[8] contains a procedure that determines an upper limit moment that can be transferred between the slab and column when subjected to an earthquake.

1.2.1.1 Lateral story drift

Flat plate-columns frames without beams and without a lateral-force-resisting system consisting of more rigid elements that limit the lateral displacements are not permitted by ACI 318 in regions of high seismicity. In this case flat plate buildings rely on a lateral-force-resisting system that limits its lateral displacement.
The story drift is defined as the story drift divided by the story height, which is the distance between the mid-surfaces of the consecutive flat plates at top and bottom of the story of interest.
It has been frequently recommended that flat plate structures should have the capability to go through a design story drift ratio of at least 0.015, including inelastic deformations[29, 30, 5].
In the force-based design approach, a static elastic analysis of the lateral-force-resisting system is performed to determine the elastic story drift δ_e. This value is then multiplied by factors, specified in IBC-06[31] to obtain the design story drift $\delta_u \leq 0.007 \div 0.025$ of the story height, including inelastic deformation.
The design story drift may reach the upper limit of IBC-06 when connections are provided with slab shear reinforcement or when the gravity load produce low punching shear stress.
ACI421.2R-07 considers the effects of gravity loads on story drift capacity, based on several experimental studies[6, 2, 7] that show the variation of ultimate story drift ratio DR_u with the ratio $V_u/\phi V_c$ for interior flat plate-column connections transferring gravity shear forces V_u and reversals of cyclic drift (Fig. 1.25). The experimental values of DR_u are compared with the design story drift δ at peak strength , divided by the story height. V_u is the

maximum shear force transferred between column and slab at failure; V_c is the nominal punching shear strength of the connection without shear reinforcement in the absence of moment transfer and it is computed according to ACI 318-05[9].

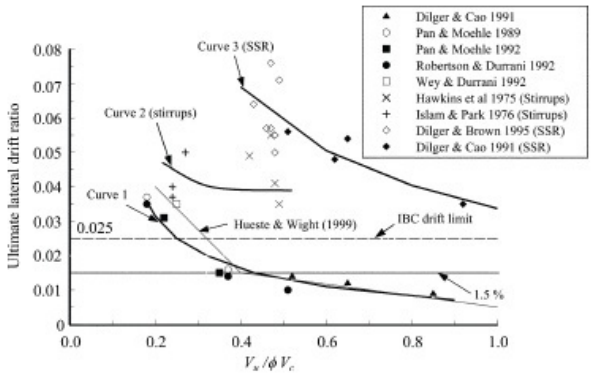

Figure 1.25: Effect of gravity loads on lateral drift capacity of interior flat plate-column connections[6, 2, 7]

Fig. 1.25 indicates that the flat plate-column connection capability to experience story drift without failure decreases with increasing magnitude of the applied gravity loads. The solid horizontal line shown in Fig. 1.25 represents the design story drift ratio of 0.015, which is frequently adopted as a minimum drift capacity. This horizontal line intersects Curve 1 at $V_u/\phi V_c \cong 0.40$, indicating that slabs without shear reinforcement can satisfy the required 0.015 design story drift ratio only if $V_u \leq 0.40\phi V_c$.
Fig. 1.25 shows that the curves representing experiments of flat plate-column connections with shear reinforcement fall well above the horizontal line corresponding to a story drift ratio of 0.015.
The slab shear reinforcement is required when the maximum shear stress at $d/2$ from the column face exceeds ϕv_c, where v_c is given by $V_c/(b_0 d)$; b_0 is the perimeter of the critical section for shear at $d/2$ from the column face and d is the average slab effective depth.
In addition, flat plate-column connections should have shear reinforcement equal to or exceeding the minimum amount given by ACI 421.2R-07[8], except when the value of V_u is less than $0.20\phi V_c$, being ϕ the strength reduction factor: $\phi = 0.75$ (ACI 318-05[9], Section 9.3.2.3).This requirement ensures that the connections can sustain the design story drift ratio $DR_u = 0.025$.
For detailed provisions regarding minimum shear reinforcement in flat plates, refer to ACI 421.2R-07.

1.2.1.2 Unbalanced design moment

According to ACI 421.2R-07[8], flat plate-column connections should have a punching shear strength able to resist the factored shear force V_u and factored unbalanced moment M_u due to gravity loads combined with the design story drift during an earthquake. ACI 421.2R-07 furnishes the methods to calculate the value of M_u and its upper limit, as explained in the following.

Frame Analysis
The moment of inertia of the slab and its supporting columns are determined according to the equivalent frame method of ACI 318, unless the layout of columns is highly irregular.
To account for the effect of cracking in non-prestressed flat plates, Vanderbilt and Corley[32] recommended to consider the moment of inertia of the slab equal to 1/3 the value of the uncracked slab strip, from panel center-line to panel center-line, to obtain a conservative estimate of the story drift.
ACI 318-05, Section R13.5.1.2, recommends the use of 25 to 50% of the uncracked moment of inertia of the slab to compute the elastic story drift δ_e. According to ASCE 7-05 δ_u is given by the following expression:

$$\delta_u = \delta_e \left(\frac{C_d}{I_E} \right) \tag{1.6}$$

where $C_d = 1.25 \div 6.5$ and $I_E = 1 \div 1.5$ are dimensionless factors specified by ASCE 7-05, depending on the inherent inelastic deformability of the lateral-force-resisting system and the occupancy importance of the structure, respectively.
Flat plate-column frames not designated as part of the lateral-force-resisting system experience the same lateral displacements as those of the lateral-force-resisting system. Thus, connections should be designed to transfer shears and moments associated with δ_u obtained from Eq. 1.6. Accurate determination of shears and moments associated with δ_u is not possible, but for design purposes, a simplified elastic analysis is proposed by ACI 421.2R-07.
The unbalanced moment caused by factored vertical forces that exist during an earthquake should be added to the moments due to the lateral drift.
To avoid underestimation of the unbalanced moments transferred between the slab and the columns for a given value of δ_e, the unbalanced moments M_u should be determined by an elastic analysis, but with the moment of inertia of the slab equal to 50% of the value of the uncracked slab and using the values of the moments of inertia of the uncracked columns(ACI 318-05, Section R13.5.1.2).

Simplified elastic analysis
The unbalanced moments transferred between the slab and the columns un-

der the elastic story drift δ_e can be determined by a linear analysis of simplified equivalent frames both for interior and exterior columns (Fig. 1.26). The slab is assumed to be simply supported at locations of controflexure lines assumed at midspan. The column is assumed to have hinged supports at controflexure points assumed approximately at the midheight of the story. The horizontal displacement δ_e is introduced at the upper ends of the columns as shown in Fig. 1.26. The value of δ_e can be estimated by any rational analysis; for example, it can be calculated using an elastic analysis of the lateral-force-resisting system subjected to the lateral forces as specified by IBC-06 or ASCE 7-05.

The unbalanced moment, due to horizontal seismic force, transferred between the column and the connected slab is equal to the sum of the end moments at the column ends above and below the flat plate-column connection. Additional unbalanced moments caused by factored vertical forces that can exists during an earthquake should also be considered. The smaller of the total unbalanced moment computed using this procedure and the upper limit given in the following paragraph, should be used.

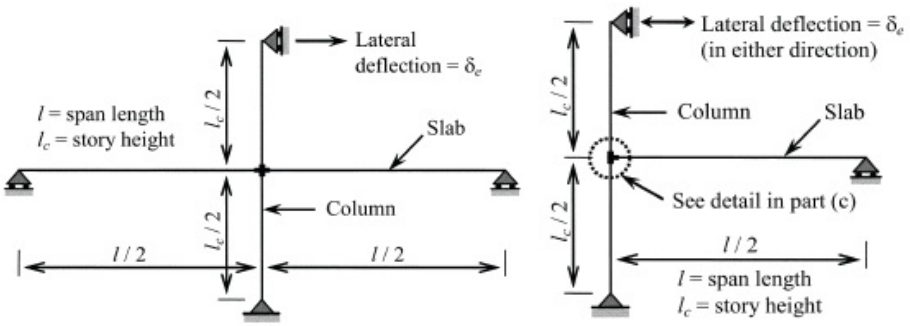

(a) Interior slab-column connection

(b) Edge or corner slab-column connection

Figure 1.26: Linear analysis of simplified equivalent frames

Upper limit for M_u

The value of the unbalanced moment corresponding to the displacement δ_e can be higher than the value that produces ductile flexural failure. Provision of shear reinforcement in this case would not increase the value of the unbalanced moment strength.

Based on finite element analyses (Megally and Ghali 2000b) and experiments (Megally and Ghali 2000a) on flat plate-column connections transferring shear combined with moment reversals, the following upper limit can

be set for the value of M_u:

$$M_u \leq \frac{M_{pr}}{\alpha_m} \tag{1.7}$$

where M_{pr} is the sum of the absolute values of the probable flexural strengths of opposite critical section sides of width $c+d$. $\frac{M_{pr}}{\alpha_m}$ represents the magnitude of the unbalanced moment that will develop the yield strength of the flexural reinforcement. When this occurs without a punching shear failure, the flat plate-column connection will experience substantial drift and not lose the ability to transfer gravity loads, thus avoiding collapse.
The equations (Eq. 1.8 and 1.9) expressing the empirical coefficient α_m are based on finite element results:

$$\alpha_m = 0.85 - \gamma_v - \left(\frac{\beta_r}{20}\right) \tag{1.8}$$

$$\alpha_m = 0.55 - \gamma_v - \left(\frac{\beta_r}{40}\right) + 10\rho \tag{1.9}$$

where:

γ_v is the fraction of moment transferred by vertical shear stresses in the slab

β_r is the ratio l_x/l_y or l_y/lx when the transferred moment is about x or y axis, respectively; l_x and l_y are the projections of the critical section at $d/2$ from the column face on its principal axes x and y, respectively

ρ ratio of the tensile flexural reinforcement

Notice that the value of M_u can be substantially greater than M_{pr}, meaning that the transfer of unbalanced moment can mobilized the flexural strength of the slab over a width considerably greater than $c + d$.

Design of shear reinforcement
When shear reinforcement is provided, the nominal shear strength (expressed in stress units) is given by:

$$v_n = v_c + v_s \tag{1.10}$$

where v_c and v_s are the nominal shear strengths provided by the concrete and shear reinforcement, respectively. ACI 421.1R-99 limits v_n to $2/3\sqrt{f'_c}$ or $1/2\sqrt{f'_c}$ MPa, respectively, when the shear reinforcement is SSR or stirrups. This two limits should be increased by 25% in seismic design when the shear stress due to V_u/ϕ alone does not exceed $1/3\sqrt{f'_c}$. This is because the maximum shear stress is caused mainly by M_u, rather than by V_u. the value of v_c is limited to $0.125\sqrt{f'_c}$ MPa in seismic design (ACI 421.1R-99).
A summary of the steps explained previously for computing the paunching shear strength of flat plate-column connections is given by the flow chart shown in Fig. 1.27.

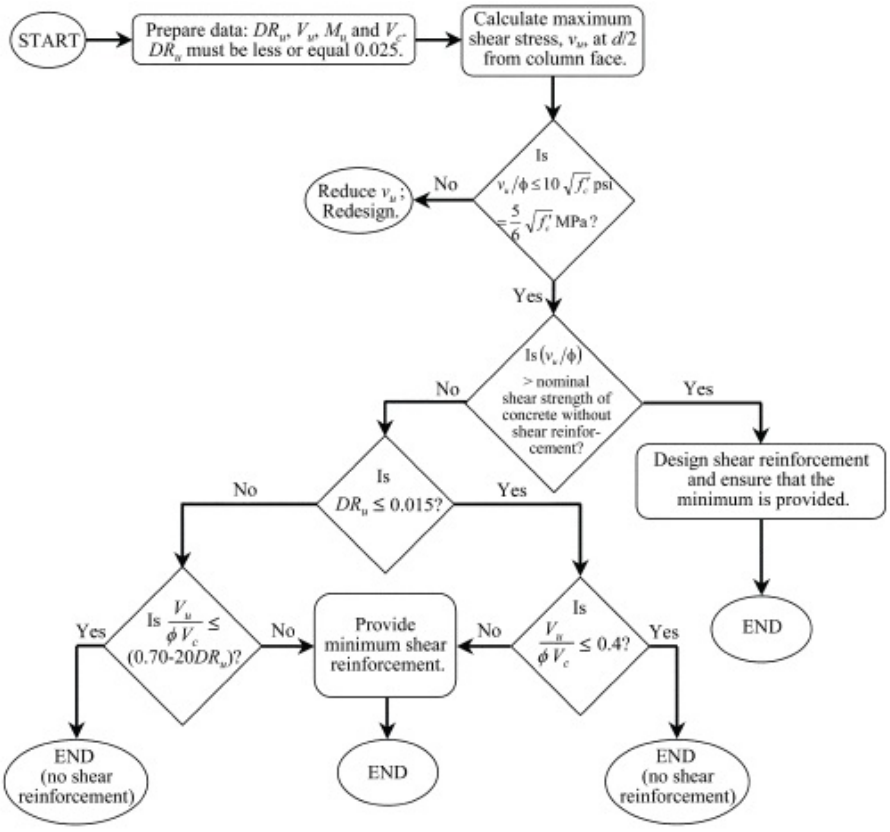

Figure 1.27: Steps for punching shear design of earthquake-resistant flat plate-column connections[8]

Finally notice that ACI 318-05 provisions for shear reinforcement design are relevant for flat slab-column connections not designated as part of the lateral-force-resisting system. Shear reinforcement beyond the requirements of ACI 318-05 is reccomended when $V_u/\phi V_c > 0.4$.
Fig. 1.28 displays the criterion for shear reinforcement requirement. A point in Zones 1 nd 2 represents the case when $V_u > 0.4\phi V_c$; with such high value of V_u combined with unbalanced moment reversals, the ductility can be ensured only with shear reinforcement. ACI 421.2R-07 is consistent with the code in recommending shear reinforcement in Zone 3 (zone of relatively high DR_u). In addition, for ductility purposes, the minimum shear reinforcement should be provided.

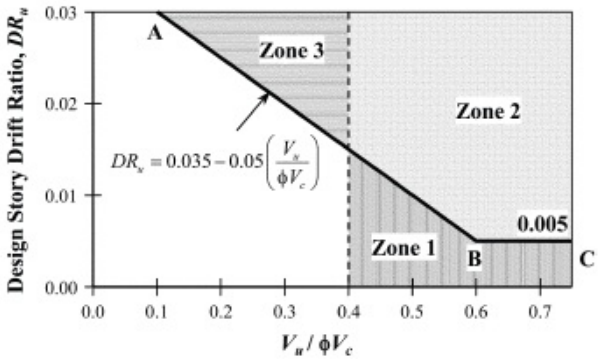

Figure 1.28: Requirement for shear reinforcement criterion[9]

Chapter 2

Grid Model for Flat-Slab Structures

The aim of this master degree thesis is to apply a grid model[33] presented in the following sections for the non-linear static analysis of the seismic response on a flat-slab floor (see Cap. 3), tested experimentally to punching failure under gravity and lateral loads.
The grid model considered[33] reproduces the non linear behavior of flat-slab structures; the inelastic response of the structure is concentrated in point hinges introduced into beam finite elements, modeling the response in bending, torsion and shear. This type of model permits to estimate internal actions at slab-column joints; the description of their non-linear behavior allows to evaluate the whole slab structural response up to failure. In particular, it is possible to asses connections safety with respect to punching and structural deformability, in terms of interstory drift ratio,under horizontal lateral loads.

2.1 Fundamentals of the grid model

The slab is represented by a grid of beam finite elements, fixed at joints, arranged in two orthogonal directions; the columns are modeled with two beam elements, one above and one below the slab, fixed to the plate (Fig. 2.1).
The beam finite elements have been defined as beam-column elements, thus including the effects of flexural, torsional, axial and shear deformation. Six degrees of freedom are activated at each joint.
The segments between the nodes are made of an elastic part and plastic hinges which reproduce the flexural, shear and torsional non-linear behavior; in general two flexural hinges, located at the two extremities where the maximum bending moment is reached, one torsional and one shear hinge, located at the center since shear and torsion are constant, are present in each

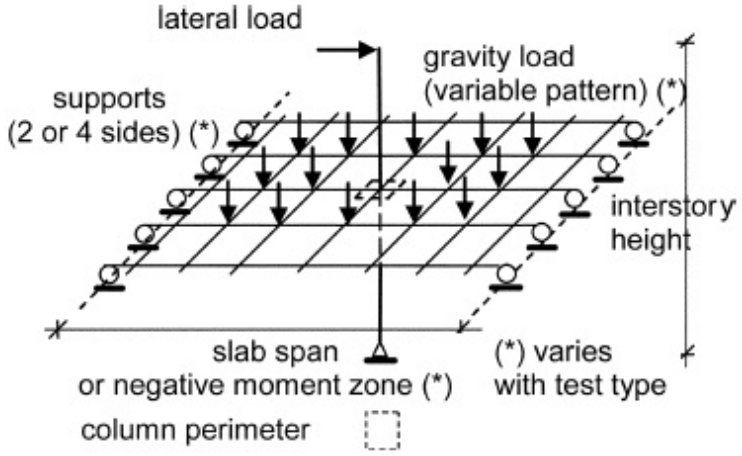

Figure 2.1: Model geometry and loads

segment (Fig. 2.2(c)).

The model has been developed by using a commercial finite element software[34], performing non-linear static analyses under displacement control.
The grid spacing must be sufficiently close in the nearby of connections in order to obtain a good approximation of the effects of load in the slab, since concentration of stresses exists in these zones; the elements can be more widely spaced elsewhere[35].
In this model (Fig. 2.2), rigid elements with length equal to the column cross-section dimensions are placed at the centre of the connection (Fig 2.2(c)). The elements intersecting the column have width equal to $c + d$ (where $c =$ side length of column and $d =$ mean effective depth of the slab), which is the width of the shear critical section according to the definition of ACI 318[9] and is considered also for torsion in the transverse direction. A shear plastic hinge has been placed in each one of these elements at a distance $d/2$ from the column face.
The flexural non-liner behavior is concentrated over a larger width than shear one and is considered equal to $c + 3d$ according to ACI 318[9]; part of this is modeled by flexural hinges of the elements framing into the columns, whereas the remaining part by ones of the adjacent elements.
As regards the other elements of the grid, two possible solutions have been taken into consideration by authors:

1. a regular spacing $c + d$ for all elements, thus simplifying the geometry and also the definition of the member properties

2. a regular spacing $2d$, leading to a rather fine grid

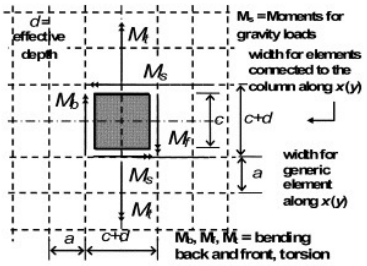

(a) Critical sections close to the column: geometry, internal bending moments and torques

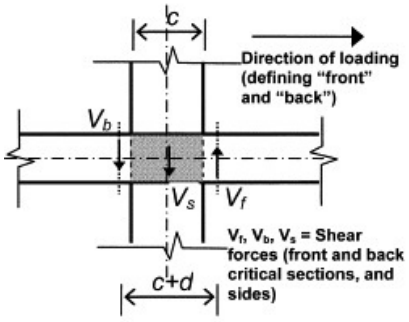

(b) Shear forces

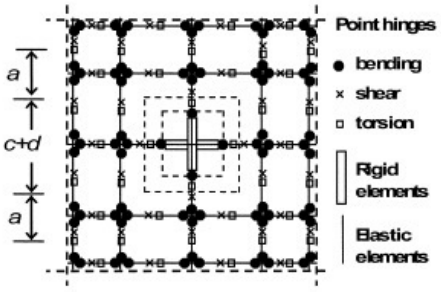

(c) Grid elements and non-linear point hinges for ACI 318[9]

Figure 2.2: Grid model

These two grid types leads to equivalent results in terms of the whole structural response and failure modes for the group of specimens analyzed by author of the model[33]. In the present thesis work, a more complicated grid spacing has been chosen, as described in section 4.1, in order to adapt the model to the particular column geometries of the test slab (see section 3.1.1). Author refers to the possibility of further modifications of the grid, in order to adapt the model to other codes[33]; in particular to Eurocode 2[36] has been considered.

2.2 Properties of non-linear hinges

Each grid element is composed by an elastic part and by non-linear hinges. The former has a stiffness determined considering the effect of shrinkage and construction stresses[13, 10], causing cracking in slab previous to the action of lateral loads; for this reason half of the initial stiffness is proposed for all elements[37]. The plastic hinges instead, which are lumped in singular points, are characterized by relations that link bending moment, shear and torsion with the inelastic curvature, shear distortion and twist angle, respectively.
These relations have been described with a phenomenological approach and using different models according to the internal action considered, as described in the following paragraphs.

2.2.1 Bending moment

The moment-curvature relations have been obtained analytically for each beam element, starting from the sectional geometrical characteristics, reinforcement and material characteristics. In order to do this, a sectional model[12] with non linear constitutive relations is used, based on perfect bond and plane sections assumptions. This model takes into account also the effects of confinement given by stirrups on the compressed concrete.
The obtained moment-curvature relations are then approximated with trilinear relationships (Fig. 2.3) which will be provided as an input to the model. The length of the flexural plastic hinges are taken equal to d (effective depth of the slab), according to tests[38].
Notice that simplifications are considered: the bond-slip of longitudinal reinforcement and interaction with shear are not considered[39, 13].

2.2.2 Torsion

In flat slab structures subjected to horizontal loads, high torsional moments develope along the elements transversally oriented with respect to the direction of loading; in particular elements oriented in this way and being

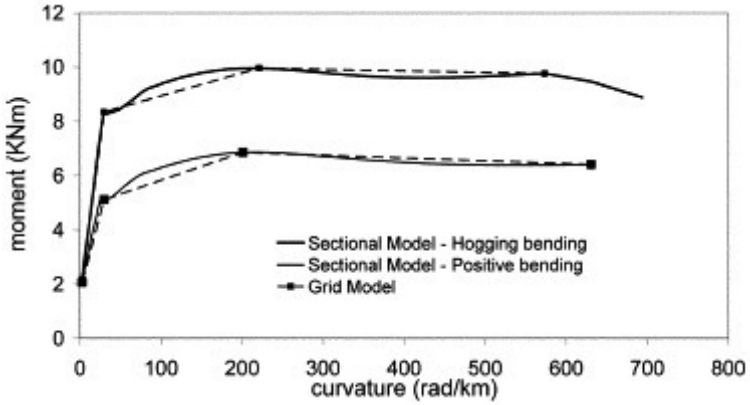

Figure 2.3: Typical moment-curvature relationship and trilinear approximation

in the nearby of connections are the most torsionally stressed. Thus, the grid model[33] used, contains also the definition of torsional plastic hinge, as explained in the following.
A simplified phenomenological approach has been used for the relation between torque and twist, with the capacity M_{tu} and the corresponding twist ψ_u. Torsion tests[11] for slabs with and without transverse reinforcement measured capacities corresponding to shear strength much larger than for a beam without transverse reinforcement, as consequence of the confinement given by the membrane actions in the plate. Notice that the response was ductile and the presence of stirrups did not modify the behavior substantially; these results are considered by the author[33] for the definition of the model.

Torsion Capacity
The torsional capacity M_{tu0} for the elements placed at the four sides of the connection is evaluated on the basis of a model for slab-column connections formulated by Park and Choi[40].
In their model the slab is represented by isoparametric bidimensional finite elements (*shell*) with nine nodes, based on Mindlin's theory of thick plates. Within its thickness a series of these finite elements is placed. In this way it is possible to describe the deformation due to the combined action of shear and flexure, existing int he zone around the connection. This model[40] provide also the state of stress at the interface of the critical zone at failure.
Park-Choi model[40] was validated by the comparison with 51 test specimens. By integration of stresses obtained within the critical surface, it is possible to estimate bending moment, shear and torsion moment acting on each side of the connection.
Considering Fig. 2.4(a),representing a typical slab-column connection, front

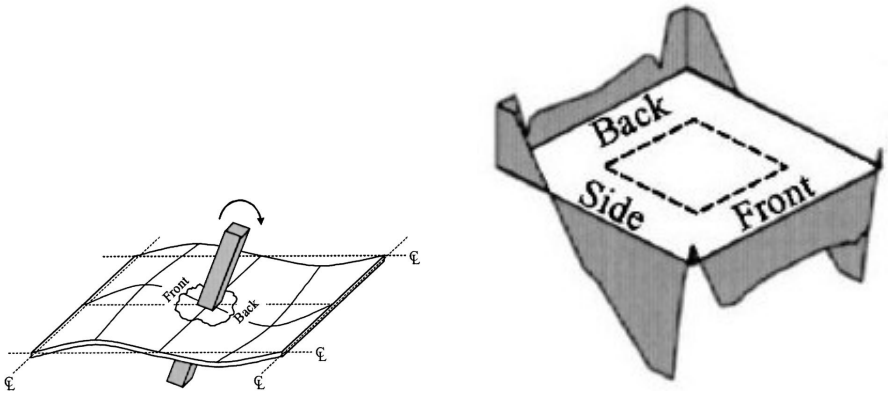

(a) Flat plate-column connection subjected to unbalanced moment

(b) Shear stresses along the critical perimeter due to the unbalanced moment

Figure 2.4: Typical connection subjected to unbalanced moment

and back sides of the critical perimeter are subjected to an elevated bending moment, whereas the lateral sides are subjected to a bending moment lesser than the yielding one, since the unbalanced moment does not increment the bending moment at the lateral sides of column. As consequence, the shear stress along the lateral sides (Fig. 2.4(b)) reach values locally higher than ones along back and frontal sides, which are also strongly damaged by flexure.
Notice that in a slab damaged by bending moment, the shear force is principally sustained by the compressed zones, where, in addiction to the shear stresses, also membranal compression stresses are present. It is necessary to take into account for this fact.
Along the lateral sides of the critical perimeter, subjected to bending moment given by gravity loads, usually lesser than the yielding value, compressive stress is assumed to vary linearly within the slab thickness. The relation between acting bending moment and the maximum compressive stress of concrete is defined as:

$$M_g = A_{sf2} f_s z = A_{sf2} \left(\frac{d-c}{c} \sigma_e \frac{E_s}{E_c} \right) z \tag{2.1}$$

where:

A_{sf2} sectional area of the tensile longitudinal reinforcement

f_s stress in the longitudinal reinforcement

z internal level arm

E_c concrete elastic modulus

E_s steel elastic modulus

c neutral axis depth

σ_e maximum concrete shear compressive stress

The maximum shear stress (v_{us}) along lateral sides is equal to the summation of the two components given by shear and torsional moment, transmitted by the unbalanced moment, acting on these sides of the critical perimeter. The relation is the following:

$$v_{us} = \frac{V_{Gs}}{(c+d)d} + M_t \frac{c+d}{2J'} \tag{2.2}$$

where:

J' polar moment of inertia of the section of width $c+d$ defined as $J' = 2d^3(c+d)/12 + 2d(c+d)^3/12$

V_{Gs} shear force acting along the considered side

M_t torsional moment acting along the considered side

The shear V_{Gs} is known, being the shear stressing one of the beam elements adjacent to the column due to gravity loads only, and it can be obtained by an elastic analysis; values of v_{us} and M_t, which correspond to failure, are instead unknown.
Park and Choi[40] propose an equation that expresses the ultimate shear stress (v_{us}) as function of the compressive stress (σ_e). The relationship between the two variables is obtained by aforementioned equations solved using values of M_G, V_{Gs}, M_t at failure, which are obtained from numerical results of the analyses based on tthe finite element model defined by authors themselves[40]. The equation interpolating the results obtained (Fig. 2.5), is the following:

$$\frac{v_{us}}{v_c} = 5 - 2.5\left(\frac{\sigma_c}{f'_c}\right) \tag{2.3}$$

where v_c is the uniformly distributed shear strength and f'_c is the concrete compressive strength.

As it is possible to observe in Fig. 2.5, the shear strength along lateral sides decreases with the increasing of the perpendicular compressive stress due to flexure; thus this equation consider the interaction effect between normal and tangential stresses.
In the grid model[33], since it is necessary to evaluate the ultimate torsional moment of the beam elements adjacent to the column, firstly solicitations V_{Gs} and M_G have to be evaluated from an elastic analysis; then it is possible to compute σ_e due to M_G and from this value v_{us} is obtained. Finally, M_t

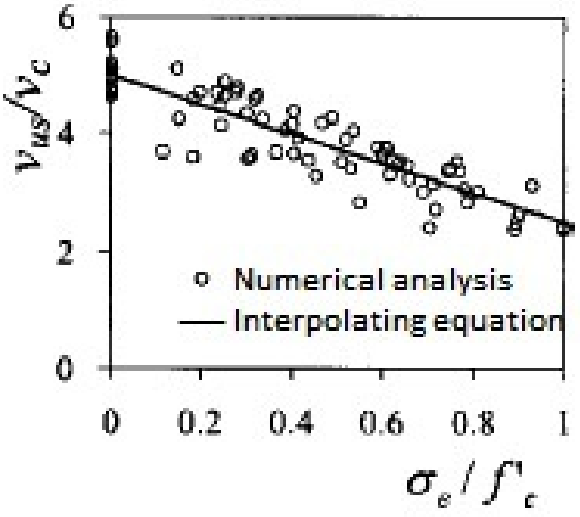

Figure 2.5: Numerical data and interpolating equation

is computed inverting equation 2.2.
Thanks to this torsional model, it is possible to determine a resistant shear stress value, in absence of shear and bending moments, up to a maximum of five times the resistance for pure uniform shear (v_c). Rigorously, this prediction holds only without shear reinforcement; in fact its effect is to decrease the level of interaction between M_t, V_{Gs} and M_g.
For this reason, for elements provided with shear reinforcement, it is necessary to compute the hypothetical resistant torsional moment without shear and bending moment solicitations, thus obtaining M_{tu0} ($>M_{tu}$). This value is then reduced on the basis of circular interaction law[41] (Fig. 2.6), linking shear and torsional moment, and from this, the value of M_{tu} to use in the model, is obtained. The equation used is the following:

$$1 = \left(\frac{M_{tu}}{M_{tu0}}\right)^2 + \left(\frac{V_u}{V_{u0}}\right)^2 \tag{2.4}$$

where:

V_u acting shear

V_{u0} resistant shear

For the elements of the grid model[33] placed externally to the critical zone, an elastic-perfectly plastic behavior is defined, with the ultimate torsional moment computed using a resistant shear stress value equal to $0.58\sqrt{f_c}$[41],

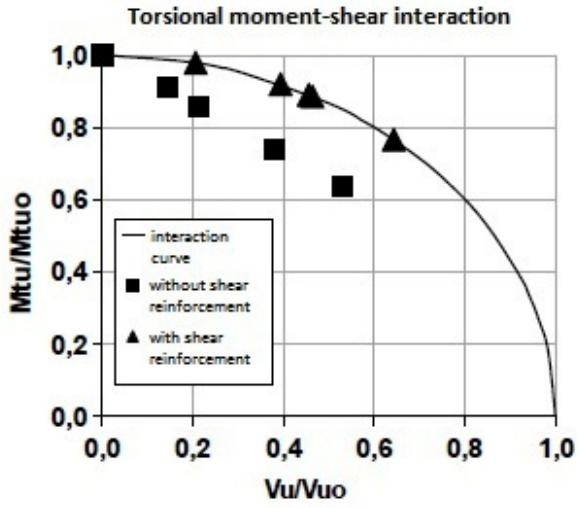

Figure 2.6: Numerical data and interpolating equation

thanks to the approximated equation of torsion for stretched rectangle:

$$\tau = \frac{M_t b}{J} \tag{2.5}$$

where:

$J = ab^3/\chi$ approximated torsional moment of inertia

a, b minor and major dimensions of the rectangular section of the element, rispectively

χ coefficient which is function of the ratio of minor and major dimension (a/b)

Twist Angle at Torsion Capacity

The values of ultimate twist angle ψ_{u0} (at torsion capacity) measured experimentally for specimens without transverse steel[11] is used[42] (Fig. 2.8).
For specimens with transverse steel, the values of ψ_{u0} are obtained by a model for reinforced concrete beams with transverse reinforcement[10]. This model represents the beam, at ultimate condition with cracked concrete, by a lattice composed by steel ties (yielded reinforcing bars) and compressed concrete struts (Fig. 2.7). The torque as a function of plastic rotations per unit length ψ is obtained. For detailed description of the application of the torsion model refers to Collins and Mitchell publication[10].

The plastic hinge length is provided as an input to the grid model and it is equal to $1.5d$, corresponding to experimental observations[43, 13, 11]. Thus,

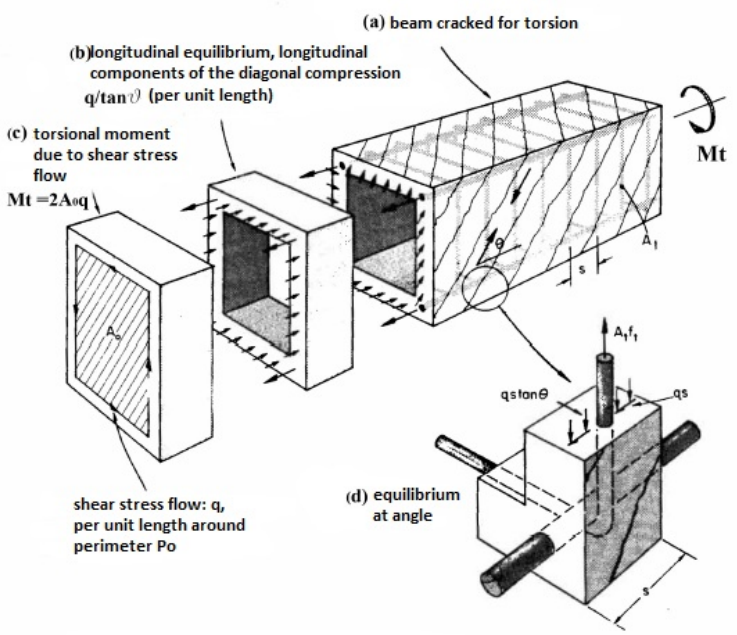

Figure 2.7: Torsional model for reinforced concrete beams with transverse reinforcement

multiplying the calculated ψ_{u0} by the hinge length, torsion angle are obtained. The results for the specimens analyzed in the paper[33] are shown if Fig. 2.8 as a function of the transverse steel ratio.
The method to obtain the behavior of the torsional plastic hinge is quite laborious, then author[33] provide a law that interpolates the values of ψ_u and which is function of the geometrical and mechanical properties of the section. In Fig. 2.9 values of twist angles, obtained from the torsional model[10], and the interpolating curve are represented. The interpolating function has the following expression:

$$\rho_u = -0.0063ln\left(\frac{p_{st}}{f'_c}\right) - 0.0071 \tag{2.6}$$

where p_{st}=A_{st}/s is the transversal reinforcement ratio and in which S_{st} is the area of transversal reinforcement and s is their spacing. When the interaction with shear and moment determines a capacity reduction from M_{tu0} to M_{tu}, the twist angle ψ_{u0} is reduced to ψ_u, proportionally to M_{tu}/M_{tu0} (Fig. 2.10).

As regard connections with SSR, a perfectly plastic branch is assumed in the torque-twist relation on reaching the torsion capacity, to consider the improvements given by this type of reinforcement[6, 2, 44].

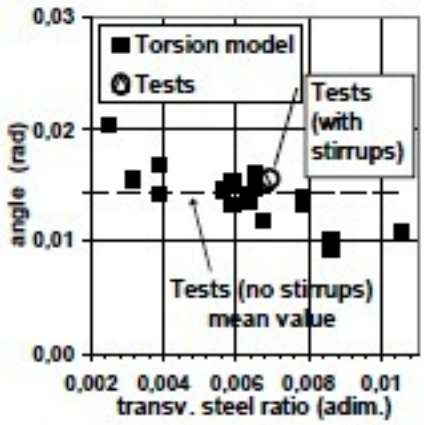

Figure 2.8: Values of angle θ_u from the torsion model[10] and tests[11]

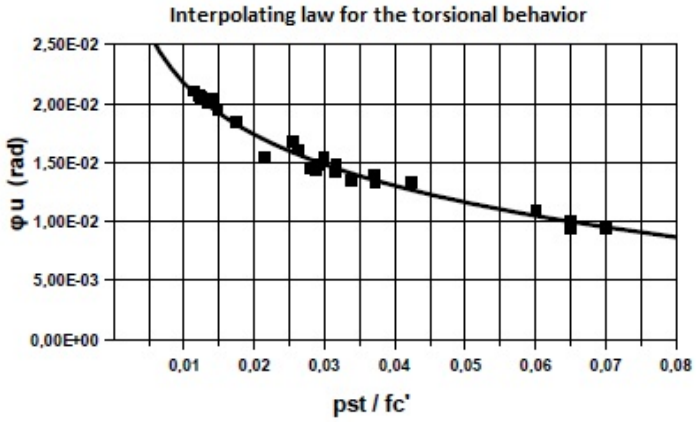

Figure 2.9: Values of twist angles obtained with torsional model[10] and their interpolating function

Normalized Diagram
The following considerations hold for the elements adjacent to the column, inside the critical zone. A tri-linear relation is used, with a first branch beyond cracking up to the yield point, followed by a segment up to the capacity M_{tu} and angle ψ_u, and a softening branch. The diagram calculated by the torsion model described in the preceding paragraph[10] is used for this purpose. The values are normalized using the maximum torque and the corresponding twist angle, obtained in the analyses. The piece-wise linear diagram is obtained connecting the points at cracking, yield and ultimate. Finally, the ordinates and abscissa of the diagram are multiplied by the cross section capacity M_{tu}, obtained by Park-Choi model[40], and the corresponding twist ψ_u to obtain the piece-wise linear curve used in the calculations.

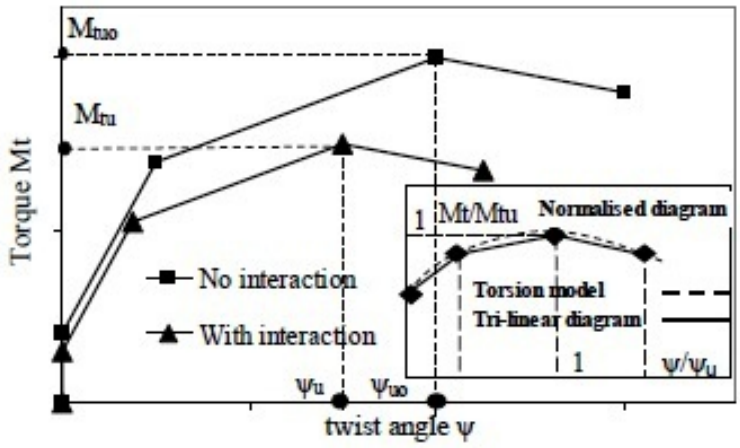

Figure 2.10: Tri-linear approximation of the torsion response

2.2.3 Shear

The shear non-linear response is particularly important for elements placed in the critical zone of connections, since in these areas shear stresses are the highest.
The relation linking shear and non-linear deformation is based on the punching capacity V_u at the critical section and the corresponding deformation γ_u; also in this case, a phenomenological approach has been used to derive the model.

Shear Capacity
The punching shear capacity on one side of the critical perimeter is computed as:

$$V_u = v_n(c+d)d \tag{2.7}$$

according to ACI 318[9, 44], where the strength $v_n = \frac{1}{3\sqrt{f'_c}}$ with no shear reinforcement. With transverse reinforcement $v_n = v_c + v_s$, where $v_c = \frac{1}{6\sqrt{f'_c}}$ and $v_s = \frac{A_v f_y}{bs}$. Notice that b is the critical perimeter and s is the spacing of reinforcement with cross-section area A_v and yield strength f_y. For the outer elements without shear reinforcement, a linear reduction of the strength from $1/3\sqrt{f'_c}$ to $1/6\sqrt{f'_c}$ is considered[2], moving from the column face to a distance equal to $4d$.

Strain at Shear Capacity

The values of ultimate shear strain γ_u for slabs without shear reinforcement have been obtained by a linear interpolation of the optimal values for modeling the experimental punching in tests carried out on slab-column connections[33]. In Fig. 2.11 the fitting curve is shown, whose equation is the following:

$$\gamma_u = 0.0092 \left(\frac{p f_y}{\frac{1}{3}\sqrt{f_c}} \right) - 0.011 \tag{2.8}$$

where γ_u is function of a non-dimensional parameter which includes the longitudinal reinforcement ratio (p) and the strength of materials (f_c, f_y). For

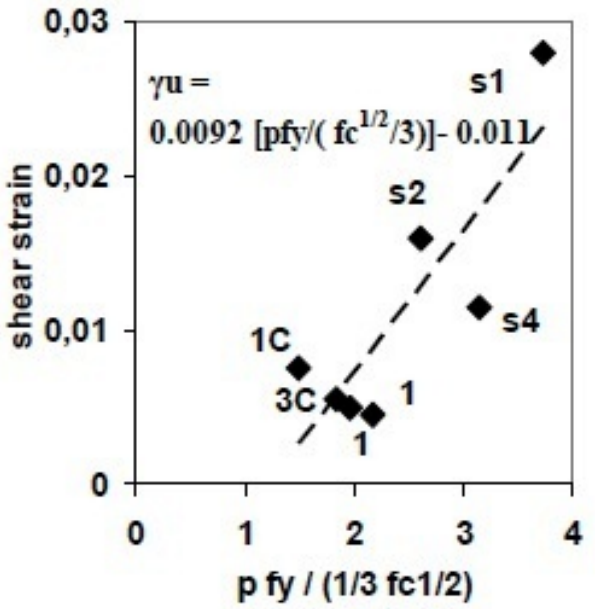

Figure 2.11: Ultimate shear strain γ_u: fit for specimens without shear reinforcement

slabs with shear reinforcement the strain at yielding of transverse steel γ_y and strain at failure γ_u are obtained from a sectional model[12], as it is done

for reinforced concrete beams. This is justified by the fact that the yielding and failure of transversal reinforcement occurs when concrete is already cracked, thus beneficial effects which increase the punching shear capacity due only to concrete are lost. This reasoning explains the reduction of the resistant contribute of concrete in presence of transversal reinforcement from $1/3\sqrt{f_c}$ to $1/6\sqrt{f_c}$, being the latter strength value for "one way" solicitations (e.g.: beam).
Values of γ_y at yielding of transverse steel and γ_u, computed for the specimens analyzed in the article considered[33], are shown as function of transverse reinforcement ratio (Fig. 2.12).

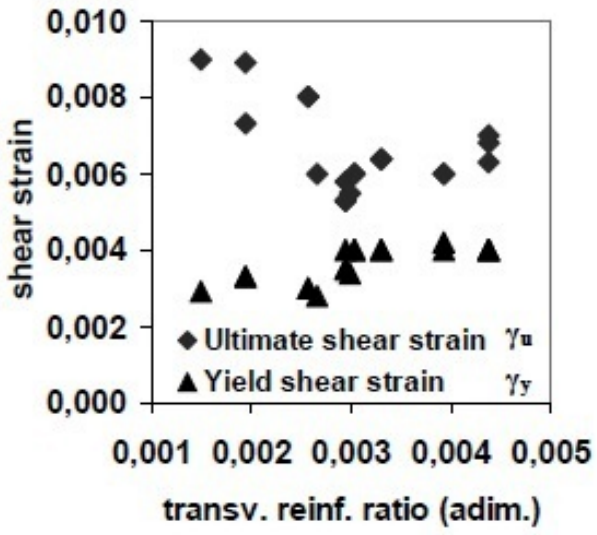

Figure 2.12: Yield strain γ_y and ultimate shear strain γ_u obtained by the sectional model[12] for specimens with shear reinforcement

Normalized Diagram
First of all it's necessary to compute the shear-strain response as for a beam section subjected to pure shear, using the sectional model[12] describe before. The section of the element has a width equal to $c + d$ and an height corresponding effective depth d of the slab. The values of the diagram obtained are then normalized using its maximum shear force and the corresponding strain. The path of the diagram is approximated with a tri-linear relation connecting the points at cracking, yield (if shear reinforcement is present) and ultimate. The ordinates and abscissas of the diagram are multiplied by thee cross section punching shear capacity V_u and the ultimate strain γ_u in order to obtain the curve that will be inserted as input in the model (Fig.

2.13).
Finally notice that the plastic hinge length is taken as the length of the part of the slab where diagonal cracks develop; test results show that this is approximately between d and $2d$[43, 45] depending on the slab reinforcement ratio and the material properties. In the present model, the plastic hinge length is taken equal to $2d$.

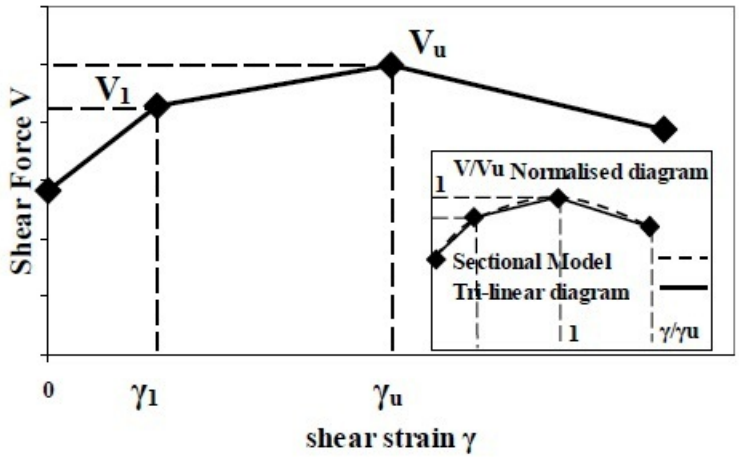

Figure 2.13: Relation between shear force and inelastic strain: tri-linear model

Chapter 3

Test Results

The grid model describe in chapter 2 has been applied on a real study case, consisting on an experimental tests on a flat-plate structure under vertical and lateral loads, carried out at University of California at Berkeley [13]. In the present chapter, a detailed description of this study case will be done in terms of geometry, reinforcements and loadings in order to better understand all the various and numerous aspects of the experimental test.

3.1 Description of the test slab

3.1.1 Geometry of the slab

The prototype slab (Fig. 3.1) represents a portion of a typical flat-plate floor of an intermediate story of a multi-story office building. This slab has three bays in each direction and a 203 mm slab thickness. Story height of the prototype is 3.05 mm and bay width is 6.86 m and 4.57 m for long and short directions, respectively.
The scale model (Fig. 3.2) used for the experimental study has dimensions equal to 40% of ones of the prototype. The length of each bay is 2.74 m and 1.83 m for long and short directions, respectively. The slab is 81 mm thick. Columns extended above and below the slab as shown in Fig. 3.2. The columns stubs above the slab were 0.30 m long, and their purpose was to anchor the column longitudinal reinforcement and to provide continuity of the column through the floor; the inferior column stubs were 1.2 m long with pinned connections at the extremities.
Four different column cross-sectional geometries were chosen (Fig. 3.1, 3.2) in order to collect data related to the effects of column rectangularity: rectangular columns with aspect ratio 2:1 were used in the east half of the floor, whereas squared columns in in the west half part (Fig. 3.1, 3.2). With this layout, the structure is symmetric about the floor centerline along the long direction.

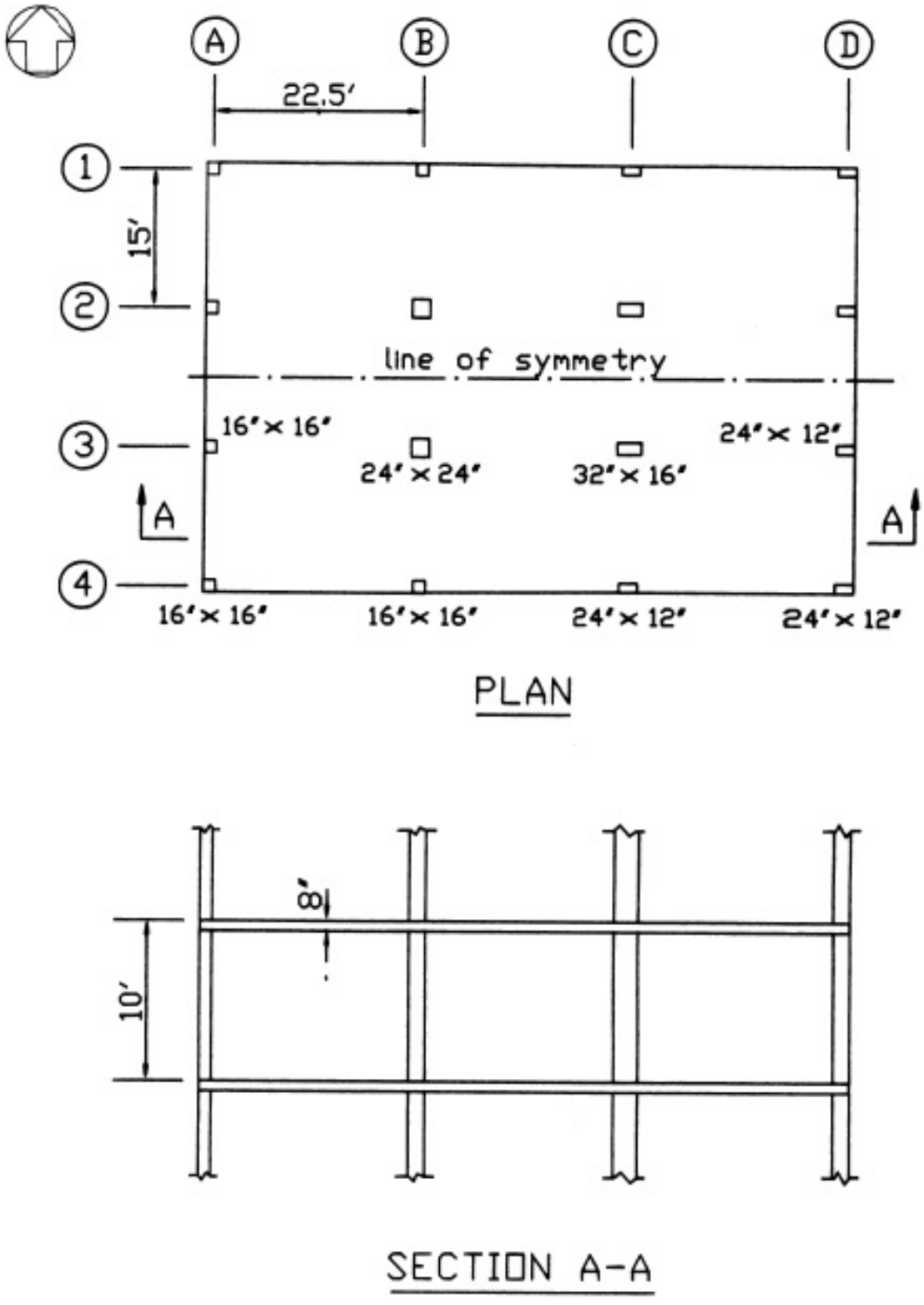

Figure 3.1: Layout of prototype slab (units in feet and inches)

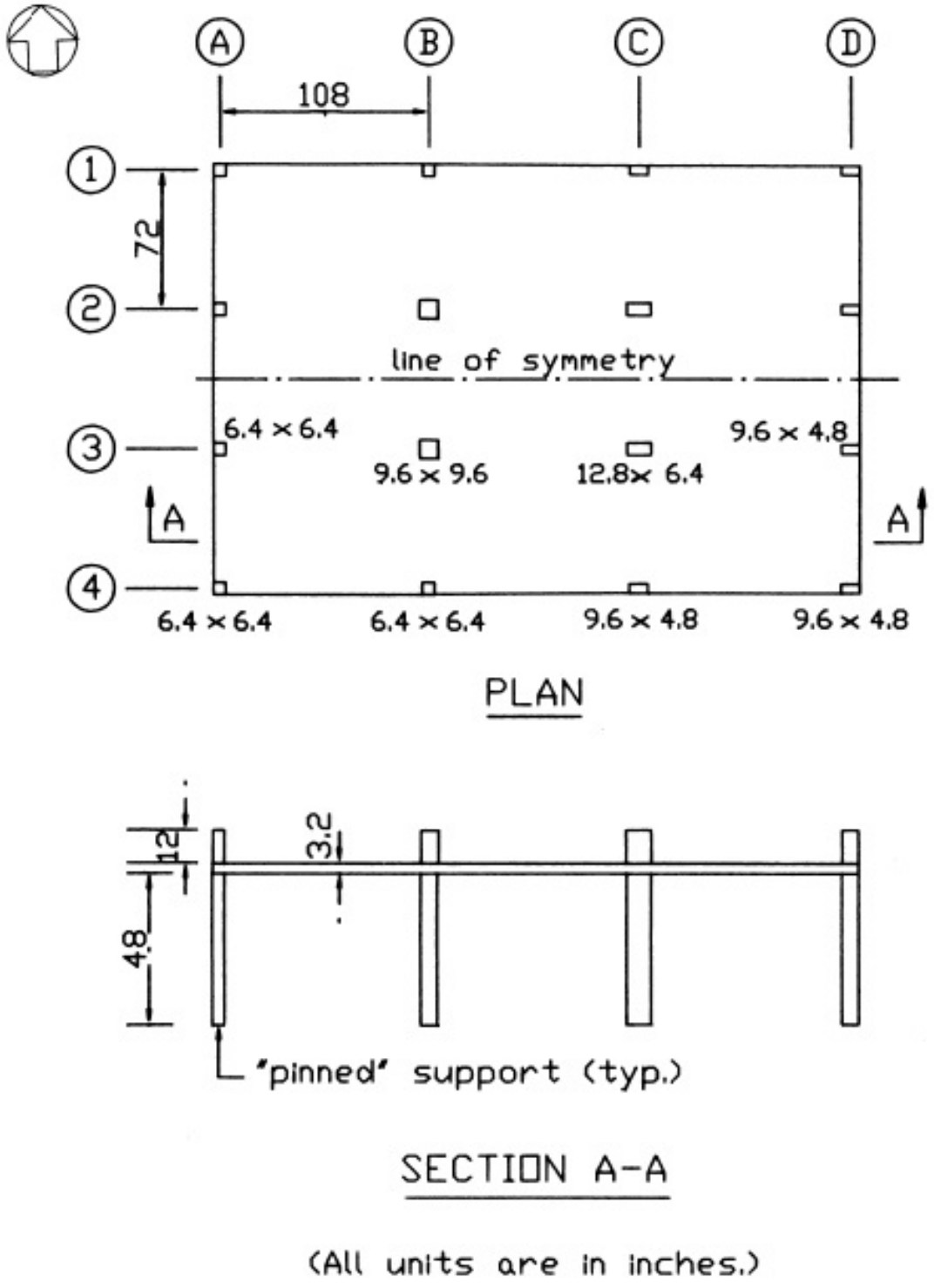

Figure 3.2: Layout of test slab

3.1.2 Materials characteristics

The concrete used had a design compressive strength of 21.9 MPa; the use of low compressive strength concrete is to exacerbate problems associated with shear and unbalanced moment transfer. Slab reinforcement used for slab are deformed bars with cross-sectional area $A_l = 32$ mm^2 ($\phi = 6.4$ mm) with an yield strength $f_y = 462.6$ MPa, whereas the ones for columns have have $A_l = 199$ mm^2 ($\phi = 15.9$ mm) with $f_y = 536.4$ MPa. Columns transverse reinforcement was smooth bars of cross-sectional area $A_l = 32$ mm^2 ($\phi = 6.4$ mm) with $f_y = 337.8$ MPa. Notice that no transverse reinforcements are used for the slab.

3.1.3 Layout of reinforcements

The prototype floor slab was designed by authors following the general procedures embodied in the ACI 318-83 Code[46], although some liberty was taken regarding selection of design moments; this was done in the interest of testing the validity of the validity of the American Code procedures and of more liberal procedures. All load factors and strength reduction factors of ACI 318-83[46] were applied in the design. The prototype design quantities were subsequently scaled for the model slab.
The actions acting on the slab were computed by the Direct Design method of the ACI 318-83 Code[46] for gravity load moments, whereas lateral load analysis for wind loads was based on the effective beam width model of Pecknold[47]. Gravity and wind load effects were combined according to the ACI 318-83 Code provision 9.2.
If geometry of the floor slab was symmetric about a floor centerline in the long direction as already cited (Fig. 3.2), a different choice was done by the authors for the layout of reinforcements, which are different on either side of that longitudinal centerline because of the two different design philosophies used, as specified in the following.
South of the centerline, all connections were proportioned for shear and moments computed as specified above, with the provisions for shear and moment transfer, and all reinforcements details fulfilled, according to the ACI 318-83 Code.
North of the centerline, redistribution of moments between the connections was assumed by authors. The objective of the redistribution was to alleviate requirements for negative moments; the released negative moments were redistributed to the positive moment regions of the column strips where the mount of reinforcement was controlled by requirements of maximum spacing. With the redistributed moments, midspan reinforcement was stressed near yield under the design ultimate loads.
The two different design philosophies resulted in notable differences in re-

quired reinforcement on the North and South halves of the floor slab, as it is possible to notice from Fig. 3.3 to Fig. 3.6.
Uniform continuous bottom steel was adopted. According to moment redistribution, two bottom rebars were added in the exterior panels as in Fig. 3.6. Additional bottom reinforcement was provided at the interior slab-column connections B3 and C3, as in Fig. 3.5 and Fig. 3.6, to resist progressive collapse due to punching shear failure. Finally, notice that interior connections B3, C2 and C3 were provided with bottom reinforcement satisfying recommendation proposed by Collins and Mitchell[19] without strength reduction factor; whereas interior connection B2 was provided with bottom reinforcement half of that recommended.
Figure 3.7 shows sectional details of slab reinforcement at the discontinuous slab edges of the model. The slab rebars with 180° hooks were placed within a width bounded by lines located four slab thickness ($4h$) beyond column face. Outside this width, bars with 90° hooks were provided. The slab reinforcement parallel to the long direction was placed in the outer layers of both the top and bottom (Fig. 3.7), which results in an effective depth of 70.6 mm (2.78 in.) for the long direction and an effective slab depth of 64.3 mm (2.53 in.) for the short direction.
Column reinforcement (Fig. 3.8) was selected by authors to ensure that the column parts extending below the floor slab would posses strengths exceeding transfer moment strength of the slab-column connections. Their design conformed to the ACI 318-38 Code Appendix A.9 "Requirements for frames in regions of moderate seismic risk".

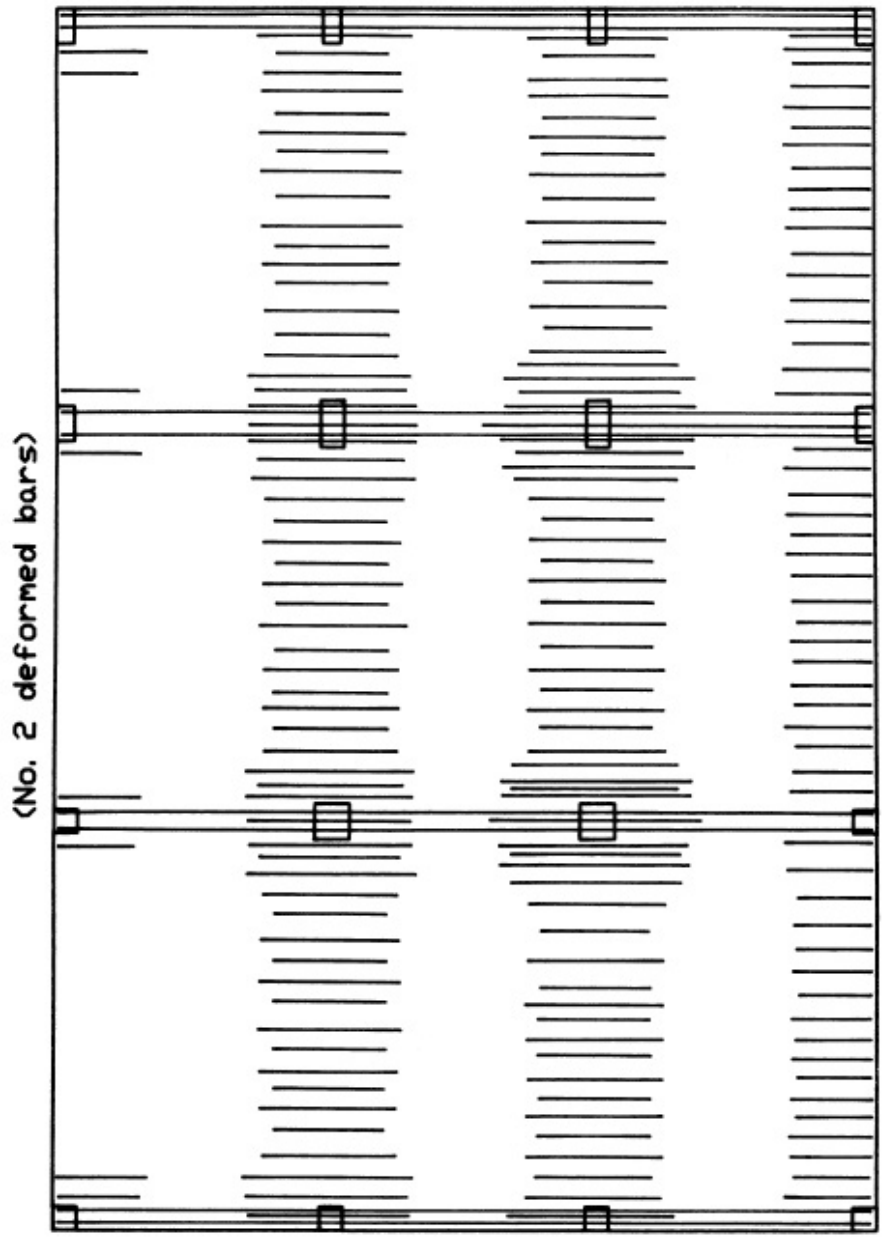

Figure 3.3: Model slab top steel layout - N-S direction

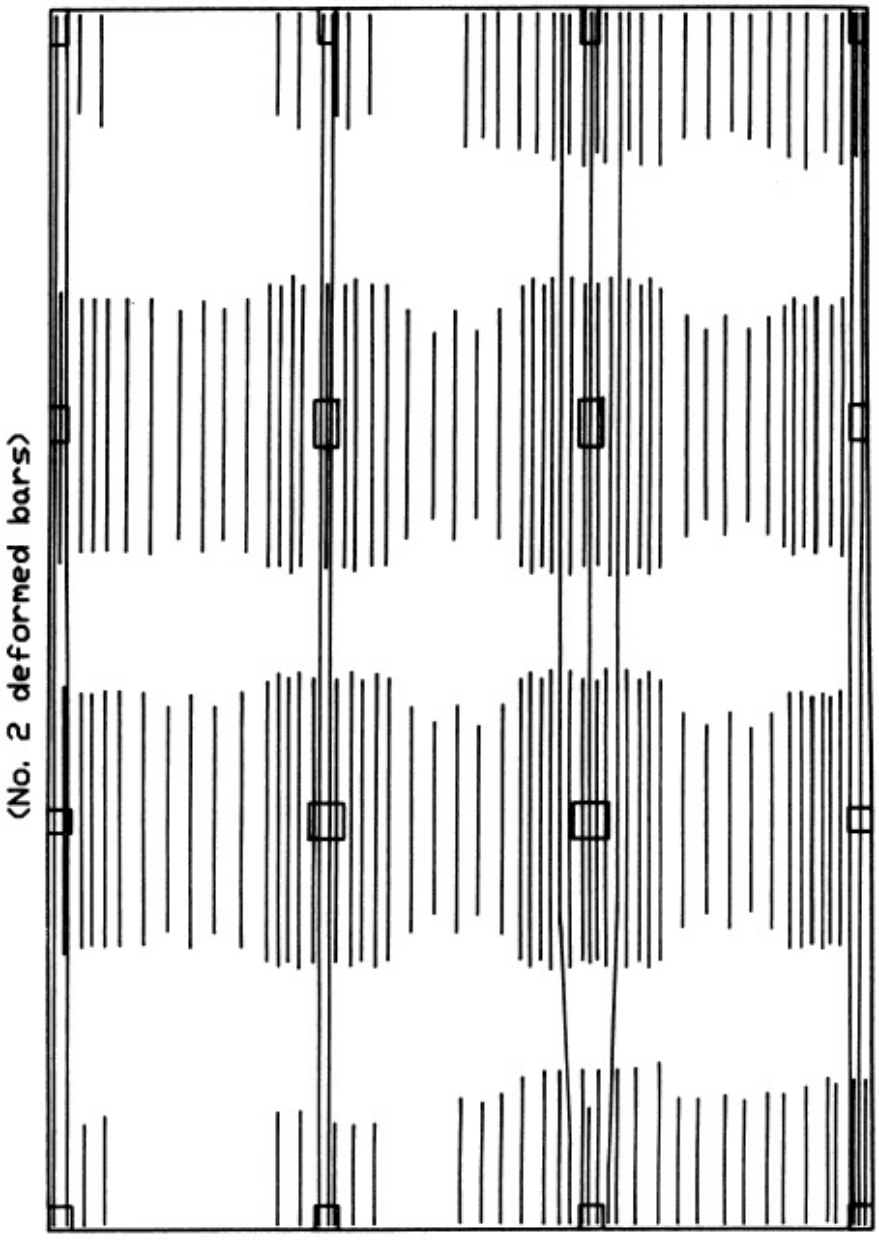

Figure 3.4: Model slab top steel layout - E-W direction

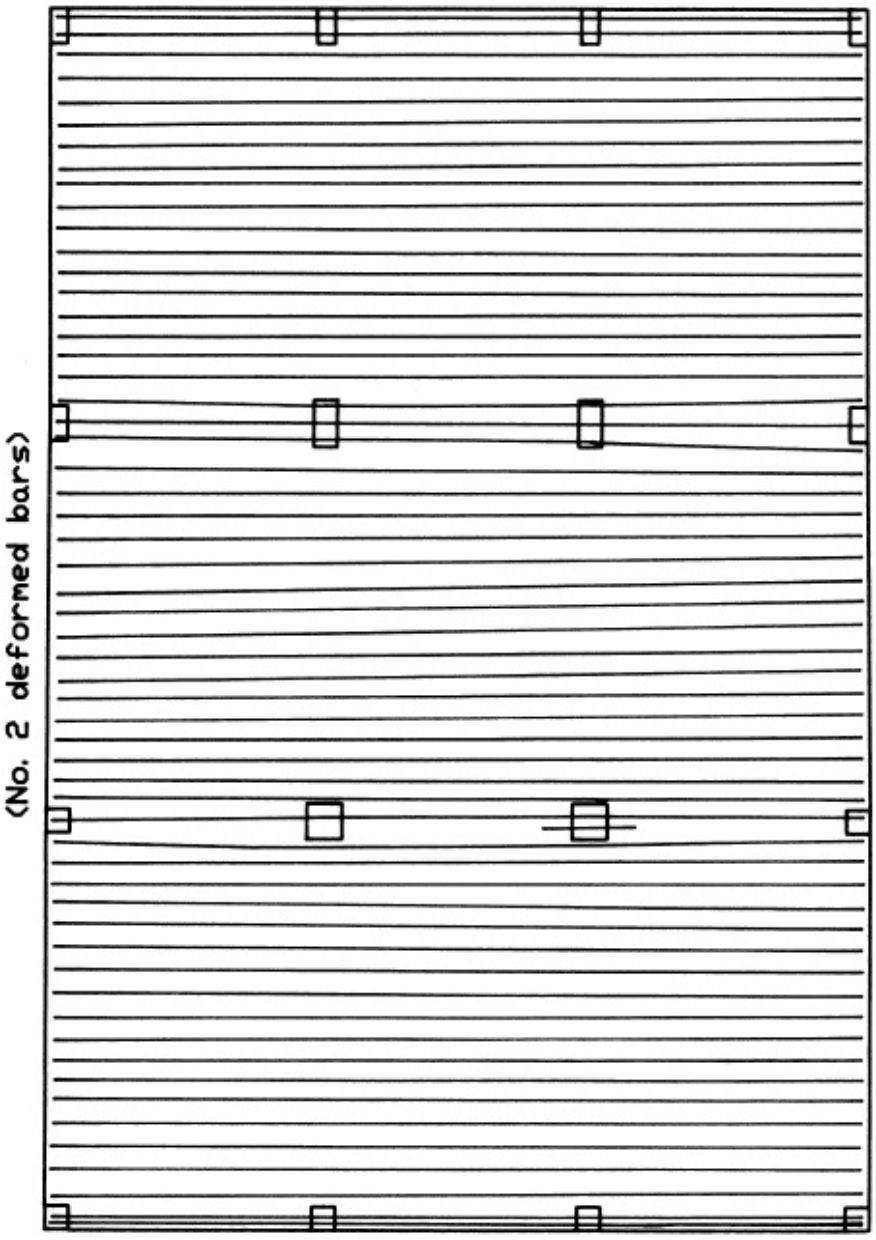

Figure 3.5: Model slab bottom steel layout - N-S direction

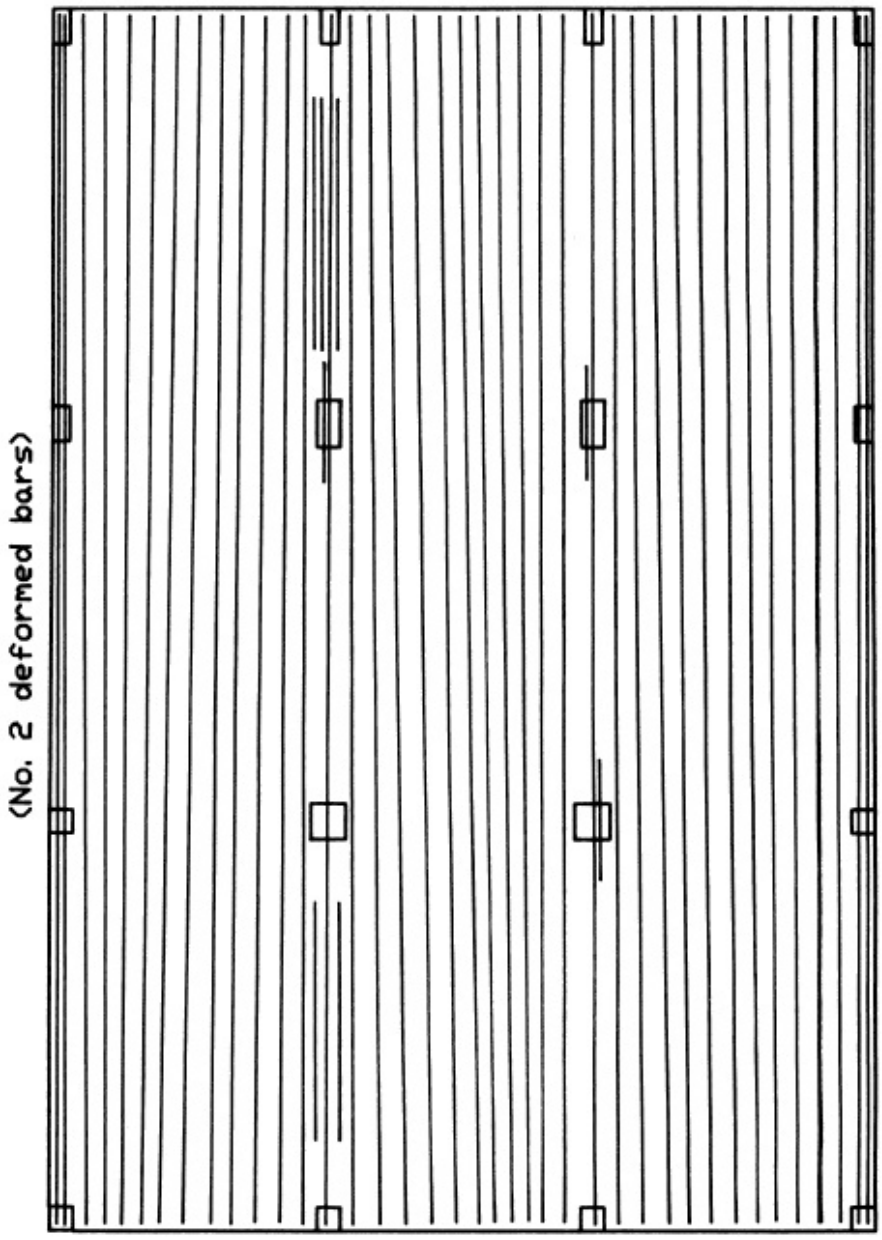

Figure 3.6: Model slab bottom steel layout - E-W direction

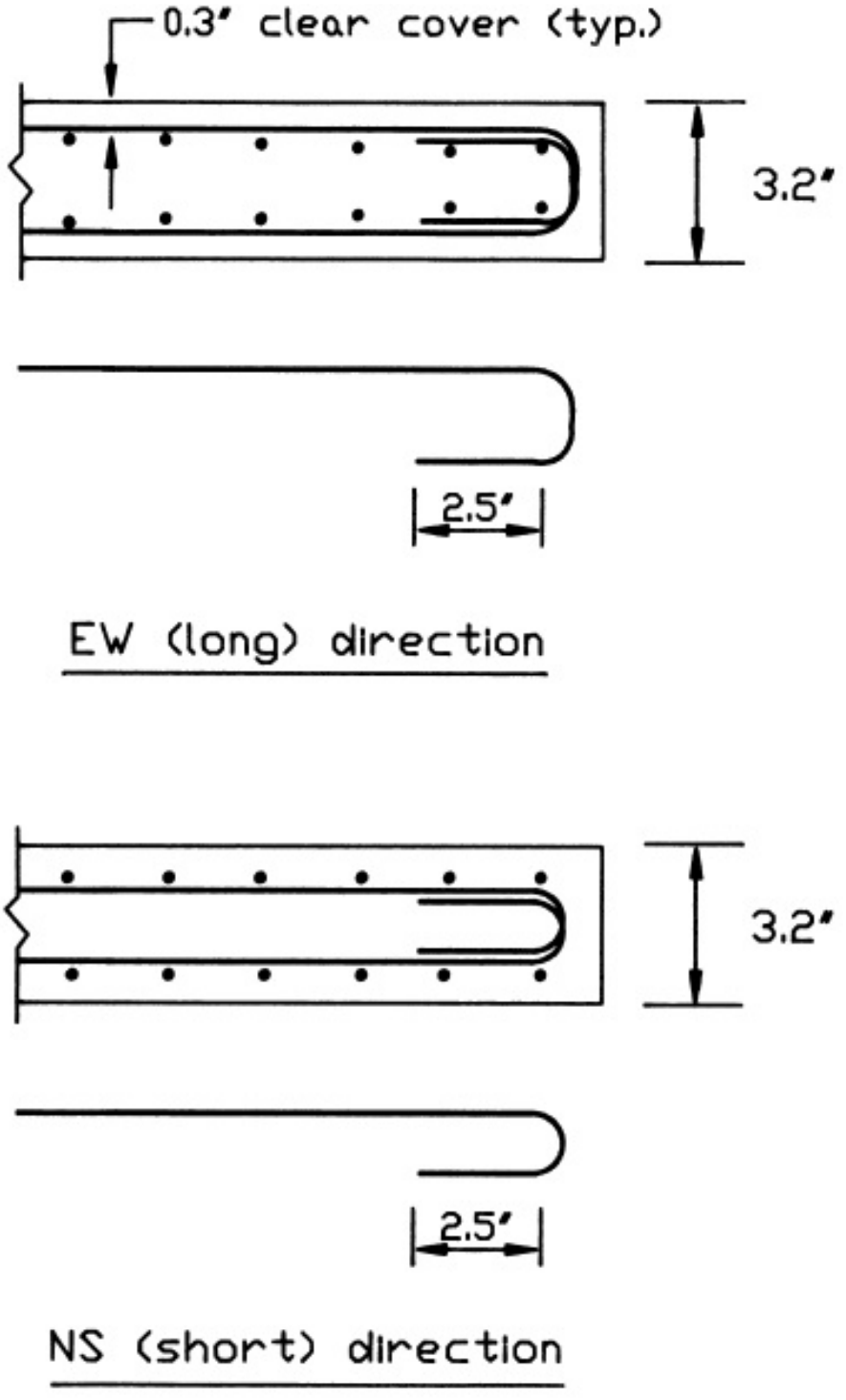

Figure 3.7: Sectional details at discontinuous edges of model slab (units of measure in inches)

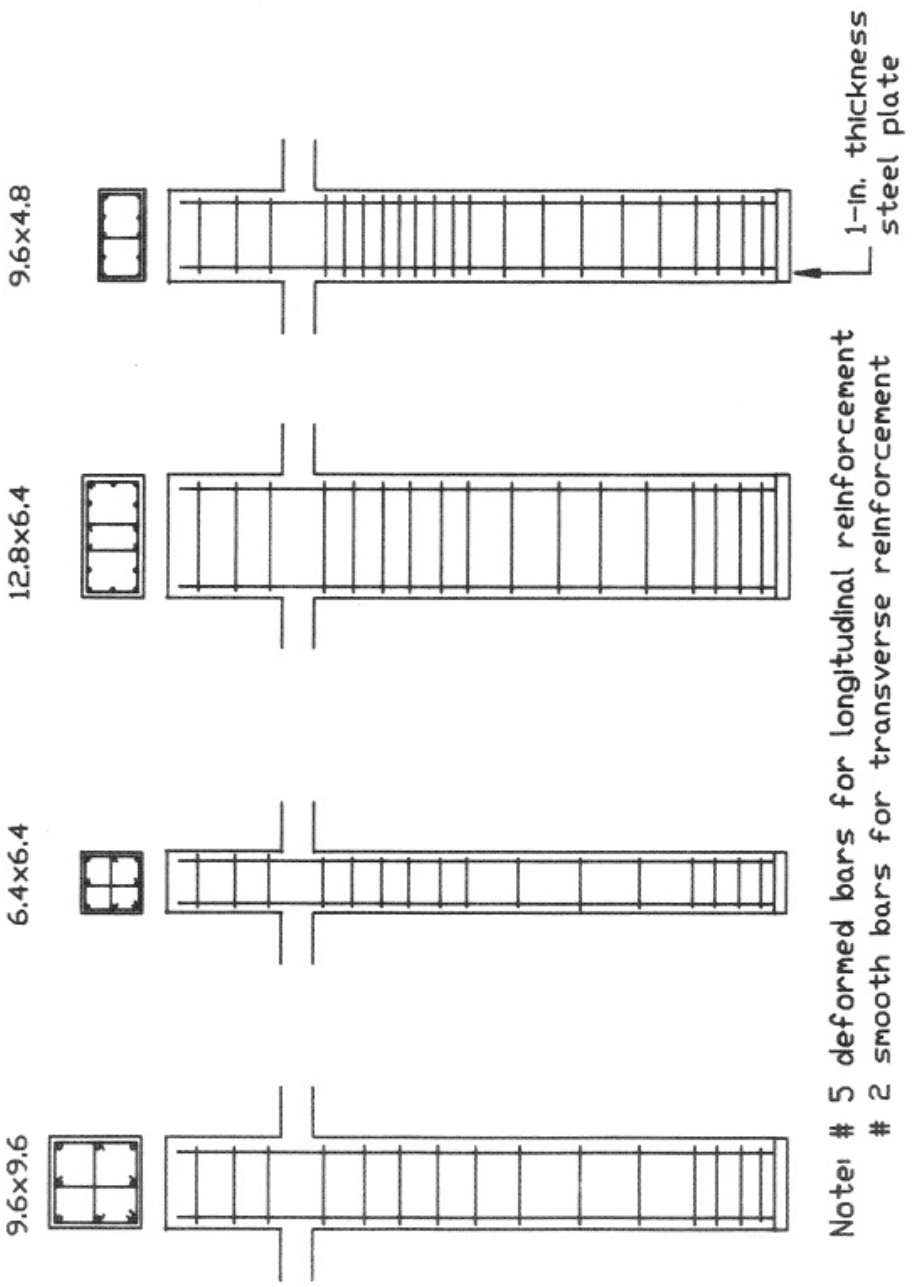

Figure 3.8: Column reinforcements of model slab (units of measure in inches)

3.1.4 Loads applied

The loads acting on the test slab are those for gravity and lateral loads. In paragraphs 3.1.4.1 and 4.2.2 loads applied will be described in details.

3.1.4.1 Gravity load simulation

Apart from the self-weight of the structure, 378 lead weights (each one 45.36 Kg) have been placed over the slab and disposed in two layers (Fig. 3.9), resulting in an equivalent uniform gravity loading of 3.73 KN/m^2. The total vertical uniform load, comprising the self-weight of the model slab, is equal to 5.65 KN/m^2.
The authors decided to roughly approximate the construction loads by a group of students standing on one panel of the model slab; this resulted in an additional gravity load on that panel equal to 2.63 KN/m^2.

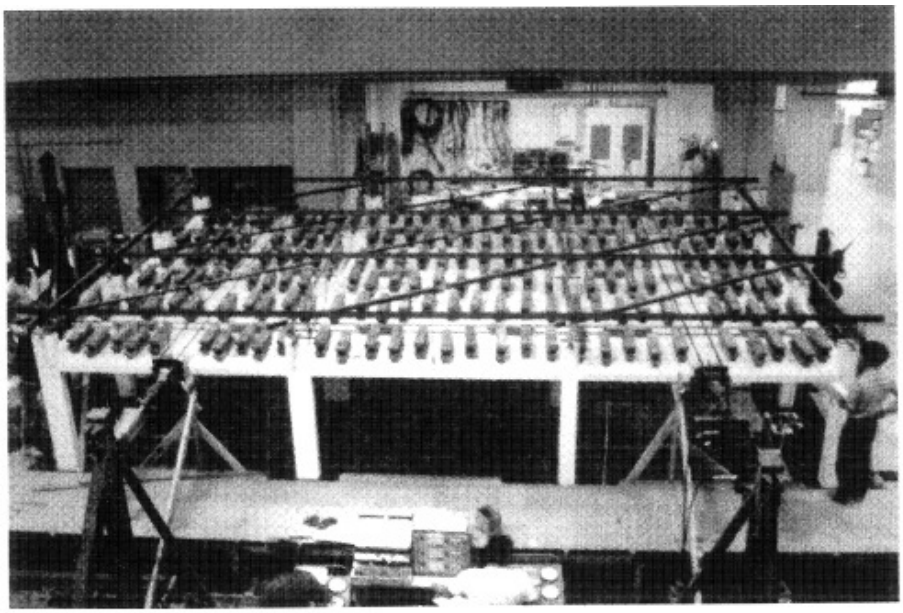

Figure 3.9: Photograph of the test slab

3.1.4.2 Lateral load simulation

Lateral loads were applied to the test slab in two principal directions (North-South and East-West) using four reversible hydraulic actuators supported on reaction frames. A schematic diagram of the lateral loading system used by authors, is shown in Fig. 3.10.

Notice that "pushing" forces from the actuators were applied through cylindrical rods acting against steel plates at the slab mid-depth (Fig. 3.10). "Pulling" forces from the actuators were transferred to the slab through the oversized loading sleeves that were connected around the slab. Being oversized, the sleeves did not restrain in-plane growth of the slab. The lateral loading system results in compressive loading against the edge of the slab regardless of the direction of loading.
Lateral tests have been actuated by displacement control.

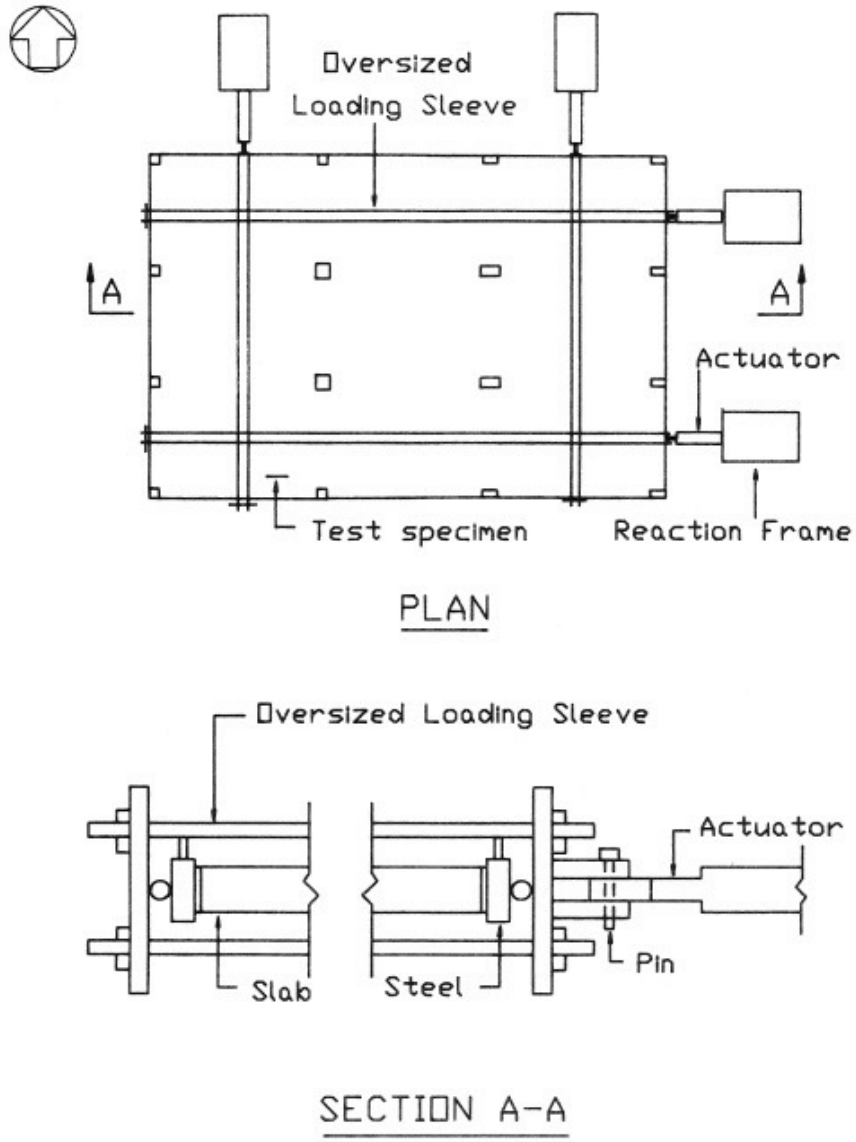

Figure 3.10: Lateral load system

3.1.5 Testing procedures

Testing of the model slab have been included gravity load tests, construction load tests and lateral load test up to failure.
Firstly, the initial structural stiffness of the structure in the two principal directions has been evaluated by tests LAT1 (N-S direction) and LAT2 (E-W direction). These two tests have been performed limiting the maximum interstory drift ratio to 1/800. At this stage of testing, gravity load consisted of slab weight (1.92 KN/m^2) only.
After that, the stiffness at occurred cracking due to service loads (test LEAD), has been measured in the two principal directions by tests LAT3 (N-S direction) and LAT4 (E-W direction), identical in terms of interstory drift to test LAT1 and LAT2.
Then, gravity loads have been increased to approximate the effects of construction loads (test CONSTR); these consisted on an additional gravity load of 2.63 KN/m^2 on the panel on which the group of student stand. The student group moved in clockwise order to test every panel. The sequence of construction loading is described in Fig. 3.11.

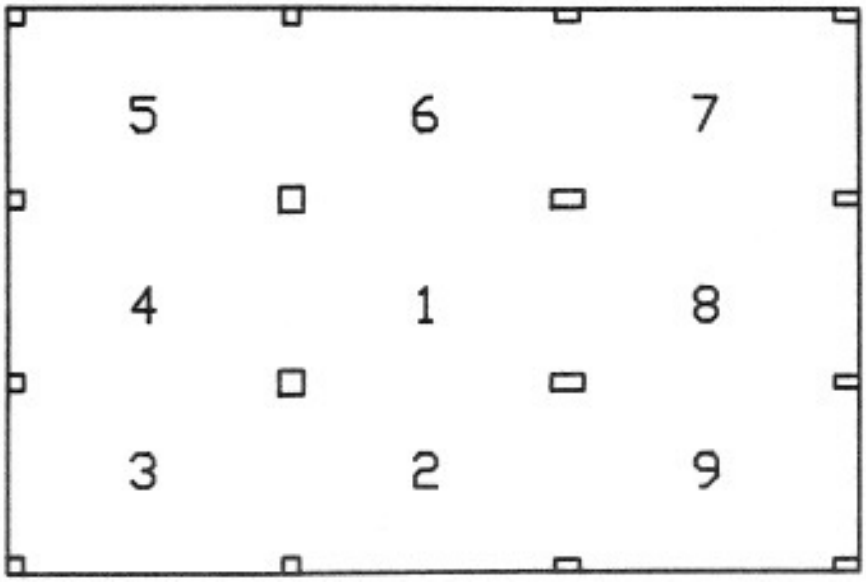

Figure 3.11: Sequence of construction loading

After all panels had been loaded and unoloaded, lateral load tests described above, were repeated for tests NS800 and EW800 in order to evaluate the effect of the gravity load history on the lateral stiffness of flat-plate frames. Finally, a group of tests with increasing lateral drifts, from 1/400 to 1/25, had been carried out in both two principal directions. The nominal lateral displacement history of each direction is shown in Fig. 3.12.

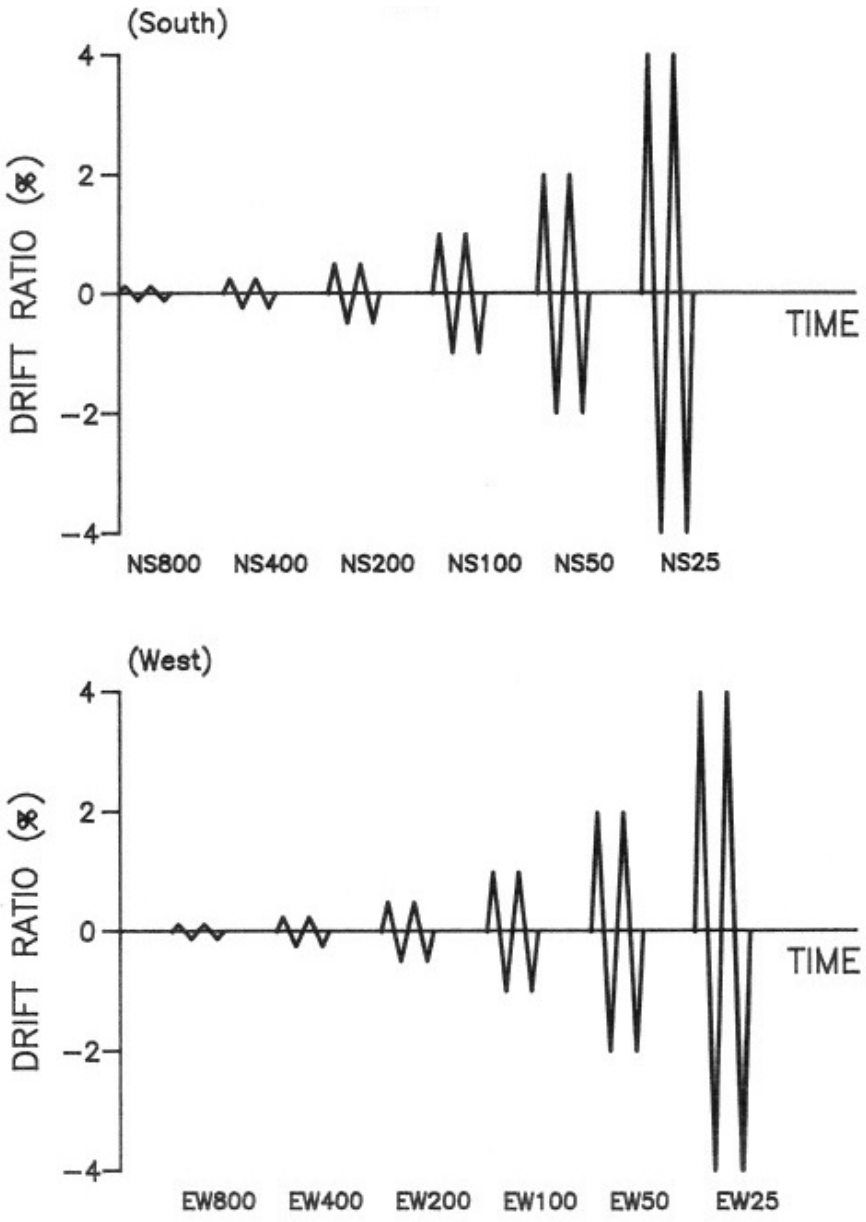

Figure 3.12: Lateral displacement history

The loading procedure was as follow: lateral drift was first imposed in the South direction, then reversed to the North direction, then returned to zero drift. The cycle was repeated once. After these two cycles in North-South direction, the same sequence was immediately applied in East-West direction. The alternating loading in the two orthogonal directions was then repeated at double the lateral drift. The tests were paused after the testing for 4% drift in East-West direction because most of the connections had failed for punching.
Finally, two cycles at 5% drift in both directions were carried out in order to test the residual vertical load carrying capacity after initial punching.
In the following, Table 3.1 containing the chronology and designation of tests referred above, is presented.

Designation	Date	Description
LAT1	11/4/86*	Lateral Stiffness, NS Dir., Drift 1/800, w/o Lead Weight
LAT2	11/4/86	Lateral Stiffness, EW Dir., Drift 1/800, w/o Lead Weight
LEAD	11/5/86	Gravity Load Test, 78 psf from Lead Weight
LAT3	11/6/86	Lateral Stiffness, NS Dir., Drift 1/800, w/ Lead Weight
LAT4	11/6/86	Lateral Stiffness, EW Dir., Drift 1/800, w/ Lead Weight
CONSTR	11/6/86	Construction Load Test, 55 psf Pattern Load
NS800	11/7/86	Lateral Load Test, NS Dir., Drift 1/800
EW800	11/7/86	Lateral Load Test, EW Dir., Drift 1/800
NS400	11/7/86	Lateral Load Test, NS Dir., Drift 1/400
EW400	11/7/86	Lateral Load Test, EW Dir., Drift 1/400
NS200	11/24/86	Lateral Load Test, NS Dir., Drift 1/200
EW200	11/24/86	Lateral Load Test, EW Dir., Drift 1/200
NS100	11/25/86	Lateral Load Test, NS Dir., Drift 1/100
EW100	11/25/86	Lateral Load Test, EW Dir., Drift 1/100
NS50	11/26/86	Lateral Load Test, NS Dir., Drift 1/50
EW50	11/26/86	Lateral Load Test, EW Dir., Drift 1/50
NS25	12/1/86	Lateral Load Test, NS Dir., Drift 1/25
EW25	12/1/86	Lateral Load Test, EW Dir., Drift 1/25
PF20	12/8/86	Post Failure Test, Drift 1/20

* Month/Day/Year

Table 3.1: Chronology of tests on the model slab

Chapter 4

Numerical Results

As previously mentioned, the aim of this master thesis is to apply the grid model[33] described in chapter 2 to a real study case consisting on a typical flat slab structure with more than one bays in both principal directions, loaded both vertically and laterally, in order to test the model for more complicated structure with respect to ones by which the model itself was validated, in particular singular connections (see Coronelli,2010[33]).
The chosen study case, as referred in chapter 3, is an experimental test on a flat-plate structure under vertical and cyclic lateral loads, carried out at University of California at Berkeley[13].
In the present chapter, the description of the setup of the grid model for this particular study case and the comparison between test results and model outputs will be presented.

4.1 Setup of the model

The grid model[33] described in chapter 2 is used in order to create a numerical model representing the test slab[?] considered in chapter 3. The aim is to represent in the best way the experimental non-linear behavior obtained from testing.
In order to design the grid to represent the test slab, indications of the Report 110 CIRIA[35] are used as reference point. Principal concepts of this, about finite element modeling, are discussed in the following.

Member Layout

The optimal grid layout should be obtained by considering the following aspects referring ti Fig. 4.1:

1. the layout should be largely based on the center-lines of the columns. This assumes that each column is represented by a point support and the slab-column connection is represented by members connecting to this point (Fig. 4.1).

2. the stiffness of members connected to the columns should be calculated for a width of slab equal to or a little wider than the column. This ensures that the local nature of the moment transfer is realistically modeled, because this is where the concentration of stress occurs.

3. lines of members should connect center-lines of panels (D1 and D2 in Fig. 4.1).

4. a line of members should be positioned at quarter panel width from the center-lines of columns (C1 and C2 in Fig. 4.1).

5. A line of members should be positioned at about a column width from the column center-lines (B1 and B2 in Fig. 4.1).

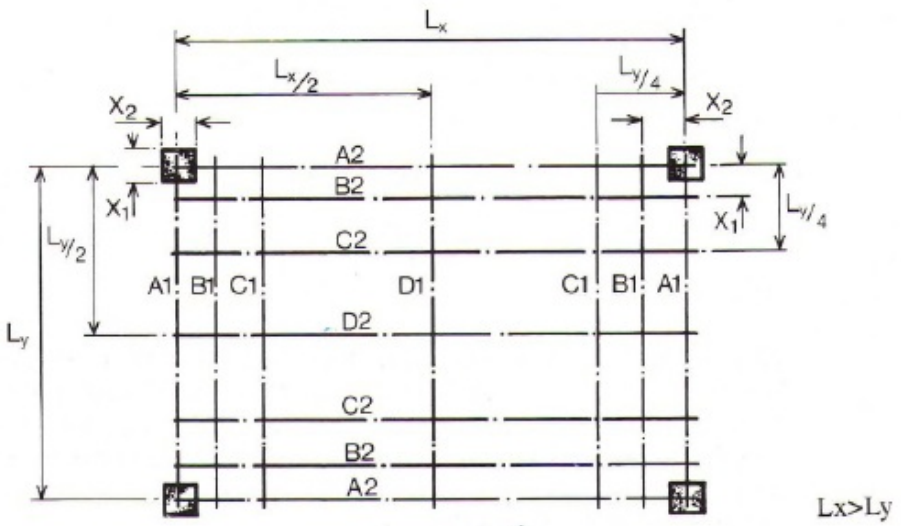

Figure 4.1: Member layout for grillage analysis

Member Width

For simplicity, the choice of the member width may be based on half the distance between the center-line of each member as shown in Fig. 4.2. At the slab edges, the width of the member depends on the position of the column relative to the slab edge. This method apparently requires the member to be eccentrically loaded, but this has not been found to appreciably affect the results.

Loading

Member loading gives more accurate results than nodal loading.

A number of different methods exist to share the load per unit of surface applied on the slab, within the different beam elements of the grid. The most accurate method, especially if distances between column center-lines

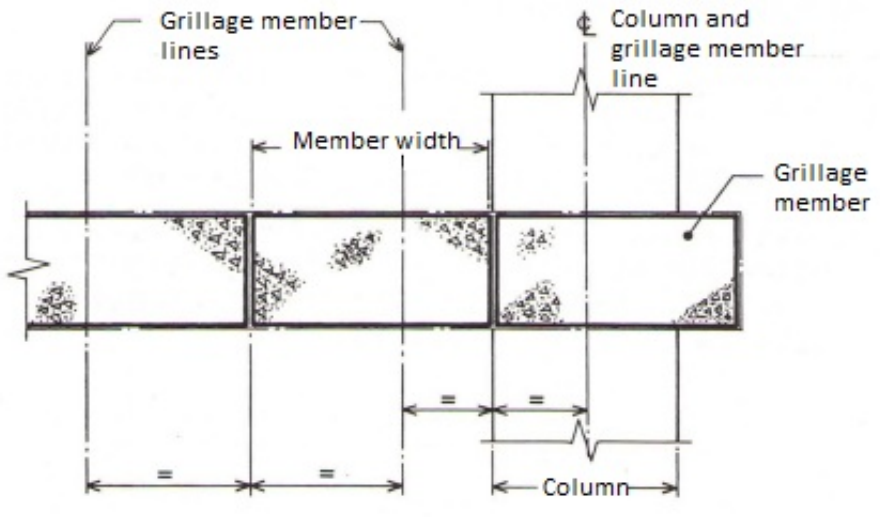

Figure 4.2: Member widths for each grillage element

are strongly different in the two principal directions, consists on considering the load acting on the slab delimited by the rectangle formed by four beams and then share it within them proportionally to their length. If, for example, the ratio between rectangle's side is equal to 3, then 1/4 of the load will be assigned to the short sides and 3/4 of the load to the long sides.

4.1.1 Grid geometry

Observing the layout of the test slab (Fig. 3.2), it is evident that the structure is asymmetrical as regard the column sections; in particular four different column sections have been used by authors of the experimental test [13] and this fact has complicated the design of the geometry of the grid, as it will be explained in the following, and in particular make impossible to use a constant grid spacing $c + d$.
In addiction, notice that the slab geometry is symmetric about the floor centerline along the long direction; thus, the grid geometry will be the same in the southern and northern part of the slab.
Taking into account as reference the guidelines given by Report 110 CIRIA [35], the following choices in modeling the grid, have been done.
It has been decided to use for the beam elements placed on the axes connecting the connections, a width equal to the major $c+d$ of the axes themselves; then, taking into account that the effective depth d is considered constant overall the slab, the leading parameter for the choice is the column side width c. For example, beam elements between connections B3 (9.6 x 9.6 in.) and

C3 (12.8 x 6.4 in.) (Fig. 3.2) have widths equal to $9.6 + d$ except for the element in the critical section of connection C3, which has a width equal to $6.4 + d$. The same width $9.6 + d$ is assigned to beam elements between connections A3 (6.4 x 6.4 in.) and B3 (9.6 x 9.6 in.), except to the element in the critical section of connection A3. To beams elements between connections C3 (12.8 x 6.4 in.) and D3 (9.6 x 4.8 in.), a width equal to $6.4 + d$ has been assigned, except for element included in the critical section of connection D3, to which a width equal to $4.8 + d$ inches is assigned. The same reasoning has been used for all the other elements placed on the axes connecting slab-column connections.
For elements not placed on the axes connecting joints, different widths are used; in particular their width is based on half the distance between the center-line of each member (Fig. 4.2). Thus, the number and the chosen positions of the axes influence the section width of the beam elements.
It has been decided to position the axes adjacent to center-lines passing through joints, at a distance equal to $c/2 + d/2$ from the center of connection with the major side dimension c, then at the border of its critical zone; this has done in order to guarantee that these axes do not intersect the critical zones of the connections lying on the same axis. For example, the adjacent axis positioned at North of connection B3 is placed at a distance equal to $9.6/2 + d/2$ inches from the joint center; the exactly same distance is used for the axis being at South of connection.
These axes are at the aforementioned distance with respect also to center of joints A3, C3 and D3, thus outside of their critical zones. The same reasoning has been applied for all the other axes being adjacent to center-lines linking connections.
For axis placed further with respect to the above mentioned axes, the widths of finite elements lying on these are chosen (in according with prescriptions of Report 110 CIRIA[35]) in order to permit that the ulterior further elements can have a regular width of $c + d$, where c is equal to the minimum side dimension in the two principal directions. In particular, for short slab direction $c_{min} = 4.8in.$ and it is used for width of elements oriented in East-West direction. For long slab direction instead $c_{min} = 6.4in.$ is the minimum column side; anyway, since the structure is asymmetrical in terms of columns sections, it is decided to use $c_{min} = 6.4$ for the west part of the slab and $c_{min} = 9.6$ for the east part. These dimensions are then used for calculating the width of elements oriented in North-South direction. This particular choice has been suggested by the asymmetry of the slab.
The using of the minimum column side for each the three aforementioned cases is based on the hypothesis that a fine grid should improve the accuracy of numerical results; obviously this choice will increase the computational cost of the analysis.
It is possible to observe the difference in grid spacing in Fig. 4.4 where the plan view of flat-slab grid model is presented.

The columns are modeled with two beam element, one below the slab grid with a length of 1.260 m (4.13 ft) and one above with a length of 0.345 m (1.13 ft). The columns stubs below the slab are pinned at their basis whereas the above ones have free ends, as in reality. The column sections are taken with the same dimensions of the ones effectively used in the test slab.
Notice that for all beam and column elements, the moment of inertia is decreased of the 50% of the original value in order to roughly take into account for concrete cracking under service loads.
The portions of columns being in the thickness of the test slab are modeled by four beam elements (*core*), positioned along the four column semi-axes, which are infinitely rigid in the slab plain, thus creating a situation similar to reality, in which the column section cannot inflect in the slab plain (see Chapter 2). In order to obtain this very high rigidity, a big fictitious section of $0.46x0.46m$ ($1.5x1.5ft$) is assigned to all the core elements. Notice that all these elements have a length equal to $d/2$, where d varies according to which column they belong to.
The four central beam elements of each connection are linked to the core elements and thus they could have very short length (Fig. 4.4).

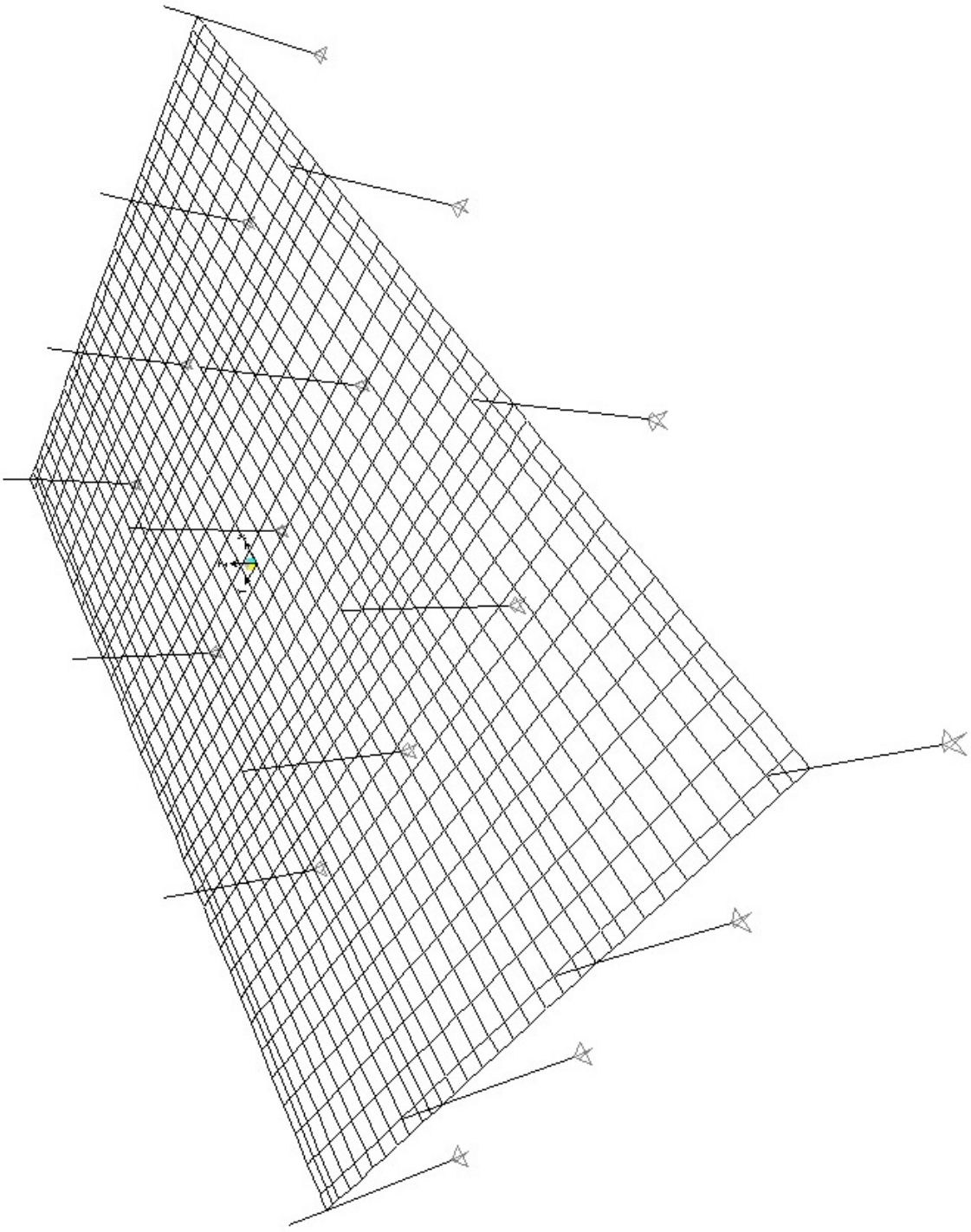

Figure 4.3: 3D view of the grid model

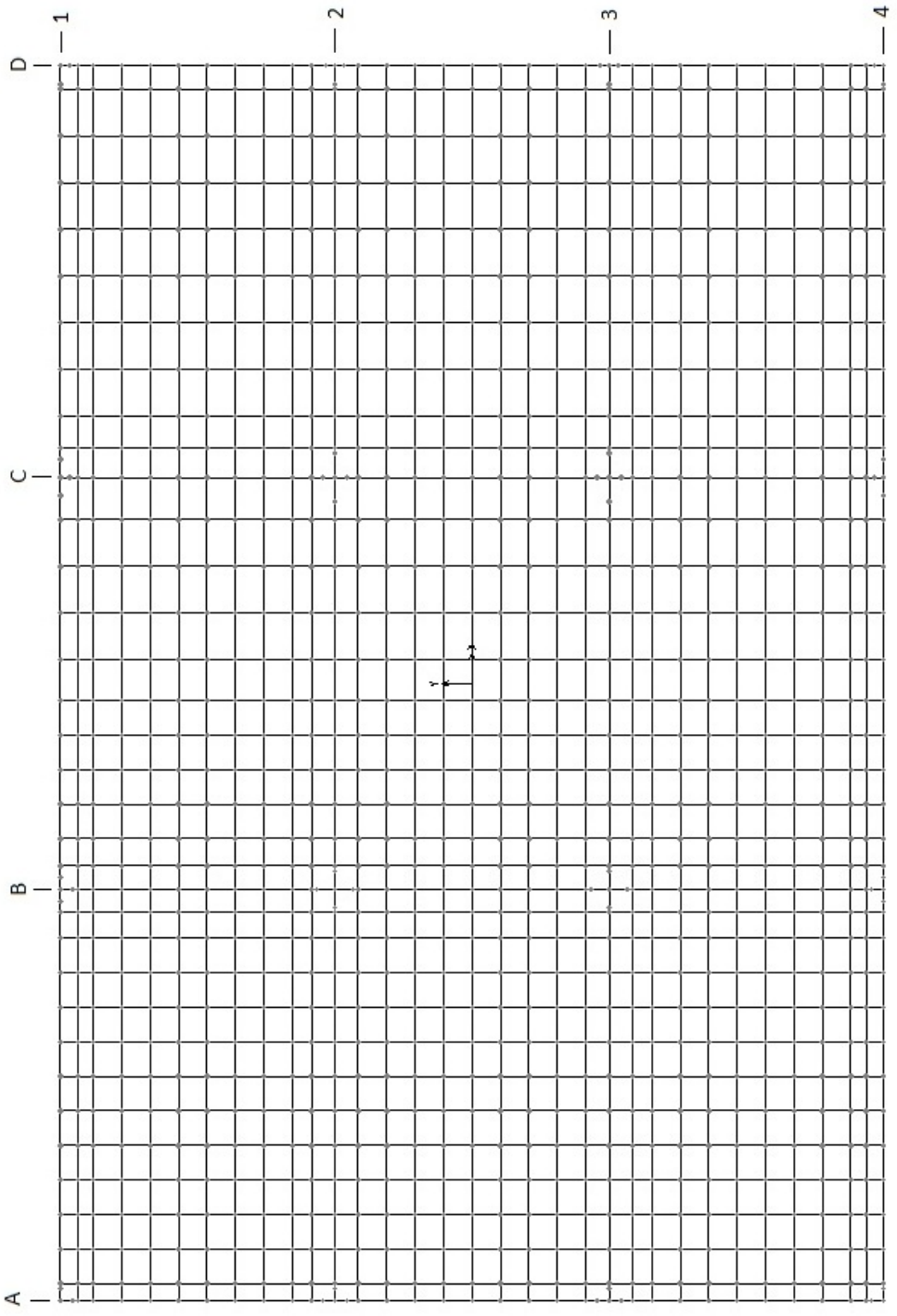

Figure 4.4: Plan view of the grid model

4.1.2 Loads applied to the grid model

The real structure is subjected to gravity and lateral loads as explained in sections 3.1.4.1 and 4.2.2.
As regard gravity loads, notice that it has been decided to not permit to the software[34] to automatically assign the self-weight to each single finite element according to its volume and specific weight, but it has been preferred to carry out from the total uniformly distributed gravity load per unit of surface being on the structure (comprising self-weight), the total load per unit length acting in the two principal directions.
In order to do this, it has been necessary firstly to obtain the mean width of the beam elements lying on the axes in the two principal directions, by dividing the slab dimensions (5.65 m for short direction and 8.43 m for the long one) by their respective number of axes (33 and 35, respectively). By this way the mean width of the elements oriented in East-West direction is equal to 0.171 m, whereas for the others oriented in the North-South direction is equal to 0.241 m.
Finally, the total load per unit length is obtained by multiplying half of the total load per unit surface for the mean width of the beam elements. The loads obtained are 0.499 KN/m and 0.681 KN/m for elements in the long and short direction, respectively.
Notice finally that these loads are not applied on the core's elements. In figure 4.5 the grid model with the uniformly distributed gravity loads is presented.
As regard lateral loads, it is tried to apply them in the same positions of the experimental test, compatibly to the refinement of the grid. The loads applied are unitary; their magnitude in fact is not fundamental since a displacement control analysis will be carried out on the model.
In Figures 4.6, 4.8, 4.7 and 4.9 lateral loads applied to the model are presented for positive and negative verse for both the two principal directions of loading.

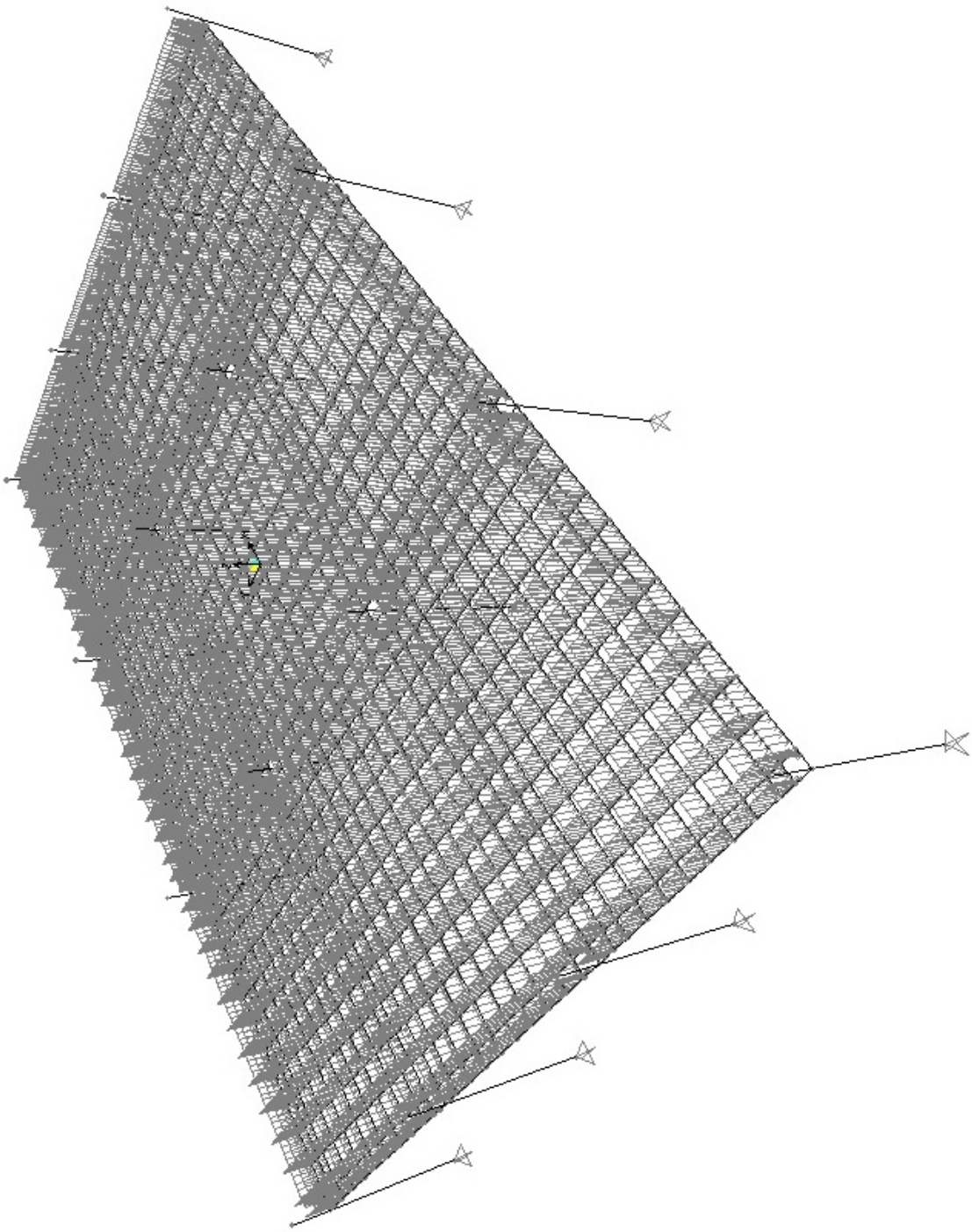

Figure 4.5: Gravity load applied on the grid model

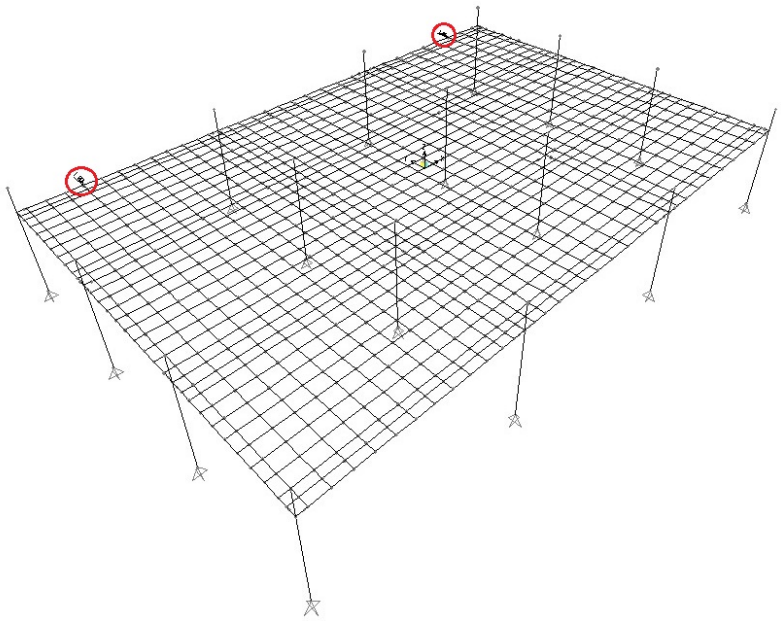

Figure 4.6: Lateral loads (red circle) applied to grid model in the positive North-South direction

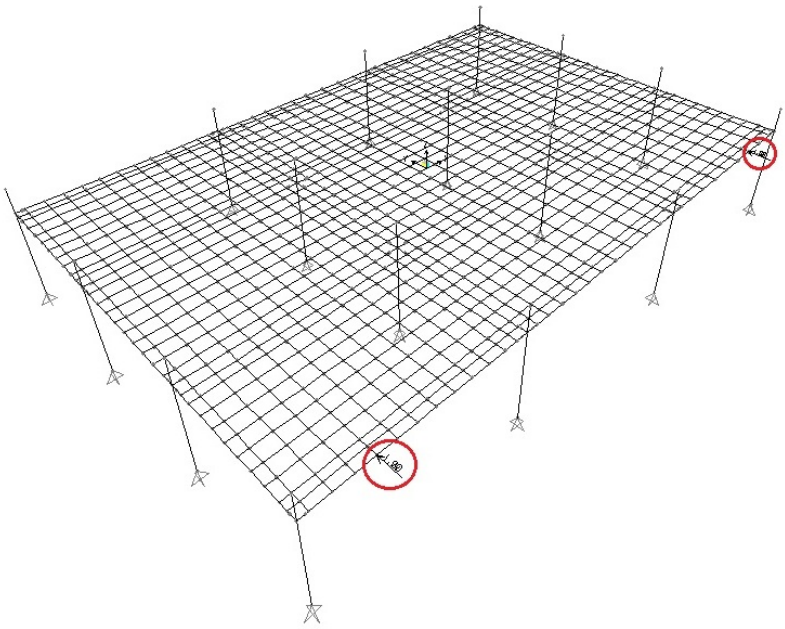

Figure 4.7: Lateral loads (red circle) applied to grid model in the negative North-South direction

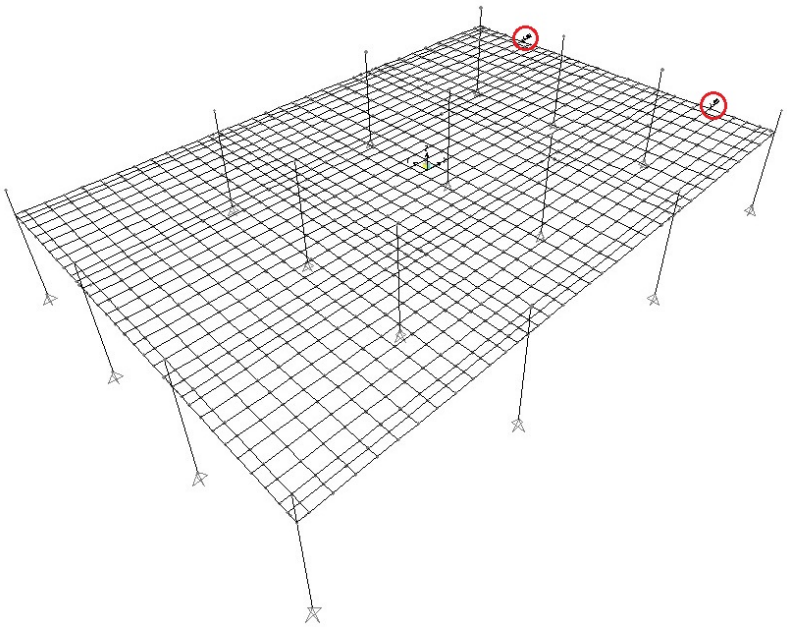

Figure 4.8: Lateral loads (red circle) applied to grid model in the positive East-West direction

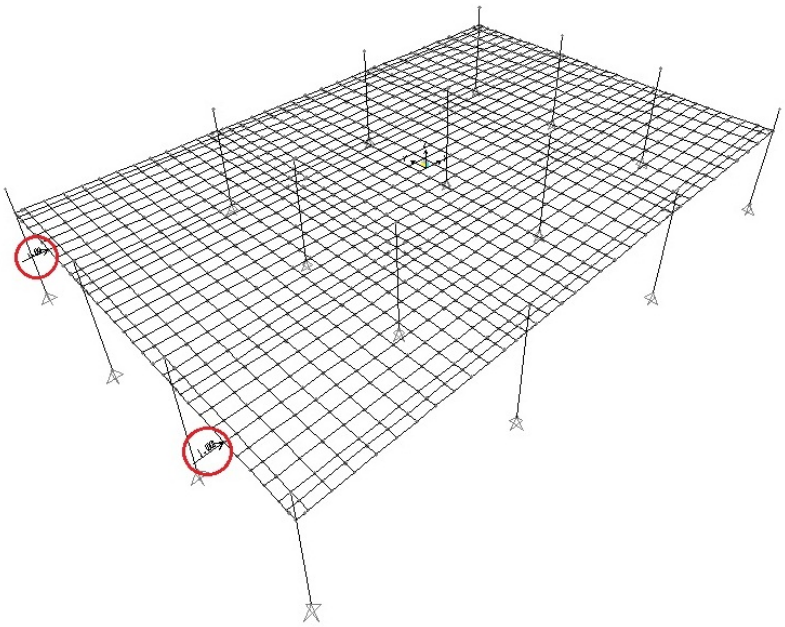

Figure 4.9: Lateral loads (red circle) applied to grid model in the negative East-West direction

4.1.3 Plastic hinges

Plastic hinges are points of the elastic frame elements in which the non-linear properties of the elements themselves are lumped. Plastic hinges are not assigned to all the beam elements of the grid model, but to ones which are the most significant because of their position in the grid; in particular they are assigned to frame elements lying on the center-lines connecting joints (except for elements of cores) and on the immediately adjacent axes. This choice is done in order to make the model more computationally light both in terms of time consumed for the definition of hinges and for the numerical analysis.
Despite this fact, definition of hinges properties results very much time consuming and this is due to the particular geometry and layout of reinforcement of the test slab. Let's explain better this fact.
Three types of hinges are defined, according to the grid model[33] explained in chapter 2: flexural, shear and torsional. The properties of all these depend on the geometry of the beams section, on concrete properties and on longitudinal bottom and top reinforcement (no shear reinforcement are present in the test slab). According to the consideration about the design of the grid geometry in section 4.1.1 and on the reinforcement arrangement in both the principal directions which is not symmetrical about the floor centerline in the long direction (Fig. 3.3, 3.4, 3.5 and3.6), many different plastic hinges have to be defined since a great number of frame elements have different geometrical and reinforcement characteristics.
In the following, considerations about the different types of plastic hinges are done.
The flexural plastic hinges properties are calculated as referred in section 2.2.1 using a sectional model[12]. Normalized diagrams, ultimate capacity ($M_{pl,u}$) and associated ultimate curvature ($\phi_{pl,u}$) are furnished as input to the model. The software[34] also require the plastic hinge length, which is defined equal to d[33].
Notice that flexural plastic hinges will be applied to all frame elements specified above; in particular high bending moments will develope at connections and at the midspan of center-lines connecting joints. Fig. 4.10 shows a typical normalized diagram of a flexural plastic hinge.
For the shear plastic hinges properties definition, a change is done with respect to the grid model[33] regarding the normalized diagram shear force-displacement (Fig. 4.11) used as input in the model. According to section 2.2.3, a tri-linear relation should be carried out from the response given by the sectional model[12]; anyway this procedure accounts for the yielding of shear reinforcement (see section 2.2.3) which, in this particular case, is not present. Thus, the normalized diagram is constructed taking into account values of $V_{pl}/V_{pl,u}$ equal to 0.2 - 0.8 - 1 - 0.8. The corresponding values of normalized shear displacement are, respectively: 0 - $0.8V_{pl,u}/G_f$ - 1 - 1.2;

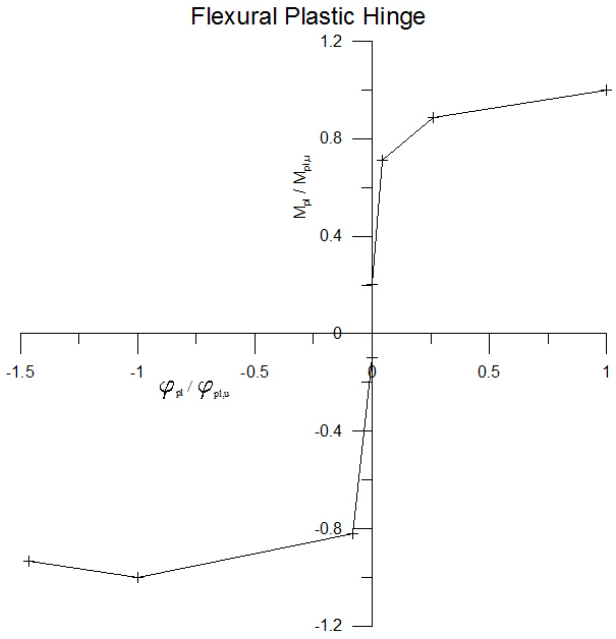

Figure 4.10: Normalized diagram of a flexural plastic hinge

in particular G_f is the cracked shear modulus (30% of the shear modulus) times the shear area of element section. These normalized diagram (Fig. 4.11) with the associated shear capacity ($V_{pl,u}[N]$) and the corresponding ultimate shear displacement ($\gamma_{pl,u}(1.5d)$), computed as prescribed by grid model[33] are used as input to the model. Notice that shear plastic hinge behavior is symmetrical for positive and negative shear.
An important remark is that shear plastic hinges have been applied only to grid elements inside the critical zone and on its border. This choice is done because shear force, acting outside the critical perimeter, are unimportant with respect to ones inside it and this means that the external elements should not show a non-linear response.
Also in the case of torsional plastic hinges properties definition, a change is done with respect to the grid model[33] regarding the definition of the ultimate twist angle. According to it, values of ultimate twist angle ψ_{u0} measured experimentally[11] should be used, since no transverse steel is present in the test slab; anyway it is preferred to use the model for reinforced concrete beams with transverse steel[10], using a fictitious shear reinforcement with little section area ($A_t = 13mm^2$) and low density ($s = 110mm$). This interpretation of the model is justified by the mechanical reason that on a beam element which is actually a part of a flat slab, a lateral confinement is applied; in addiction from a series of experimental tests[11] no substantial difference is observed in the torsional behavior of slab reinforced and not-reinforced against

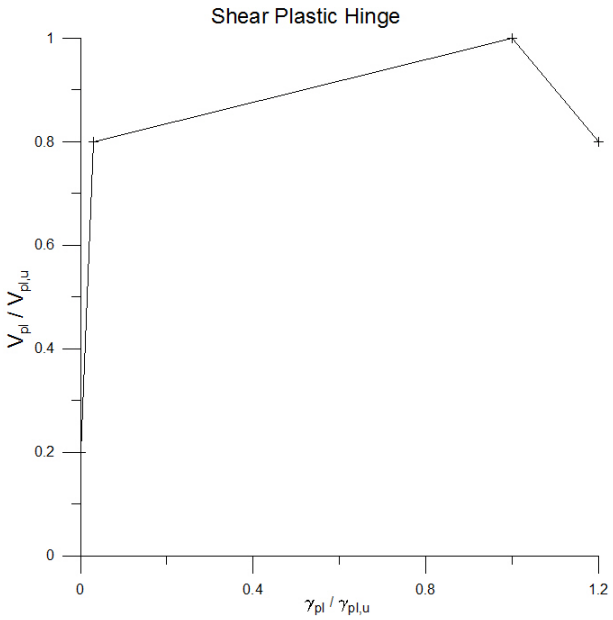

Figure 4.11: Normalized diagram of a shear plastic hinge

shear.
About reduced torsional capacity M_{tu} due to interaction effect, the Park and Choi model[40] is used, as proposed in the grid model[33]. The value of bending moment and shear acting in the slab due to gravity loads and used to reduce the value of the torsional capacity without interaction effect (M_{tu0}), are obtained by an elastic analysis of the slab grid model.
As input for the model, the normalized diagram (Fig. 4.12), the torsional capacity and the corresponding twist angle per unit length are used. In addiction, the plastic hinge length $1.5d$ is specified.
Notice that torsional plastic hinges computed in the aforementioned way are put in frame elements of the critical section and in their adjacent ones, since these parts of the structure are the most torsionally solicited. Actually, according to the grid model used[33], for grid elements that are not at the interface with the columns, elastic-perfectly plastic behavior is defined, with capacity calculated[41] with strength $0.58\sqrt{f'_c}$, as specified in chapter 2. Despite this fact, it has been decided to extend the aforementioned torsional model also to members directly outside the critical zone, in order to improve the torsional efficiency of the connections. For all the other beam elements, a non-linear torsionally perfectly plastic behavior is assigned.
Notice finally that for torsional plastic hinges of the edge and border connection, the value of ψ_u carried out from the model for R/C beams with transverse steel[10] is not used, but the half of the value is considered.

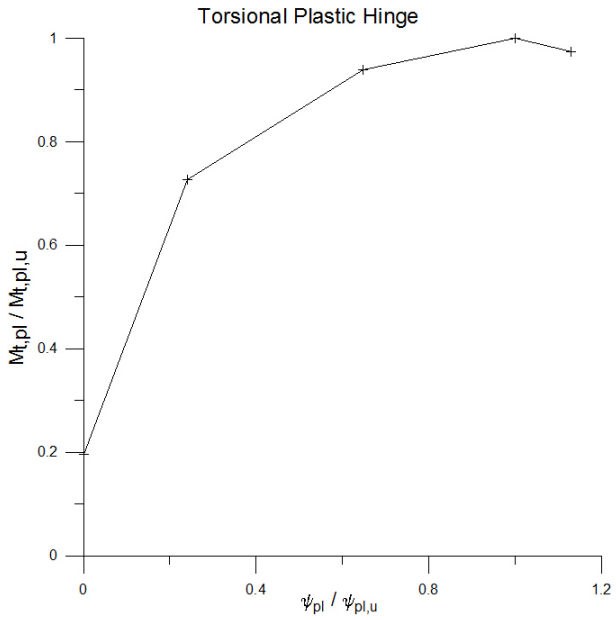

Figure 4.12: Normalized diagram of a torsional plastic hinge

4.1.4 Analysis

The procedure followed for the analysis of the model slab is the following: a load controlled non-linear analysis is firstly performed under gravity loads specified in section 4.1.2; then, starting from these results, non-linear static analyses with displacement control in both the two principal directions are carried out for horizontal loads (section 4.1.2). Notice that positive and negative verse of loading are also considered in the analysis.
The pushover analyses are performed by setting into the software[34] the node to which imposing the displacement and its desired maximum value. The node chosen is positioned in the central part of the test slab and the displacement assigned is 0.063 m (0.206 ft) corresponding to 5% drift because it's of interest to lead the structure to failure.
Notice that the pushover analyses are performed under monotonically increasing loads, thus different to the cyclic loadings applied on the test slab considered[13].
The output of the analyses are pushover curves (total lateral force applied to the structure versus its lateral displacement), values of internal actions (bending moment, shear, torsion) acting in the grid elements at each step of the analysis and the visualization of the deformed shape of the structure with in evidence the state of plastic hinges at each step. The latter permits

to immediately and quite clearly understand the failure mode of the model and its damage sequence.
The software shows the plastic hinges state according to different colors: fuchsia is the color for plastic hinge which are beyond the first cracking, yellow for these which are beyond the yielding (or the 80% of the capacity) and finally orange for these which have reached the capacity.

4.2 Comparison between test results and model outputs

The type of analyses carried out on the model are non-linear gravity load analysis and non-linear static (*pushover*) analyses, as referred in section 4.1.4. These are certainly different with respect to the cyclic and biaxial nature of the test applied on the real structure (see section 3.1.5); thus, is necessary to interpret from this perspective all the model results and their comparisons with experimental data.

4.2.1 Punching shear failure of connections of the test slab

The flat-slab structure[13] considered was tested by means of vertical and cyclic lateral loads in two orthogonal directions, as described in section 3.1.5. Before describing and comparing in details the experimental and model output data, it's interesting to have a general view of the damage and connections behavior at failure of the structural system.
As referred by authors of the experimental campaign[13], punching shear failure of connections due to lateral loads did not occur until test EW25; this means that the structure was able to resist cyclic lateral load test at 4% maximum drift for direction North-South (test NS25) without approaching punching shear resistance at connections. In the following, lateral moment-rotation curves of each joint for test EW25 are presented in Fig. 4.14.
In this figure, as specified also in its legend, three different moment scales, namely 250/100/70 in kip-in (corresponding to 28.25/11.30/7.91 KNm), are used, respectively, for interior, edge and corner connections. Small circle in a quadrant of a single graph marks the occurrence of the punching shear failure in that quadrant, which is defined as sudden loss of flexural resistance. These failures are clearly understandable by observing the paths of cycles of each single connection; in joints in which punching occurred an important loss of capacity, in terms of bending moment, between the first cycle and the second one at the same maximum drift, is observed. This particular behavior is also more evident if Fig. 4.14 is compared with Fig. 4.13, which represents the path of cycles at 1% maximum drift and in which sudden loss of bending moment capacity was not surveyed in each connection. The differences in cycles represented in Fig. 4.14 and 4.13 are absolutely clear.
The phenomenon of punching of several connections is clearly understandable also by observing the overall behavior of the structure, represented by the experimental lateral load-deflection curves reported by authors[13]. In Fig. 4.15 the entire response history to failure (4% drift) are shown; the punching failure of connections is clear for direction East-West, anyway also curves for North-South direction show a quite visible degradation of the strength.
As it is well known, shear failure is a sudden phenomenon, thus also punching failure is sudden (see Fig. 4.14) and, as referred by authors of the experi-

mental study, this occurs for several connections within a short time period. It is noted that all the interior connections (B2, C2, B3, C3) failed when the slab displaced to both the West and the East directions. Similarly, the edge connections with bending parallel to the direction of loading (B1, C1, B4, C4) failed in two directions, except the square connection B1 which survived in the East direction. The rectangular edge connections with bending perpendicular to the edge (D2, D3) failed in two directions, whereas the square connections (A2, A3) survived except A2 failed in the West direction. Notice finally that all the corner connections (A1, D1, A4, D4) survived in test EW25 except the rectangular connection D1, which failed in the West direction.

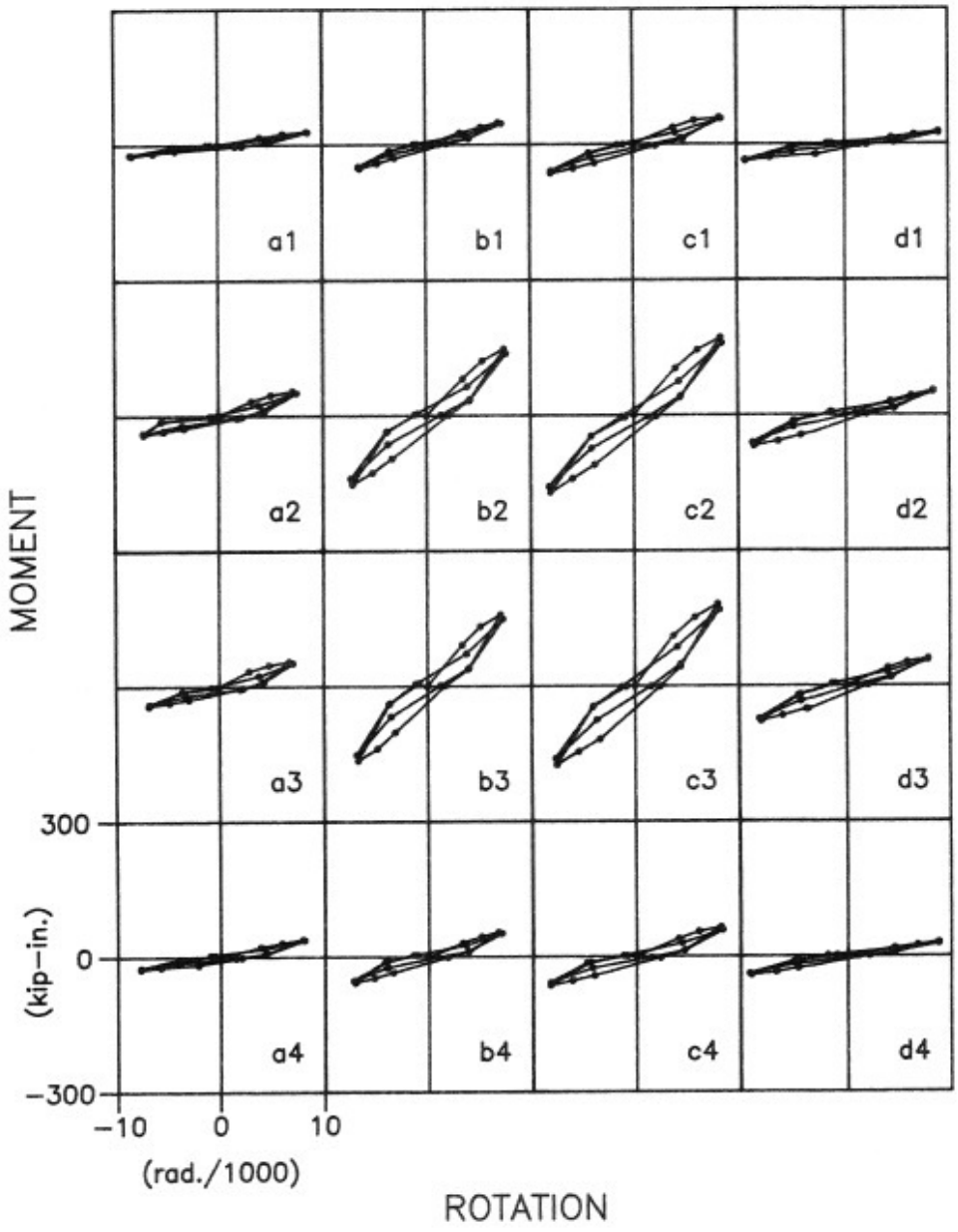

Figure 4.13: Moment-Rotation curves of connections for test EW100 for both East and West direction of the loading

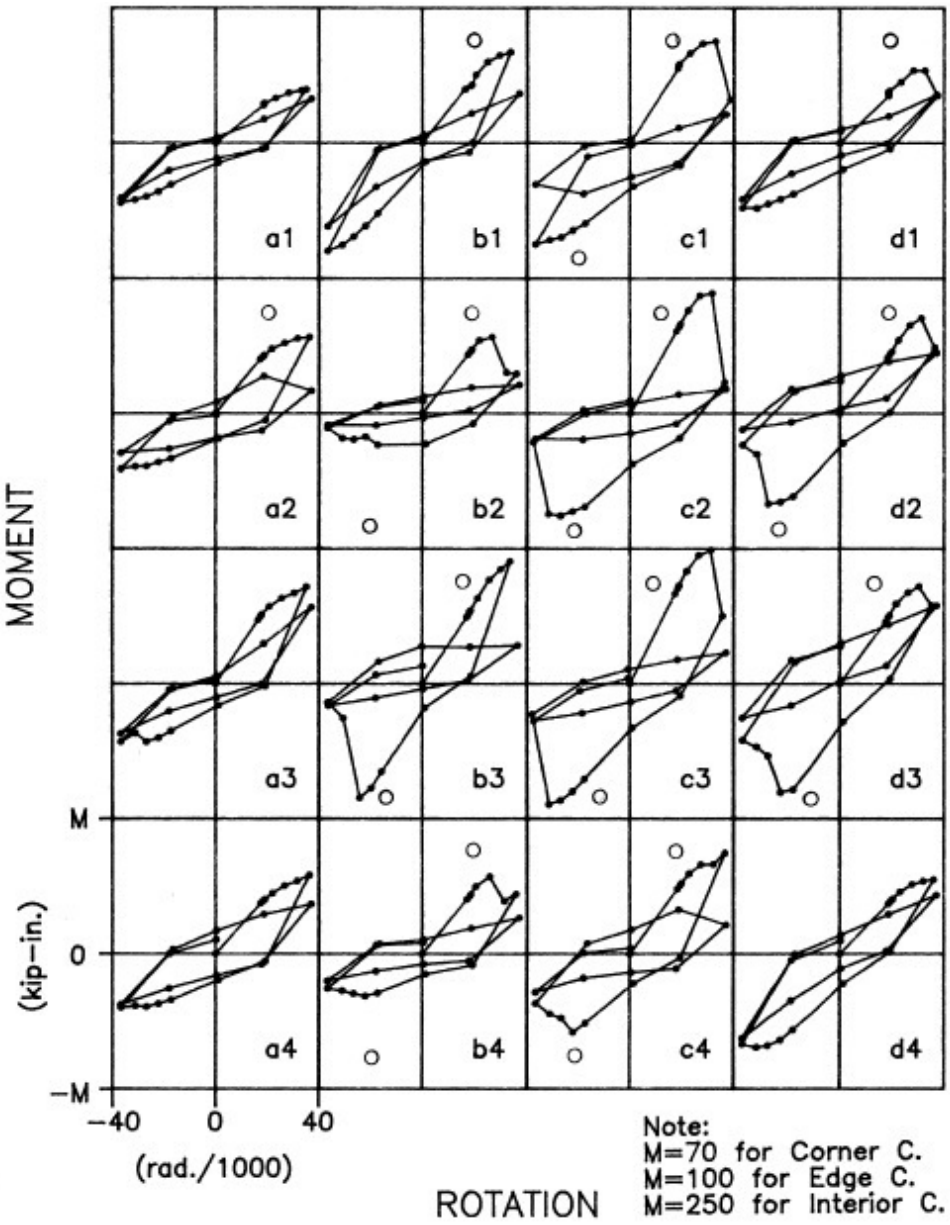

Figure 4.14: Moment-Rotation curves of connections for test EW25 for both East and West direction of the loading

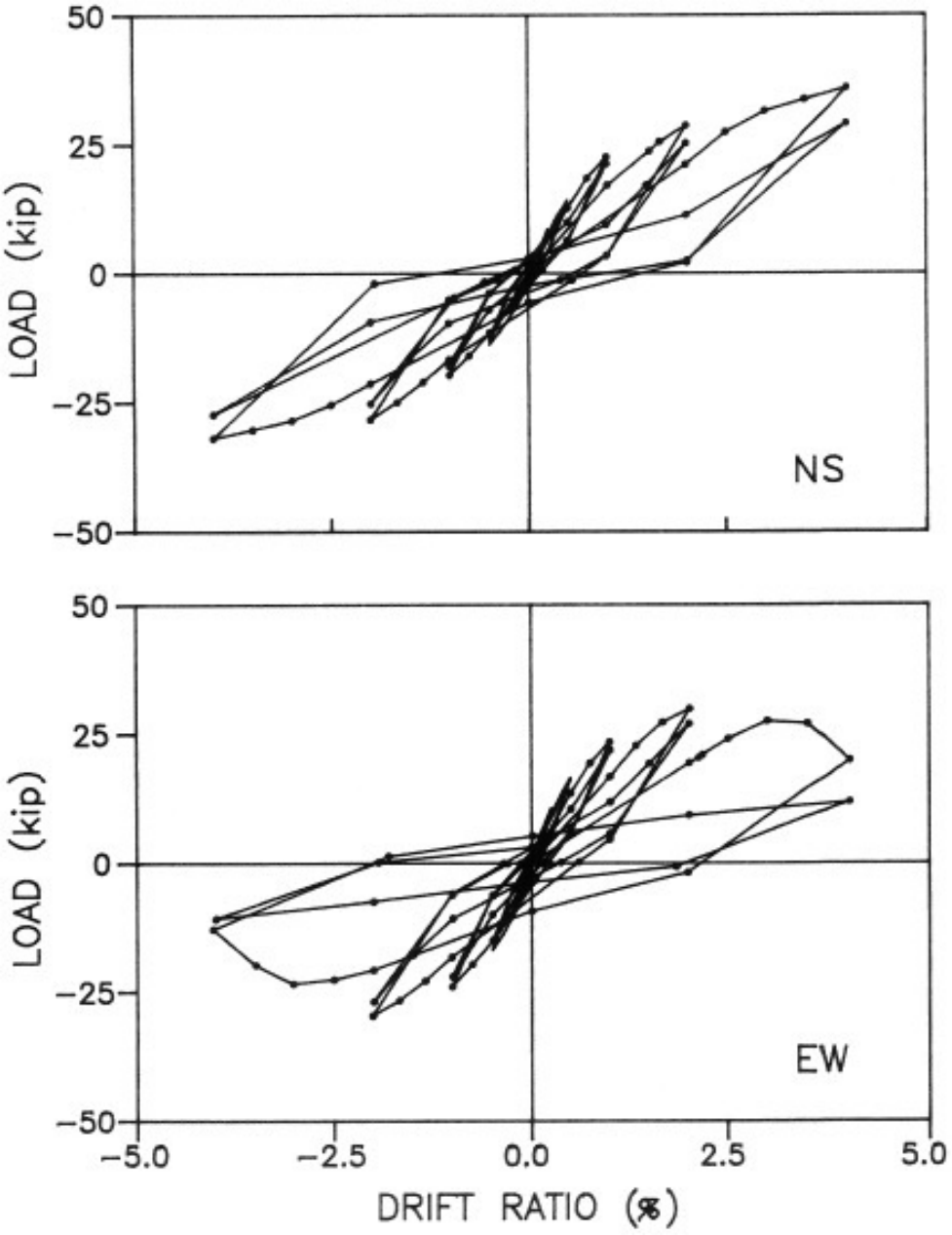

Figure 4.15: Lateral load-deflection response to failure

4.2.2 Lateral load versus deflection relationship

The report describing the experimental study considered [13], provides data about the total lateral load applied to the structure and deflection, in terms of interstory drift ratio, which is defined as the lateral deflection of the slab mid-depth divided by the column clear height of 1.22 m (4 ft). Notice that lateral drifts and loads on the test slab have been considered positive by authors in the South and West direction (Fig. 3.10).
Authors furnish data in tabular form about only the peak values (one positive and one negative) of the lateral loads and the corresponding deflections, in which gravity load effects are excluded, for each test from LAT1 and LAT2 to NS25 and EW25; lateral load-deflection curves for tests LAT1, LAT2, LAT3, LAT4, NS200, EW200, NS25 and EW25 are provided, in which it is possible to observe each single cycle. In this thesis only load-deflection response to failure are reported in Fig. 4.15.
Peak values and corresponding deflections are well suited to be compared with pushover curves carried out from the non-linear static analyses of the grid model for the two orthogonal directions of loading; in Figures 4.20 and 4.21, graphs presenting the model pushover curves and the experimental lateral load-deflection (drift) curve will be presented for both the positive and negative verses of the two orthogonal directions (N-S and E-W). Representation of the slab deformed shape and the plastic hinges activated in the frame elements are also shown in Fig. 4.22 and 4.23 only for the positive verse of loading for both two principal directions. Notice that the legend of hinges colors is specified in section 4.1.4.
The first important remark which is possible to do observing figures 4.20 and 4.21 is that the experimental responses are different in the two orthogonal directions, both in terms of resistance and drift. This particularity could be detected not only on the global behavior of the structure (lateral load-drift curves) but also in the moment-rotation envelopes of each joint, as it will be explained in section 4.2.3. This difference in all probability could be impute to the degradation of the test slab due to the particular biaxial cyclic way of loading, explained in section 3.1.5, which loads and thus deteriorates the structure firstly in North-South direction and secondly in East-West direction. This scheme has been followed by authors during the entire test.
Since the performance of slab-column structures depends primarily on the characteristics and conditions of slab-column connections, it is possible to explain the above cited aspect of the response due to biaxial loading as follows [5] (Fig. 4.16). Under uniaxial loading, resistance is attributable to torsion on faces AB and CD and shear and moment on faces BC and DA. If an uniaxially loaded connection is loaded subsequently in the transverse direction, faces AB and CD (which had previously been loaded in torsion) begin to develop torsion. The interactions between flexure, shear and torsion [41] are such that the net connection resistance in any given direction is

less under biaxial loading than under uniaxial loading. Similarly, more rapid degradation of the concrete occurs under biaxial loading.

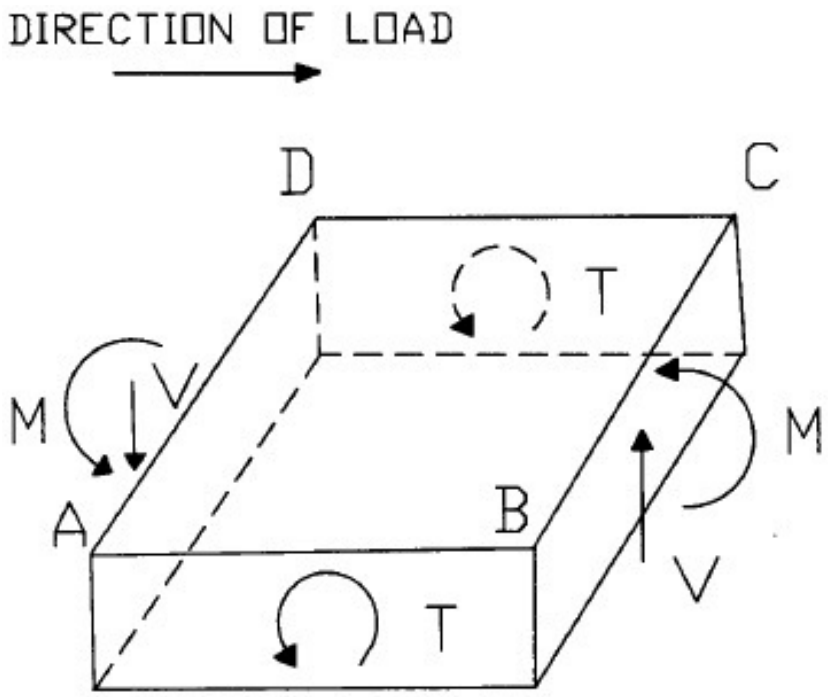

Figure 4.16: Forces on connection under uniaxial loading[5]

As regard the comparison between model and experimental curves, it is possible to notice firstly that in both the two principals directions, an underestimation of the initial stiffness of the whole structural system is detectable; this is not meaningful in the evaluation of the validity of the grid model since its initial rigidity is strongly influenced by the choice of the cracked moment of inertia of columns, which has been assumed as the 50% of the uncracked one (see Section 4.1.1). This choice will influence the structural response until non-linear effects in the slab will become predominant due to the increasing of the maximum lateral drift reached.
What is instead important to underline is the overall behavior of curves. The pushover curve in North-South direction (Fig. 4.20) appears very similar to the experimental one in terms of path and maximum lateral load whereas the maximum drift reached is higher for the second (3.3% drift for model and 4% drift for experimental test). In East-West direction (Fig. 4.21) instead, the comparison shows comparable drift (for both 3% drift) in the positive direction but also an high overestimation of the lateral loads applied (both for positive and negative direction). In negative direction numerical drift is

much higher than the experimental one, but it's worth to remember that EW25 test has been stopped because of punching of several connections has occurred. It's also worth to notice that numerical drift reaches 4.4% value in negative direction, which is much higher than 3% drift reached in the positive one. Probably, the cause is a combination of the development of the shear and torsional strength, which is influenced by the rectangularity of the columns of the east edges which plays a fundamental role in this phenomenon, as explained in the following: columns A2 and A3 (west edge) have squared sections whereas columns D2 and D3 (east edge) have rectangular sections with an aspect ratio of 2:1 and in particular their major sides are on East-West direction; this means that the torsional capacity of the beam elements lying on the slab edge and being inside the critical zone of connections D2 and D3 is much higher than the ones of edge elements in the critical zone of connection A2 and A3, since torsional capacity (Park and Choi model[40]) depends strongly on the sectional geometrical characteristics and thus on element width. Parallel to this phenomenon, it's necessary to take into account the development of punching resistance in connections which is different according to the direction of loading and thus to deformed shape of the slab. It is known in fact, that punching is likely to occur where, at the connection, negative bending moment acts, i.e. the tensioned fibers are on the top surface (as in the right part of Fig. 4.17), instead of the case of positive bending (tensioned fiber on the bottom surface as in the left part of Fig. 4.17).
When the structure is loaded toward West (positive verse), in connections A2 and A4 the acting shear force approaches before to the 80% of punching capacity with respect to what happens in connections D2 and D3 (because of the deformed shape), although the capacities of the first are higher than the ones of the second (Fig. 4.18). This induce connections A2 and A3 to redistribute actions on the other hinges, while the plastic hinges of connections D2 and D3 are still at the first stage of non-linearity.
Exactly the same phenomenon happens on connection D2 and D3 when the structure is loaded toward East (negative verse); in particular these fail for punching between 3.5% - 3.9% drift, whereas connections A2 and A3 have just overcome the first stage of non-linearity (Fig. 4.19).
The fundamental difference in the two loading case is that in the second, when shear plastic hinges of joints D2 and D3 fail for punching, these connections have also a very good torsional resistance which is able to carry the new increments of lateral loads; on the contrary in the first loading case this does not happens since torsional resistance of joints A2 and A3 are quite low, the redistribution process cannot take place and thus the analysis stops. This is confirmed by the fact that torsional hinges approximately reach their torsional capacity (Fig. 4.18(a)).
An ulterior confirm of this explanation is given by the small softening branch in the negative part of the numerical curve, after the reaching of the maxi-

mum lateral load (Fig. 4.21).
Notice that all this speech is not valid for North-South direction of loading, since the structure is symmetrical about the center-line in the long direction in terms of columns geometry. In this case what is different are layout and ratio of reinforcement; anyway this seems to not influence both the experimental and numerical response of the whole structure.

Returning to the differences in lateral loads applied in in East-West di-

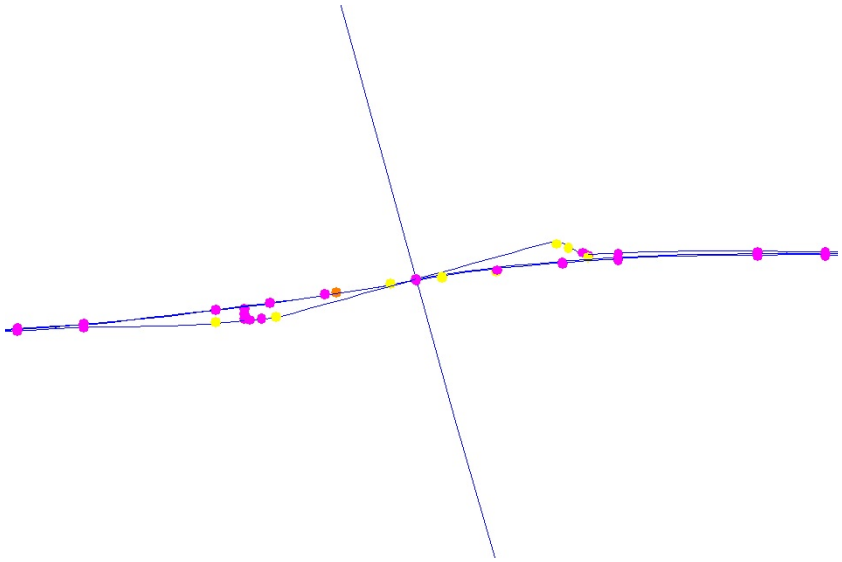

Figure 4.17: Deformation of an internal connection subjected to unbalanced moment

rection, it is certainly due to the already mentioned degradation of the test slab thanks to biaxial cyclic loads applied in sequence (see section 3.1.5), deterioration that a non-linear static analysis cannot reproduce since consists on the application on a structure of a monotonic lateral load with increasing magnitude. The gap between model and experimental curves starts approximately from 1% drift (4.21), that is the drift at which significant yield of connections was detected in the experimental tests. Thus, 1% drift could be interpret as the limit drift from which the biaxial loading start to deteriorate heavily connections and then the whole structure. Thus, at this stage of the comparison of results is already evident that the importance of the biaxial and cyclic nature of loading strongly influences experimental results, as it will be strongly confirmed in the behavior of connections presented in section 4.2.3, but this phenomenon cannot be caught by the non-linear static analysis.
In Fig. 4.20 it is possible to notice that the numerical analysis performs a lot of very small steps at nearly 2% drift, both for positive and negative

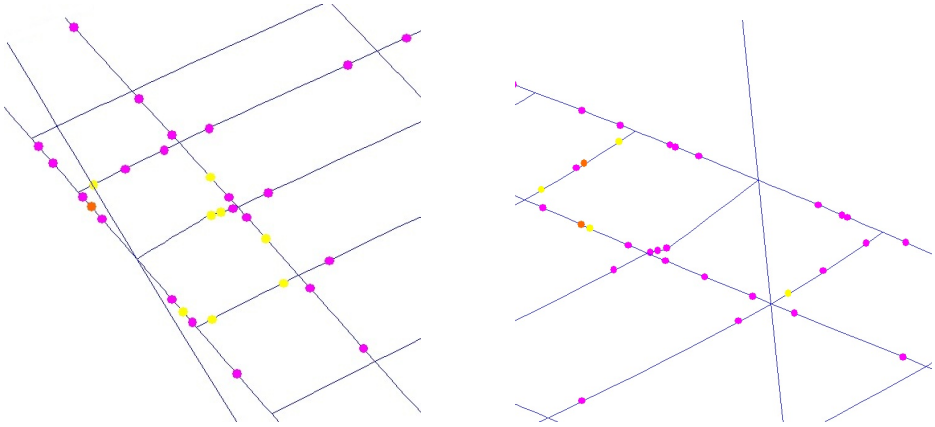

(a) State of hinges of connection A2 at 3% positive drift in East-West direction

(b) State of hinges of connection D2 at 3% positive drift in East-West direction

Figure 4.18: Comparison between hinges state

direction. This is due in both cases to numerical problems, associated to the punching of connection B4, as regard South direction of loading (positive), and punching of connection B1, as regard North direction of loading (negative); probably the model at these stage of the analyses has difficulties overcome the punching of these connections and to redistribute the loading increments to the plastic hinges still able to sustain it. This numerical phenomenon is clearly visible in Fig. 4.30 as a sudden drop.
Something similar happens for East-West direction of loading; in particular in negative direction the numerical model perform a lot of very small steps after the drift of 4%. In this case the explanation is quite simple, since at this stage of drift several connections has failed for punching (B3, C2, C3, D3, D2) and then the model has difficulties to redistribute new load increments. Despite this fact, no sudden drops in the moment-rotation diagrams of these connections are noticed.

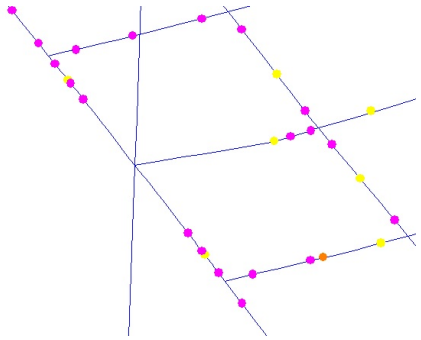

(a) State of hinges of connection A2 at 3% negative drift in East-West direction

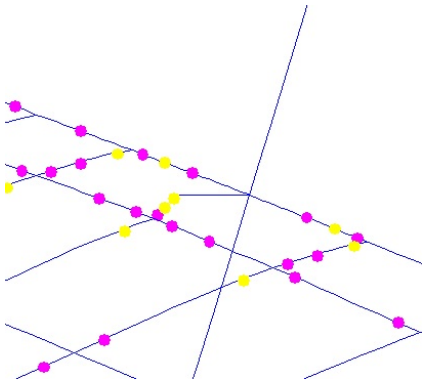

(b) State of hinges of connection D2 at 3% negative drift in East-West direction

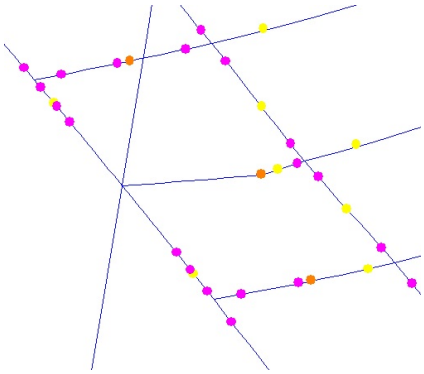

(c) State of hinges of connection A2 at 4.3% negative drift in East-West direction

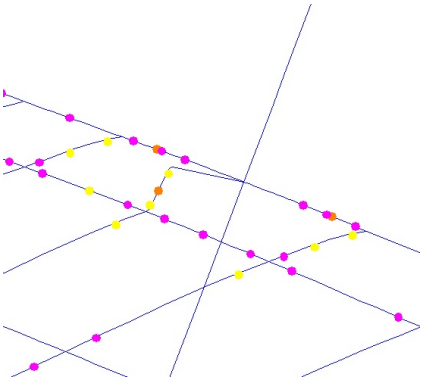

(d) State of hinges of connection D2 at 4.3% negative drift in East-West direction

Figure 4.19: Comparison between hinges state

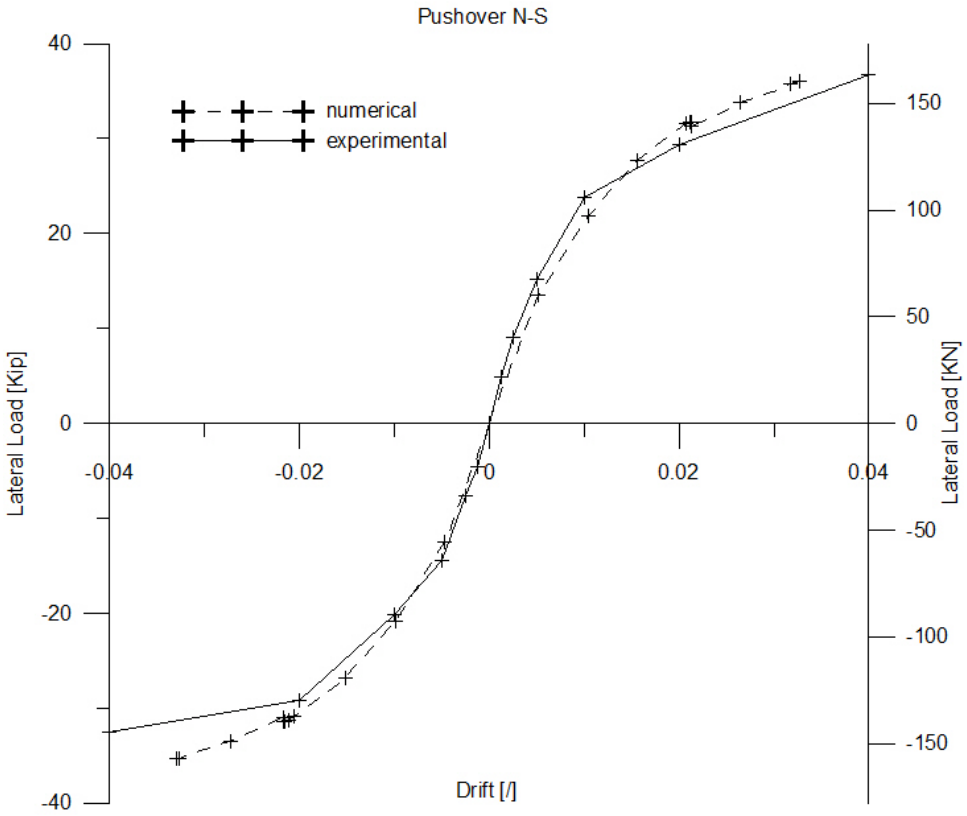

Figure 4.20: Comparison between the numerical pushover curve and the experimental lateral load-drift curve in North-South direction

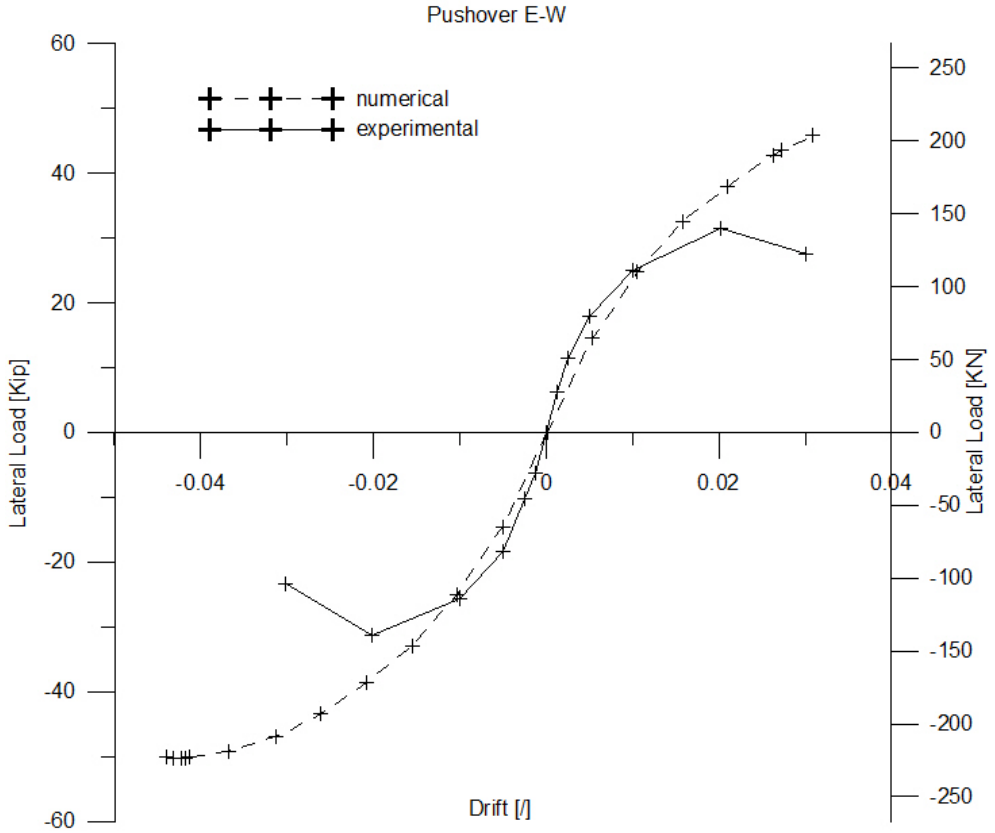

Figure 4.21: Comparison between the numerical pushover curve and the experimental lateral load-drift curve in East-West direction

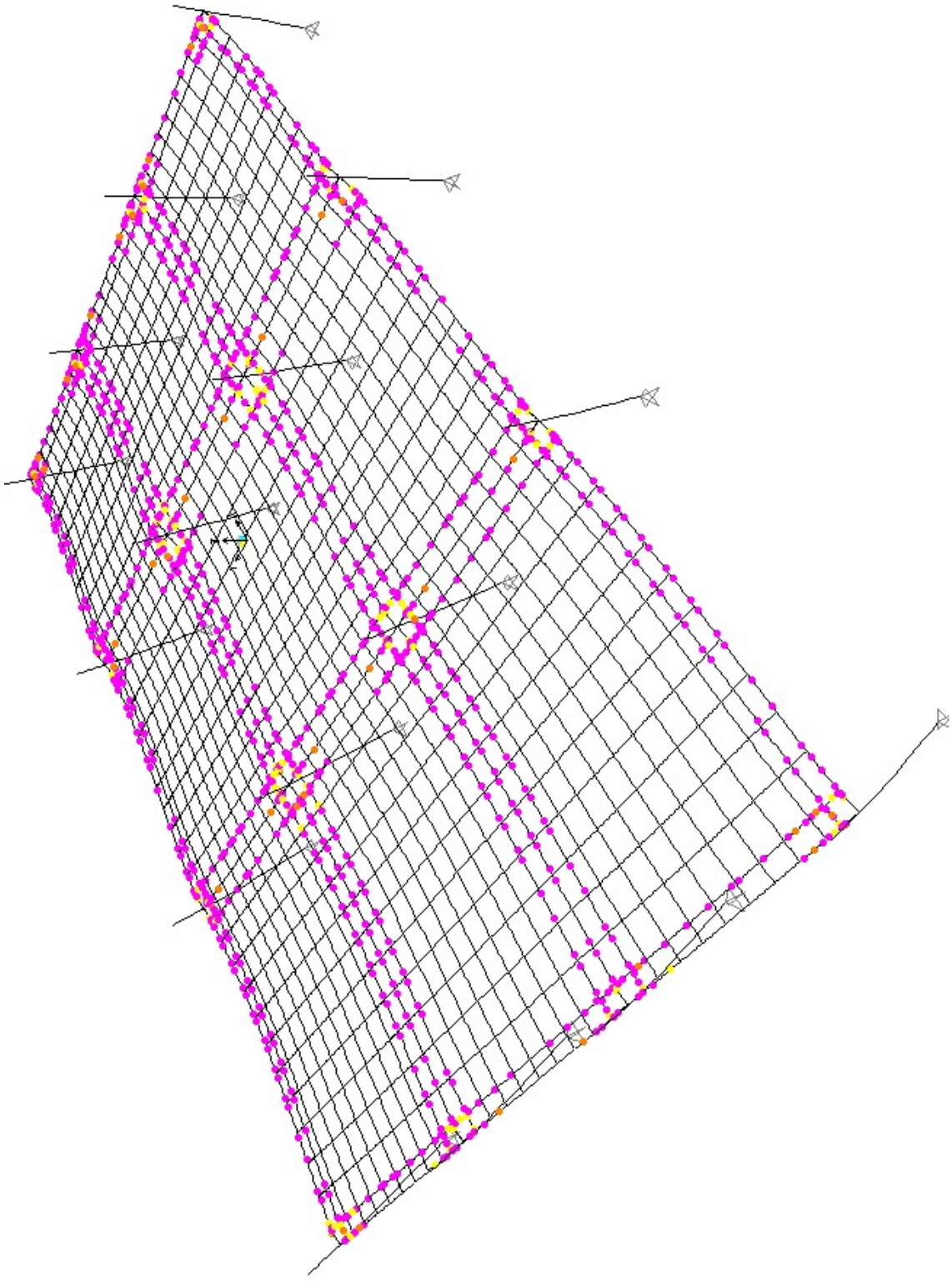

Figure 4.22: Representation of the deformed shape of slab and of the plastic hinges activated for direction West direction of loading

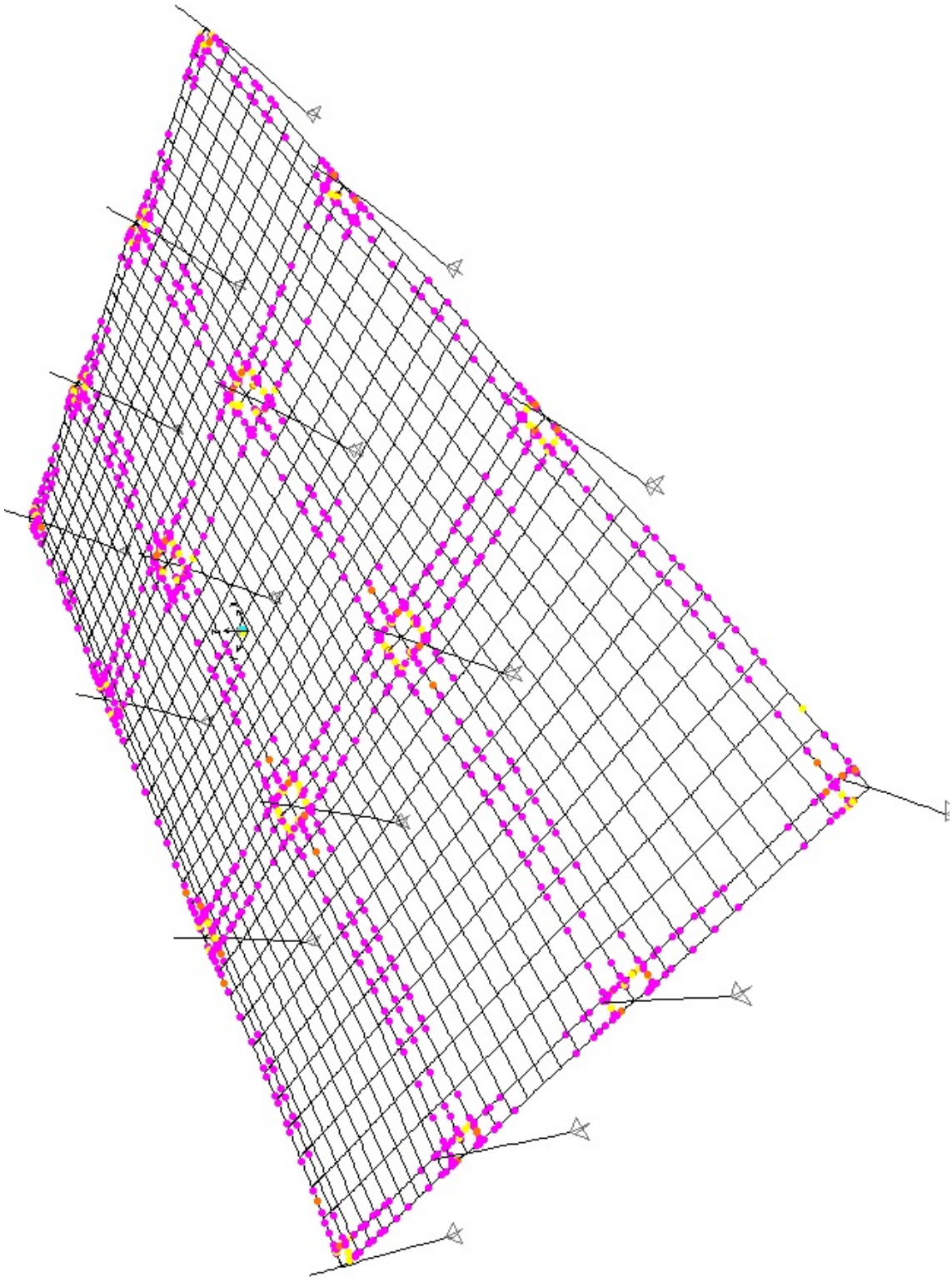

Figure 4.23: Representation of the deformed shape of slab and of the plastic hinges activated for direction South direction of loading

4.2.3 Moment versus rotation envelopes of joints

In this section a comparison between the experimental and numerical moment-rotation envelopes of joints will be presented, since it is interesting to investigate the singular behavior of each connection and how they influence the overall behavior of the whole structure.
Authors of experimental tests provided in the report[13] considered, lateral moment-rotation curves for tests LAT1, LAT2, LAT3, LAT4, NS800, EW800, NS400, EW400, NS200, EW200, NS100, EW100 and lateral moment-rotation envelopes up to drift of 4% of each connections for both the two orthogonal directions. These moments, according to authors instructions, are obtained by the product of the measured base shear (relative to the initial reading of each test) and the column height of 1.26 m (49.6 in.). Only peak values of the transfer moments and their corresponding rotations are provided in tabular form in the report and actually these data are the more interesting and more suitable for a comparison with model results.
It's worth to notice that the behavior of connections varies according to two discriminating factors: their position (internal, edge and corner) and the direction of loading (North-South and East-West). For these reasons it is decided to perform comparisons in both the two principal directions for nine connections, in particular for all the internal joints (B2, B3, C2, C3), for the south edge joints (B4, C4), for the south corner joints (A4, D4) and for the south-west joint (D3). In this way, and taking also into consideration that the slab is symmetric about the floor centerline along the long direction, all the possible connection types, at least for what regarding geometry, are considered.
In the figures presented in the following (Fig. 4.24 - 4.49), moment-rotation curves for both the two principal directions are presented for the nine connections specified above; in addiction photographs of damage of connections, for those pictures are available from the report[13], are reported.
A remark about the numerical curves presented in the following is that are composed by bending moments and rotations obtained at each step of the pushover analysis carried out with the sofware[34].
Let's start considering direction of loading North-South and in particular start focusing on corner connections A4 and D4 (Fig. 4.24 and 4.28).
First of all, it's possible to notice that the experimental envelopes (solid lines) demonstrate that yielding of connections occurs gradually; anyway the most significant yielding happens when drift reached approximately 1% and after this, a relatively plastic response is shown up to a drift of 4%. Notice that this is a general remark, holding for all connections and for both directions of loading, as shown in from Fig. 4.24 to Fig. 4.49.
As regard the comparisons for this two first cases, firstly it is possible to notice that in general the numerical envelope overestimates the experimental one, at least for drift greater than 1% in positive direction and nearly the half

in the negative one. The reason is supposed to be the progressive deterioration of connections in the experimental tests due to the particular loading procedure, for which the structure has been loaded firstly in North-South direction and then in East-West direction for increasing drift, as explained in section 3.1.5. Biaxial lateral loading procedure of testing has been proved to reduce lateral load stiffness, strength, ductility and drift capacity of slab-column connections by several research investigations, concerning singular joints for both interior[5, 48] and edge[49] connections. Has to be noticed that these study cases are different to connections A4 and D4, since they are at the corners of the flat slab; anyway it is reasonable to suppose that this deterioration phenomenon occurs also in corner connections, and if possible, should be greater than in interior and edge connections. This effects on the singular joints can be reasonably supposed to influence the overall behavior of a flat-slab structure to which the singular connections belong to. From this point of view it is possible to interpret the already cited pushover curve overestimation of the experimental lateral load-deflection curve in East- West direction (see Section 4.2.2).
Despite the differences in magnitudes between numerical and experimental lateral loads in Fig. 4.24 and 4.28, the model catch well the shape of the experimental curve showing decrements in the slope (flexural stiffness) of the graph at similar rotations of the experimental curve; thus, the general behavior of these connections is well modeled.
In Fig. 4.26 a photograph (taken from South) of the joint A4 after the tests is presented; it is possible to recognize two big diagonal cracks which are probably due to torsion arising during the cycles of test in North-South direction, since authors of the experimental tests[13] refer that no punching failure has occurred in this connection.
Focusing on elements inside critical section of connection A4, this behavior is effectively confirmed by numerical results, since no shear plastic hinges has reached failure for both two directions of loading, whereas the torsional one, placed on the south edge, experiences its capacity (Fig. 4.27(a)). Notice also that flexural plastic hinge placed at the interface of the column on the west edge, reaches its maximum resistance, suffering then a flexural deterioration process that may affect the response of this element during the following East-West test (Fig. 4.27(a)). This is what happens in reality; anyway grid model[33] couldn't catch this fundamental particularity simply because it has been not design to consider it. This is a further specification of the concept already explained in section 4.2.2 about the biaxial deterioration of the test slab, which is the principal reason for the difference between the numerical and experimental response.
The influence that biaxial interaction of internal actions has on the the definition of plastic hinges properties could be an important development of the model.
As regard edge connections B4 and C4 (Fig. 4.30 and 4.34), similar consider-

ations can be done. Numerical curves overestimate experimental ones both in positive and negative directions for connection C4, whereas connection B4 shows a step in its behavior, due to numerical problems at the punching of the connection in direction North-South. However, without this particularity, the general trend of the numerical curve is similar to those of the other connections.
As just mentioned above, connection B4 experiences punching failure for South direction of loading whereas this does not occur for both West and South loading direction (Fig. 4.33); numerical results are then the opposite of what happens in reality, since authors of experimental tests[13] have specified that shear failure of several connections occurred only during test EW25 (Fig. 4.14). This anticipated failure, which occurs nearly at 2% drift in North-South direction, is due to something not correctly defined in plastic hinges parameters. In particular, supposing that flexural and shear hinges are correctly defined, the value of the ultimate torsional twist ψ_u of torsional hinges of edge elements could be the guilty because to high, although already reduced as explained in section 4.1.3. If this is the cause, the overestimation of ψ_u may induce the torsional plastic hinge to slower develope its capacity, thus accelerating the loading process of the shear plastic hinge and leading to its premature failure.
The problem underlined above is not absolutely detected in the behavior of internal connections, which is modeled very well as explained in the following; the reason is that the grid model[33] used ha been principally calibrated on internal connections test results. Thus, a better understanding of the torsional behavior of edge connections could lead to further improvements of the model.

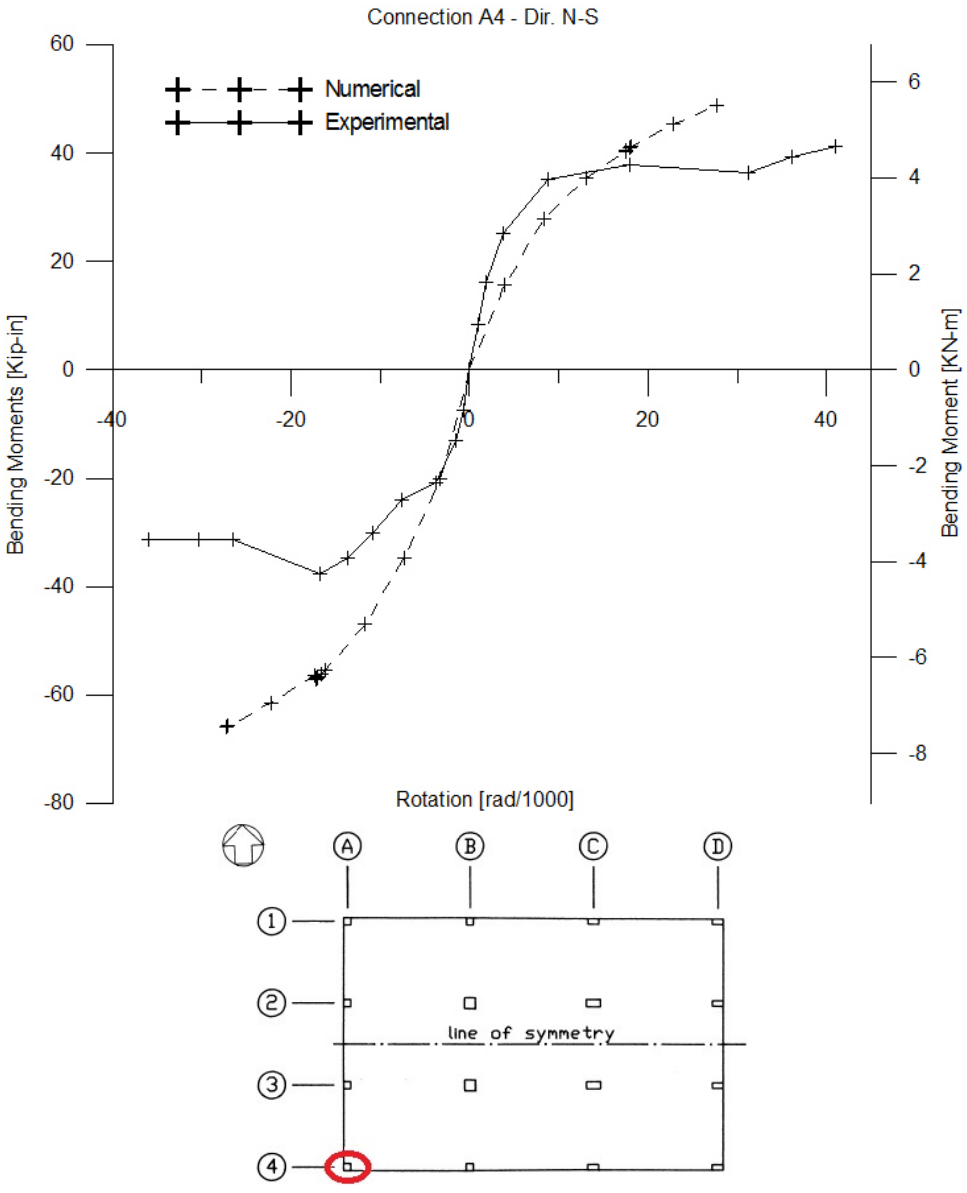

Figure 4.24: Comparison between the numerical moment-rotation curve and the experimental moment-rotation envelopes of joint A4 in North-South direction

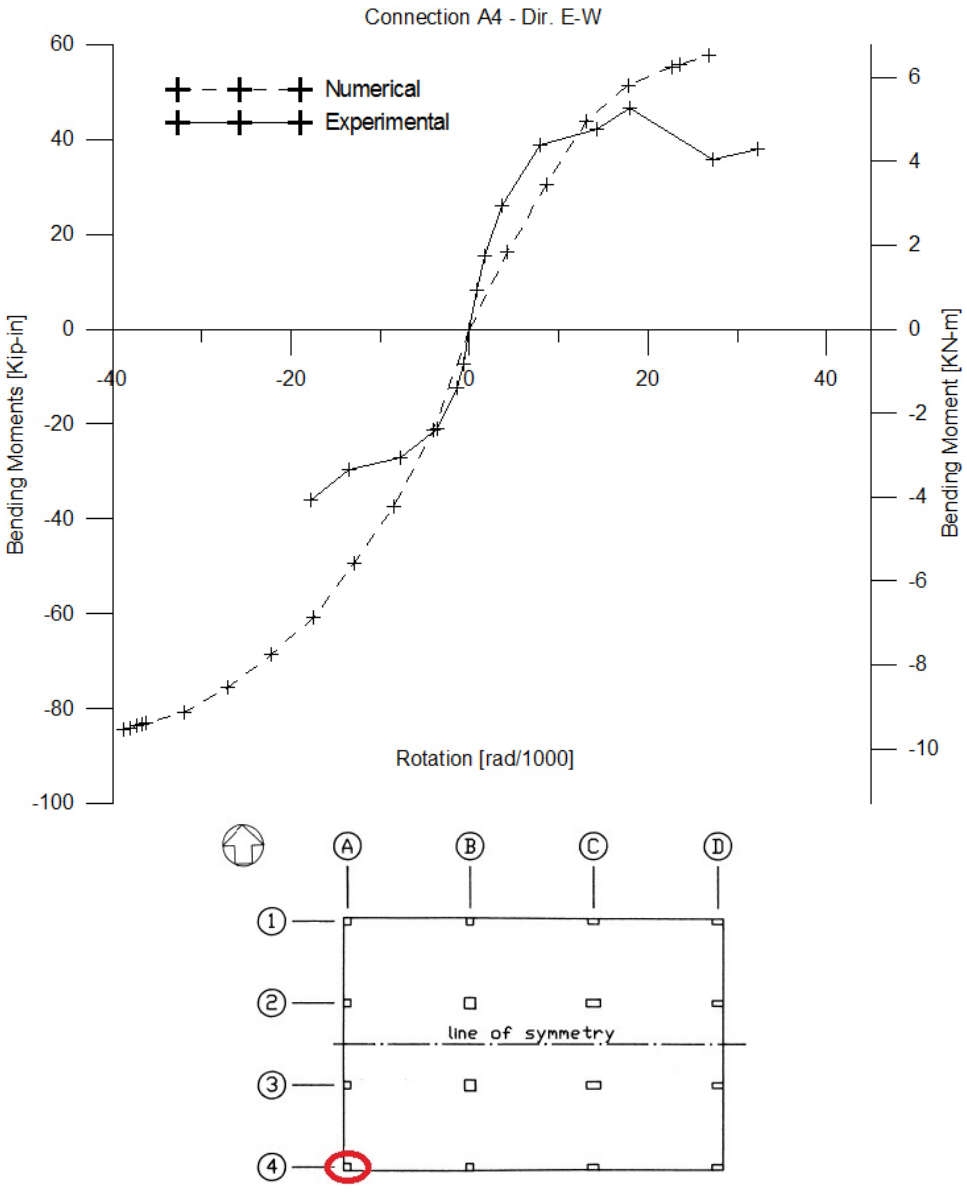

Figure 4.25: Comparison between the numerical moment-rotation curve and the experimental moment-rotation envelopes of joint A4 in East-West direction

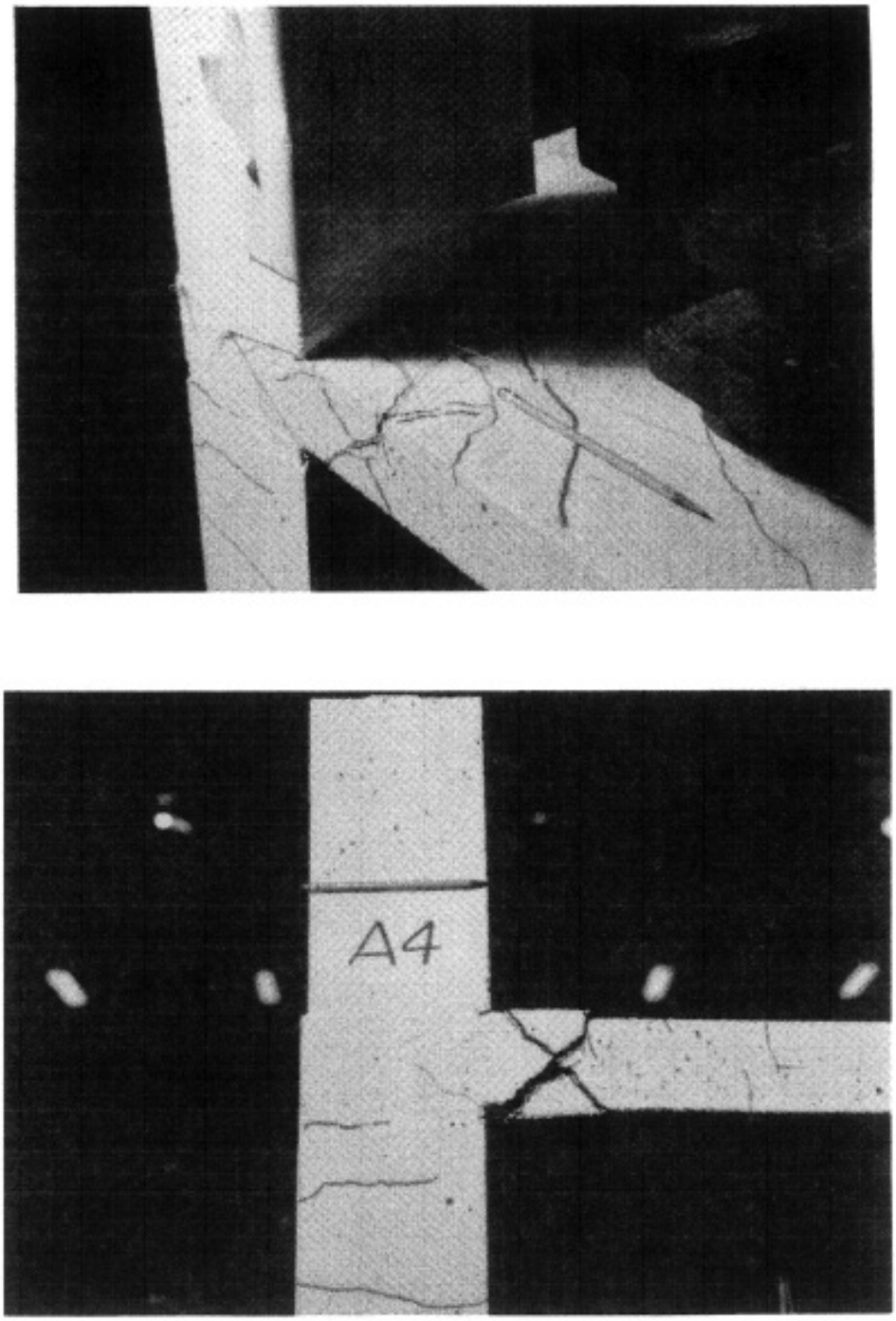

Figure 4.26: Photographs of damage of connection A4[13]

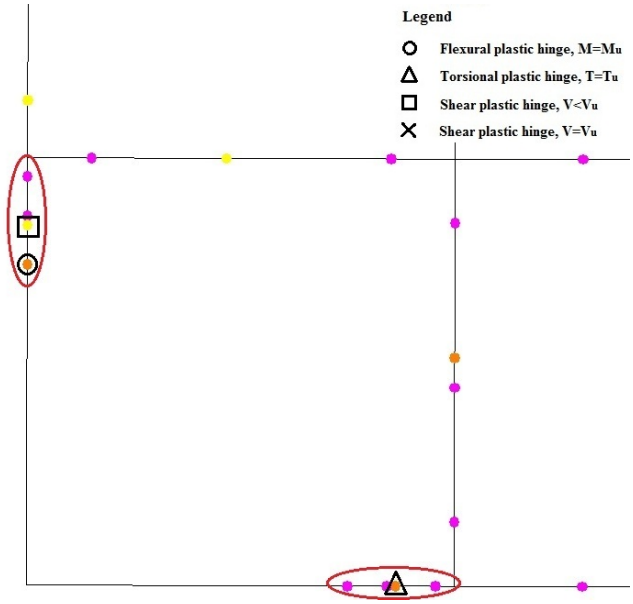

(a) State of hinges of connection A4 at 3.3% positive drift in North-South direction

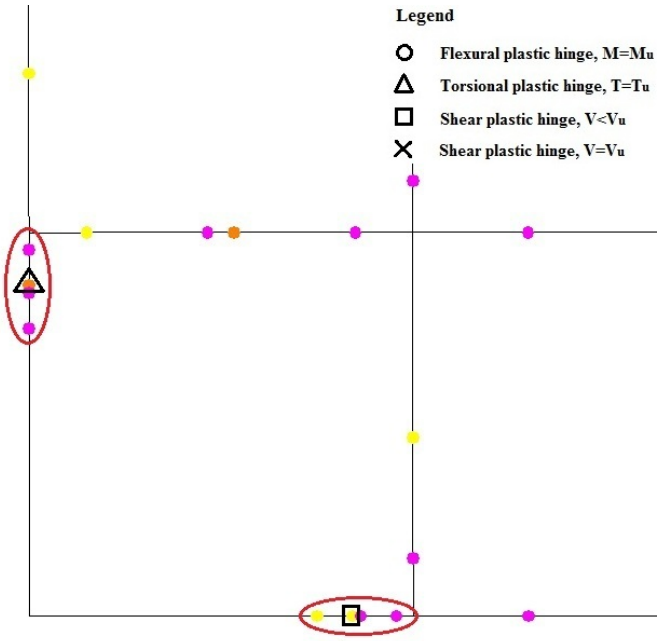

(b) State of hinges of connection A4 at 3% positive drift in East-West direction

Figure 4.27: State of hinges of connection A4 at the maximum numerical drift reached for positive loading directions (West and South). Elements in critical sections are marked with a red circle

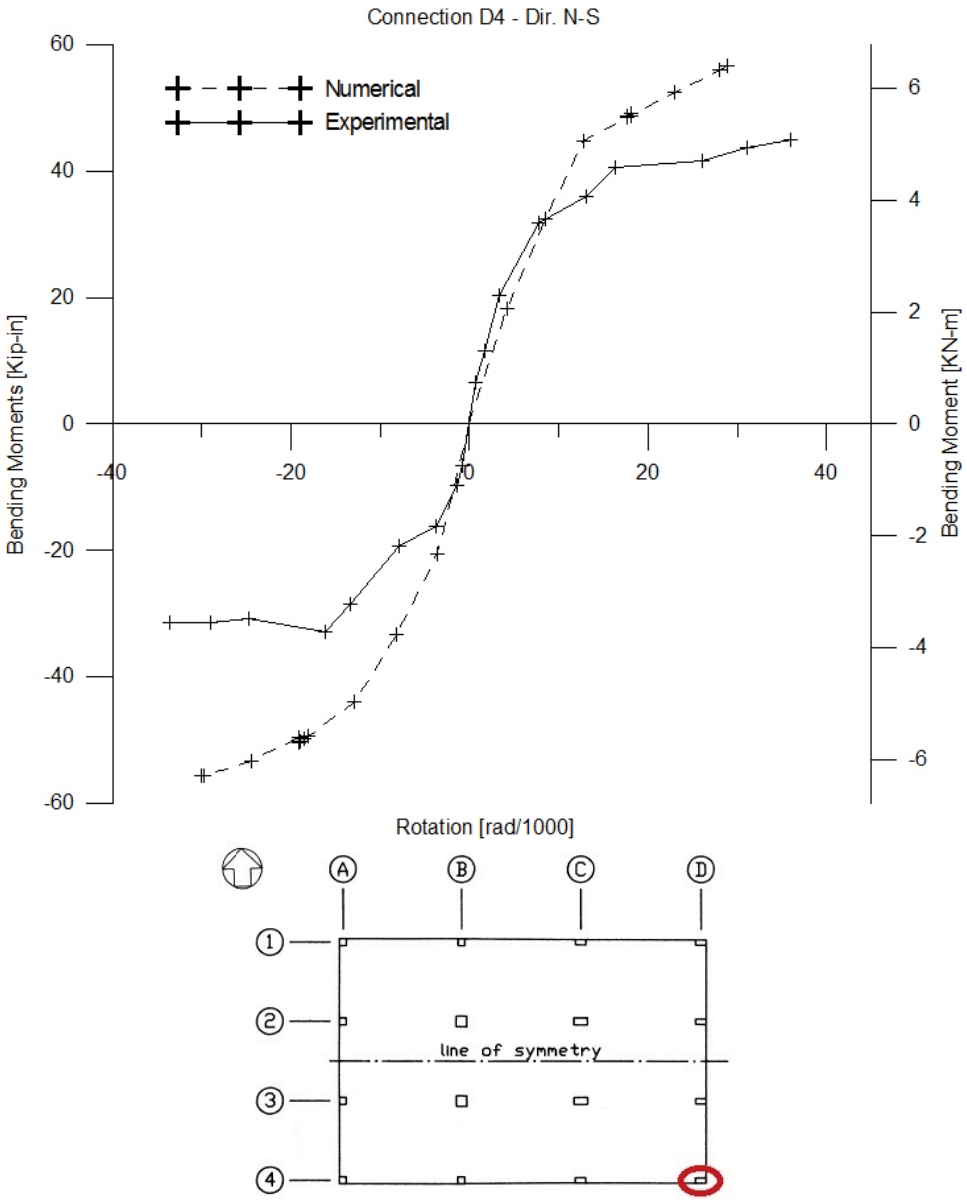

Figure 4.28: Comparison between the numerical moment-rotation curve and the experimental moment-rotation envelopes of joint D4 in North-South direction

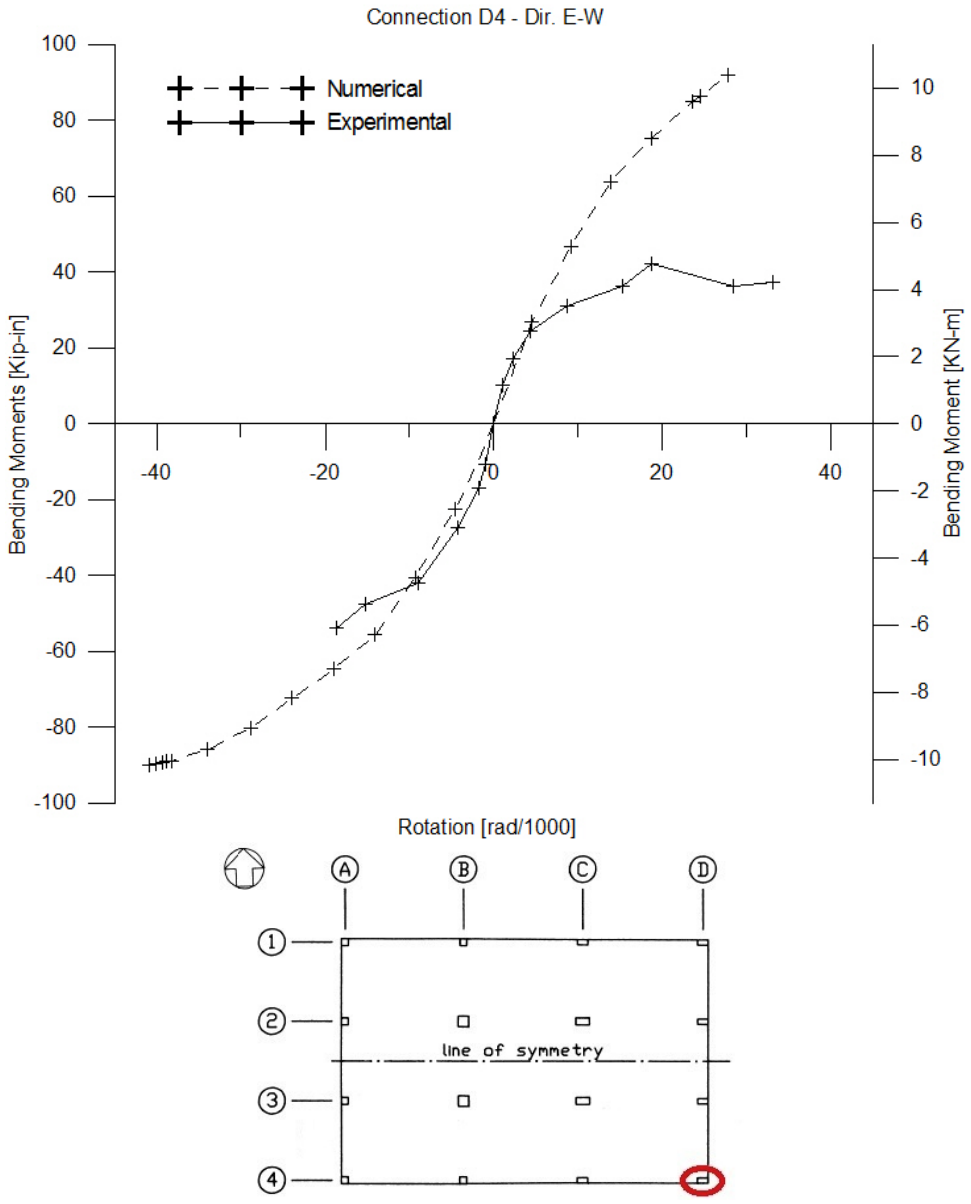

Figure 4.29: Comparison between the numerical moment-rotation curve and the experimental moment-rotation envelopes of joint D4 in East-West direction

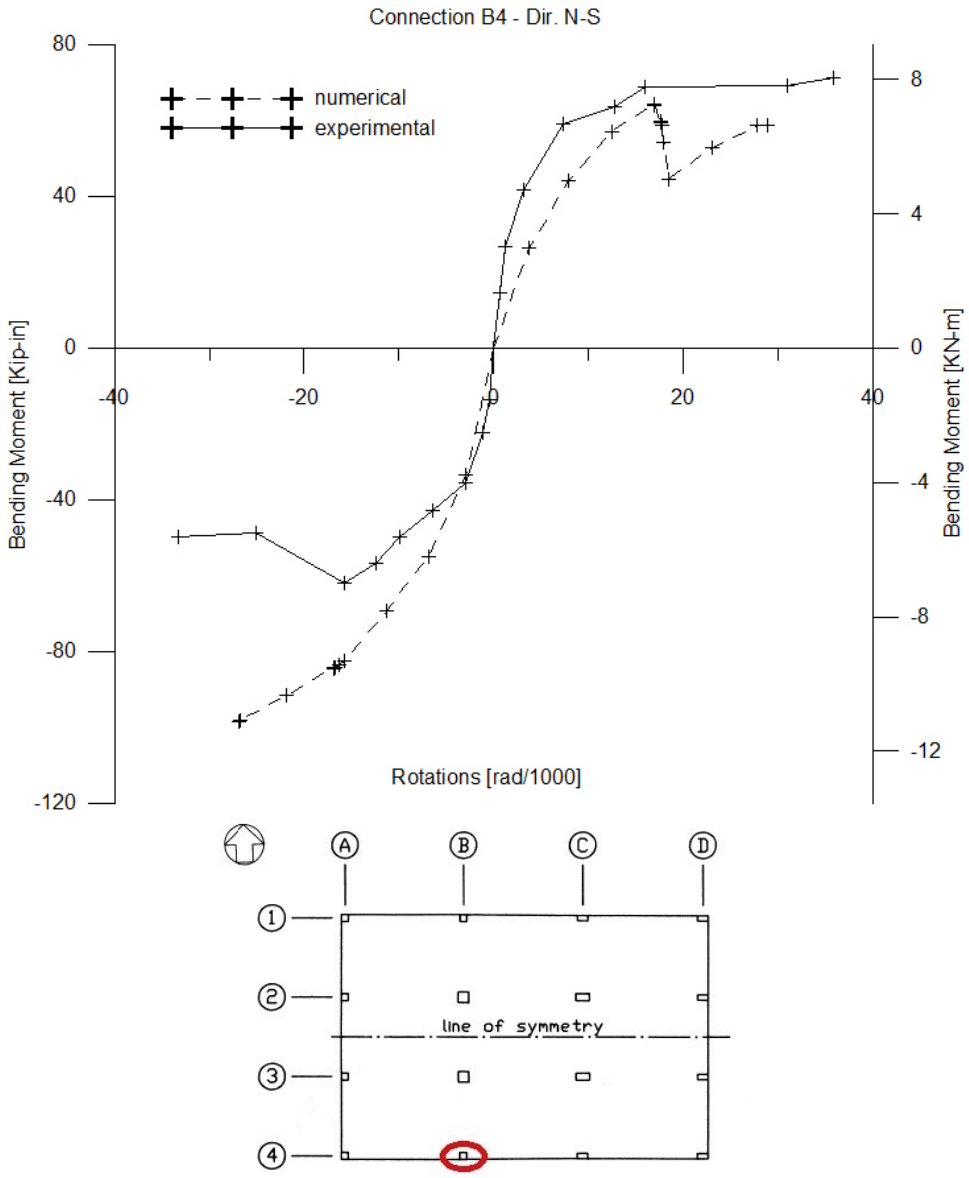

Figure 4.30: Comparison between the numerical moment-rotation curve and the experimental moment-rotation envelopes of joint B4 in North-South direction

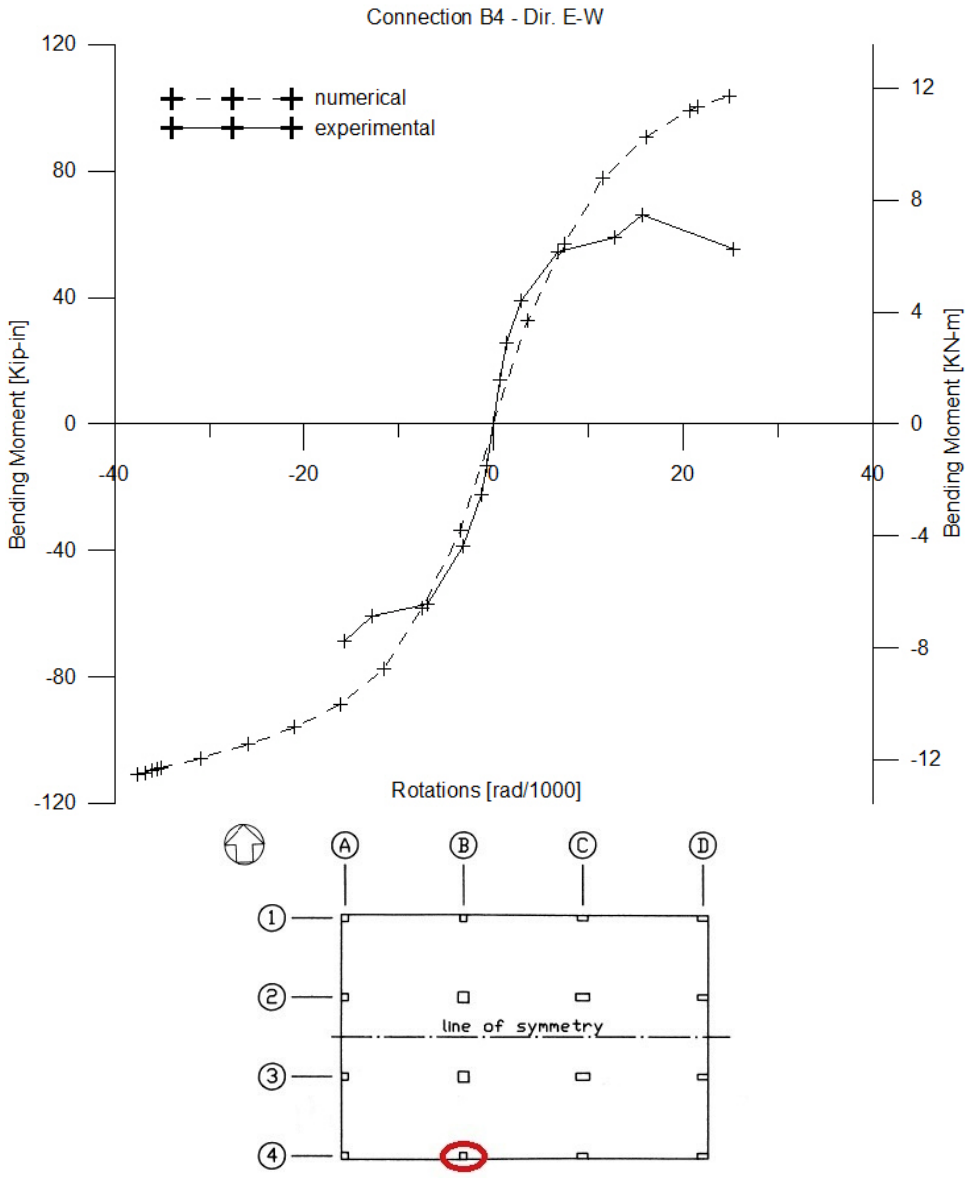

Figure 4.31: Comparison between the numerical moment-rotation curve and the experimental moment-rotation envelopes of joint B4 in East-West direction

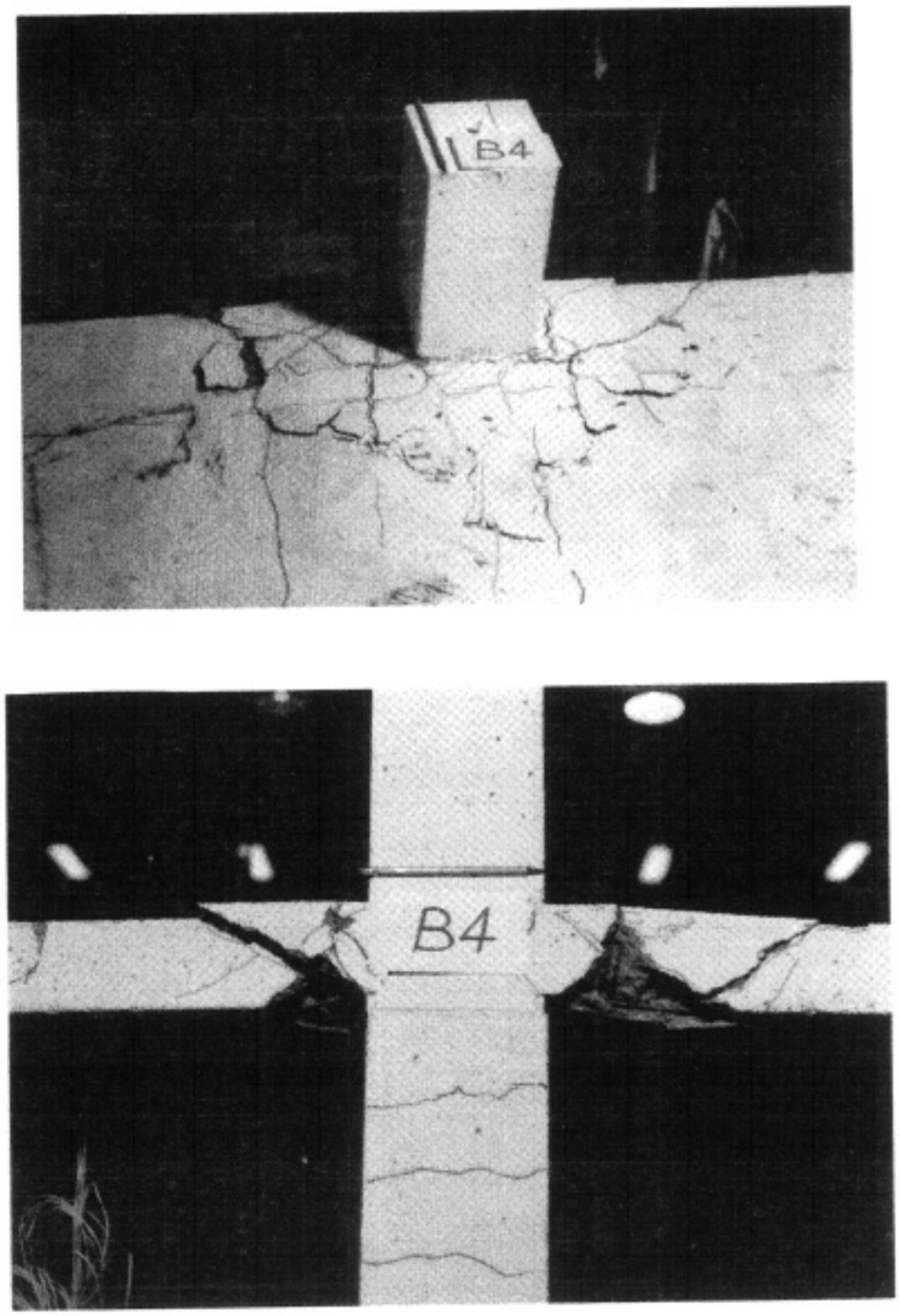

Figure 4.32: Photographs of damage of connection B4[13]

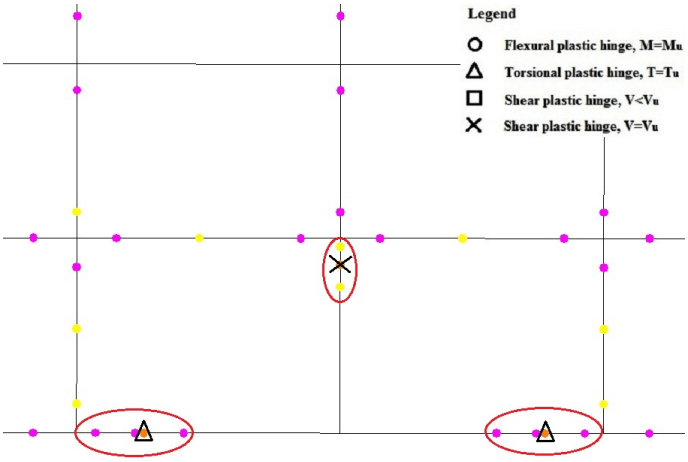

(a) State of hinges of connection B4 at 3.3% positive drift in North-South direction

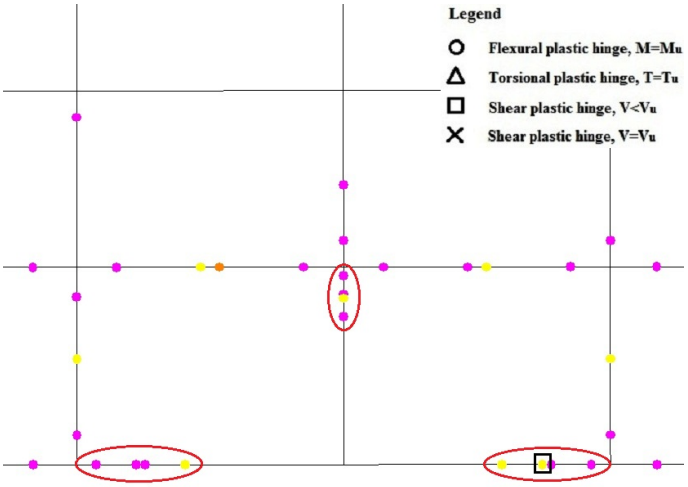

(b) State of hinges of connection B4 at 3% positive drift in East-West direction

Figure 4.33: State of hinges of connection B4 at the maximum numerical drift reached for positive loading directions (West and South). Elements in critical sections are marked with a red circle

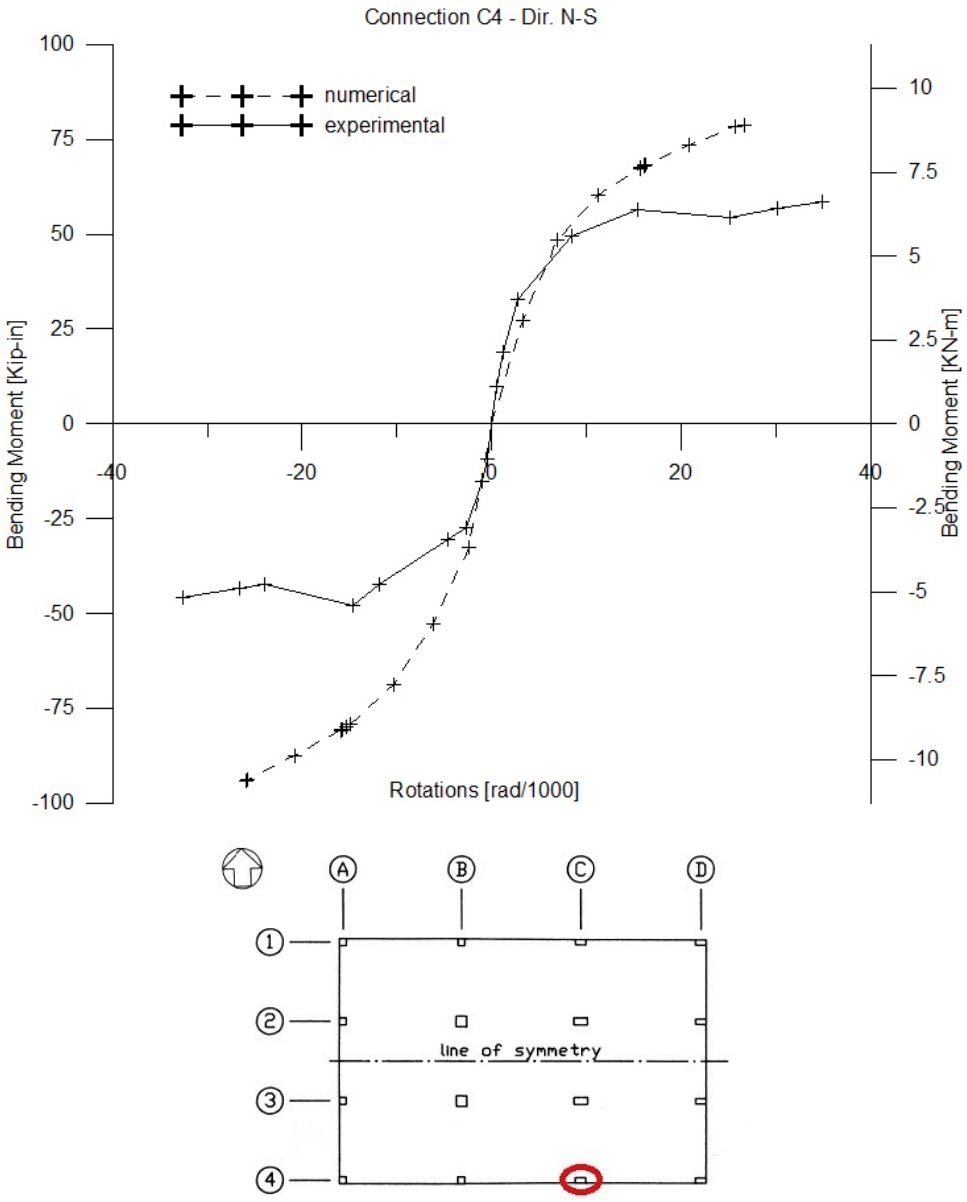

Figure 4.34: Comparison between the numerical moment-rotation curve and the experimental moment-rotation envelopes of joint C4 in North-South direction

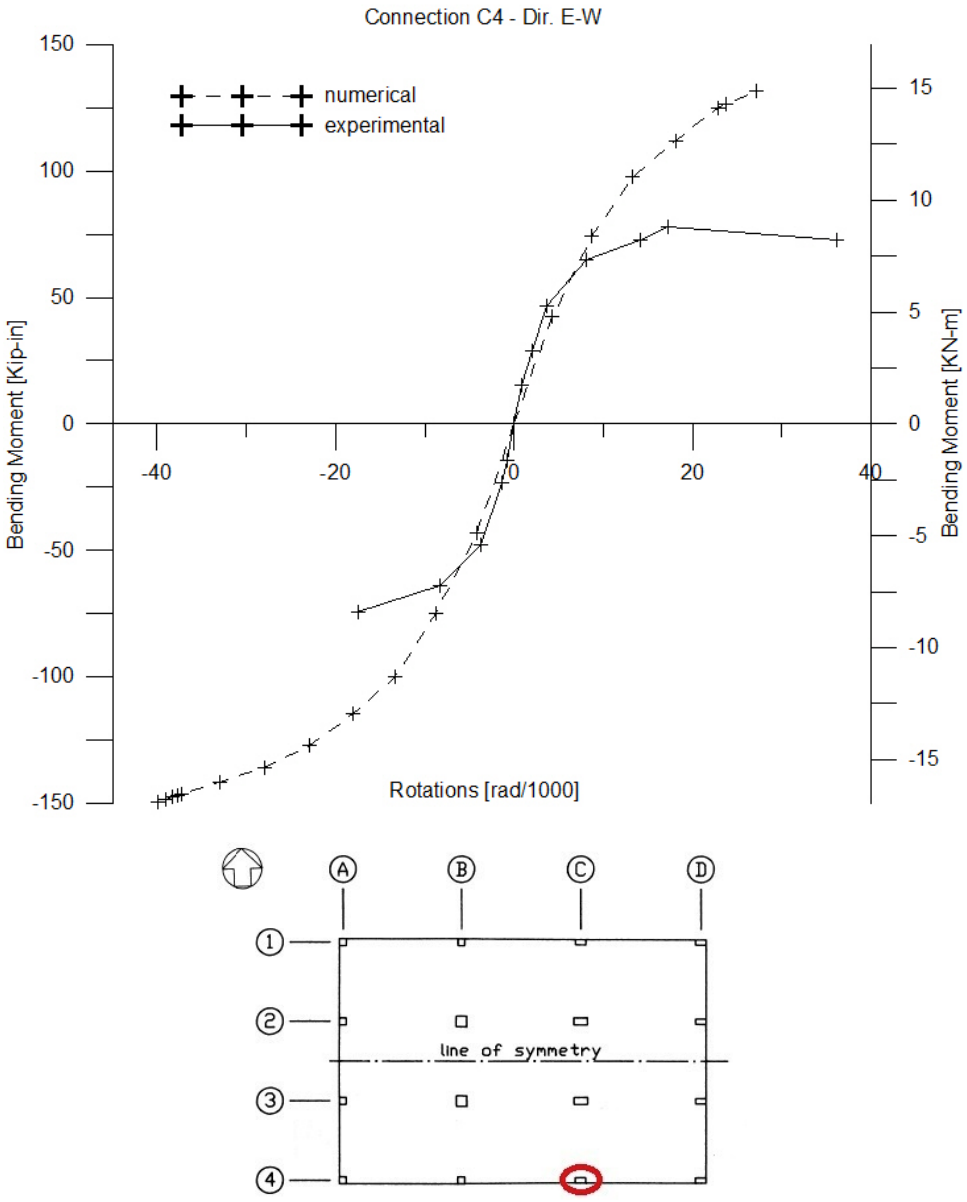

Figure 4.35: Comparison between the numerical moment-rotation curve and the experimental moment-rotation envelopes of joint C4 in East-West direction

In Fig. 4.36, 4.41,4.43 and 4.46, moment-rotation curves of internal connections B3, B2, C3, C2 are presented. It is possible to notice that the model gives a very good prediction in term of strength and general behavior; the correspondence is evident both in positive and negative parts of the graphs. This means that the model is able to well represent the structural behavior of internal connections and this is probably due to the fact that internal joints seem to lesser suffer the effects of biaxial loading, with respect to what happens for edge and corner connections. The principal reason could be the presence of the slab all around the connection and this provide it more resources with respect to an edge or a corner connection, in order to resist loads in the two principal directions. Thus, numerical curves fit well the experimental ones because the second do not show significant decrement of strength in the negative branches.
An ulterior reason is that the grid model[33] has been calibrated principally on experimental tests results regarding internal connections, it's not surprising that the model works better for these cases.
It is also interesting to notice that for internal column, differently for what happens for edge and corner columns, numerical curves slightly underestimate experimental results.
Let's now focusing on connection B3, anyway the following considerations could be widen to all internal connections.
According to experimental results[13] (section 4.14), connection B3 failed for punching shear during test EW25 for both positive and negative direction of loading at a drift of 3.3% and 2.4%,respectively. The numerical results do not confirm that since the two shear plastic hinges on the two critical elements in direction East-West, one on the left and one on the right of the connection, reach the 91% (yellow) and the 75% (fuchsia) of their capacity, respectively, for West direction of loading (positive) (Fig. 4.40(a)). For East direction of loading (negative) also numerical results show punching failure of connection, at least for shear plastic hinge on the left of the joint (Fig. 4.40(b)), whereas the right one experiences nearly 93% of its capacity. This happens at the ultimate step of the analysis, at 4.4% drift, then much higher than experimental one for which punching failure has occurred.
This difference between model and reality could be in all probability imputed to the degradation of connections due to biaxial loading, and, in particular, the explanation is very similar to the one already written for connection A4. During numerical analysis in the North-South direction, critical elements in East-West direction suffer damaging due to torsion whereas ones in the North-South direction suffer damaging due to shear and flexure (Fig. 4.39). During loading in the long direction instead, first elements should resist principally to shear and flexure, whereas the second to torsion (Fig. 4.40). Thus, what happens in reality is that elements already damaged for flexure and shear, will show lesser torsional capacity than the same virgin elements; the same reasoning holds for elements firstly damaged by torsion.

If the model[33] could take into account for this, punching failure will probably occur also during numerical analysis for positive East-West loading for drift similar to what observed experimentally.
Notice finally that torsional capacity is not reached in any of the beam elements of the critical sections, differently to what observed in corner and edge connections; this is due to their better performance against shear and bending moment.
As regard connection D3 and in particular North-South direction of loading, it is possible to notice that its experimental envelope is well represented by the analysis (Fig. 4.48), despite the fact that it is an edge connection. The reason in this case is that the load acts parallel to the border of the slab, thus, the "back" and "front" part of the slab with respect to the connection, give a comparable strength in the two opposite direction of loading.
A general remark for the comparison for moment-rotation curves in North-South direction is that the ultimate ultimate rotations of experimental curves are constantly greater then the ones obtained numerically; this is the consequence of the pushover analysis in North-South direction which does not reach the level of drift obtained from experimental tests on the slab.

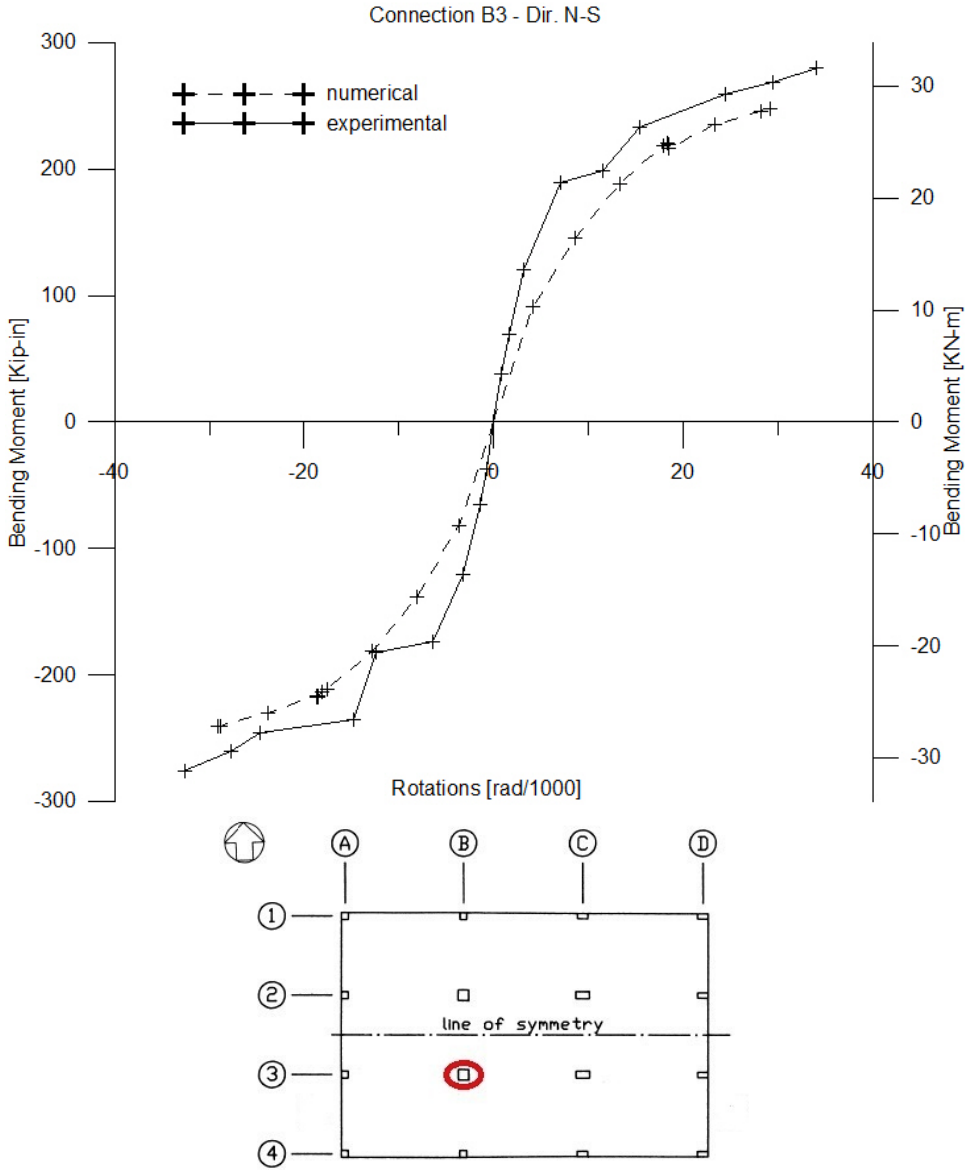

Figure 4.36: Comparison between the numerical moment-rotation curve and the experimental moment-rotation envelopes of joint B3 in North-South direction

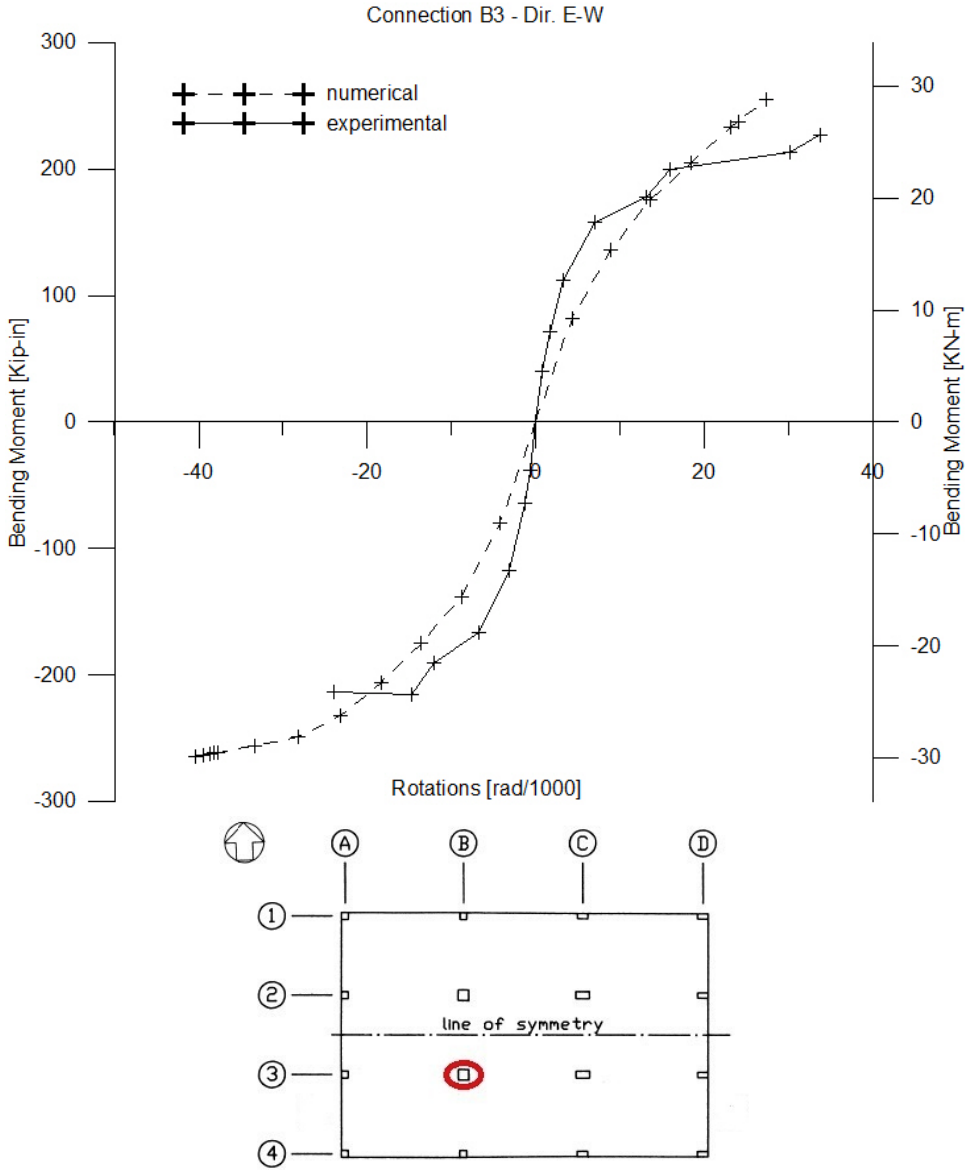

Figure 4.37: Comparison between the numerical moment-rotation curve and the experimental moment-rotation envelopes of joint B3 in East-West direction

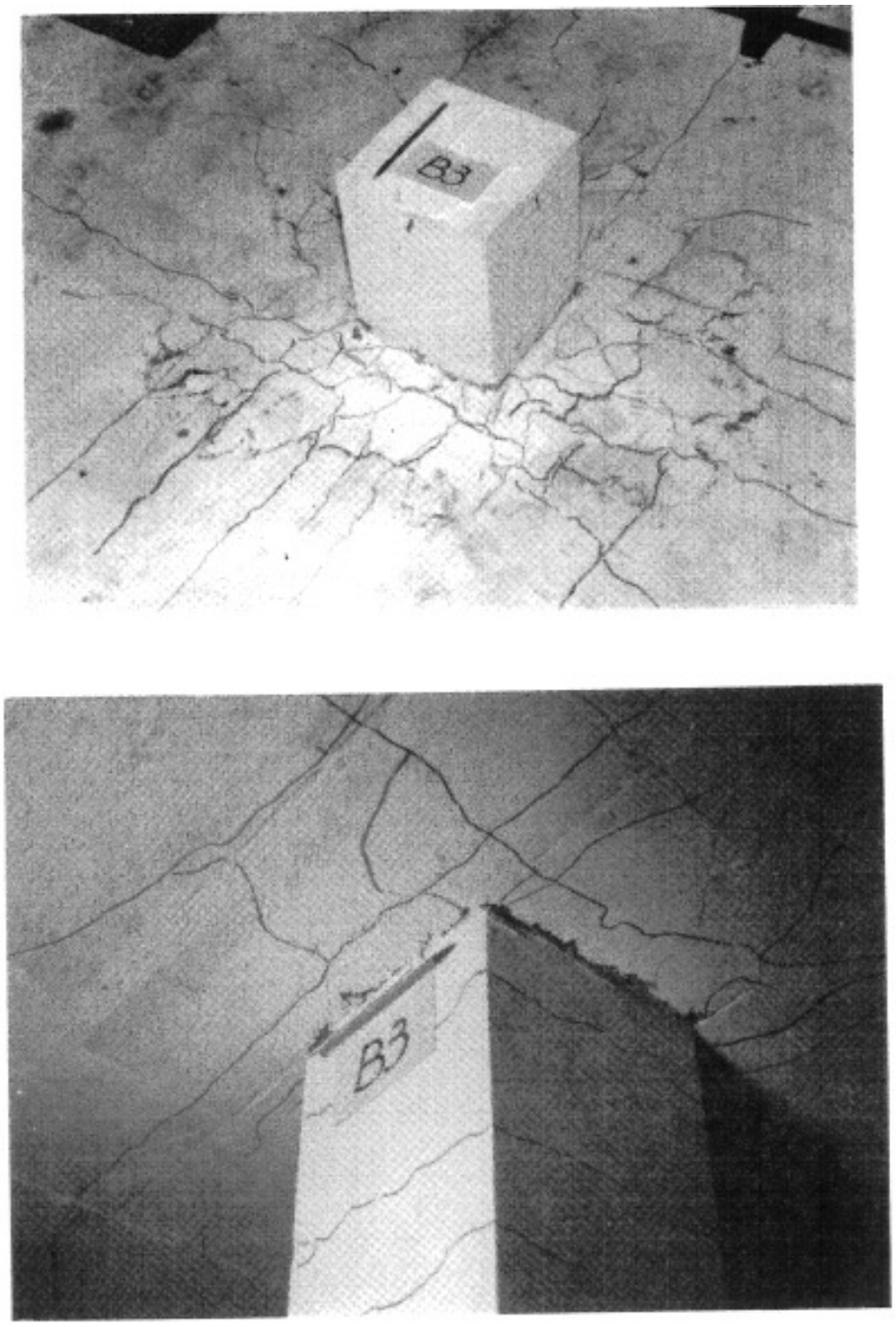

Figure 4.38: Photographs of damage of connection B3[13]

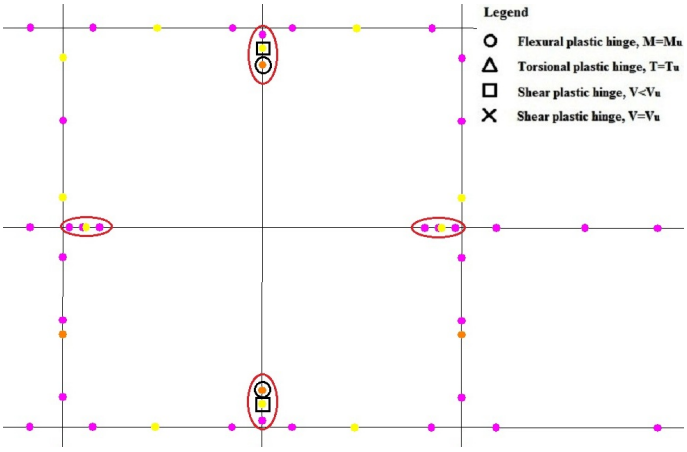

(a) State of hinges of connection B3 at 3.3% positive drift in North-South direction

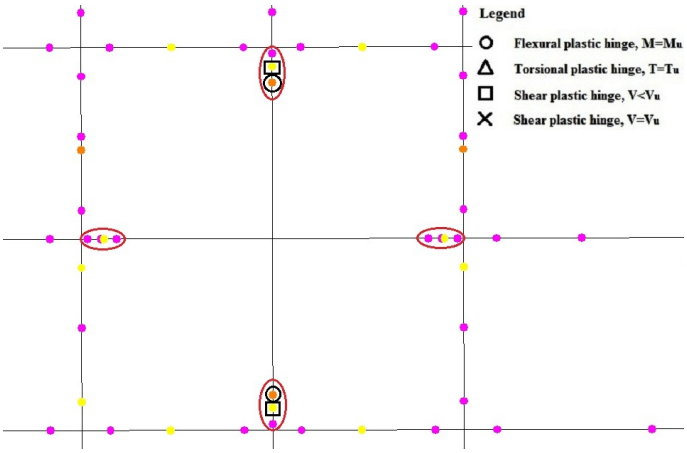

(b) State of hinges of connection B3 at 3.3% negative drift in North-South direction

Figure 4.39: State of hinges of connection B3 at the maximum numerical drift reached for positive and negative North-South directions of loading. Elements in critical sections are marked with a red circle

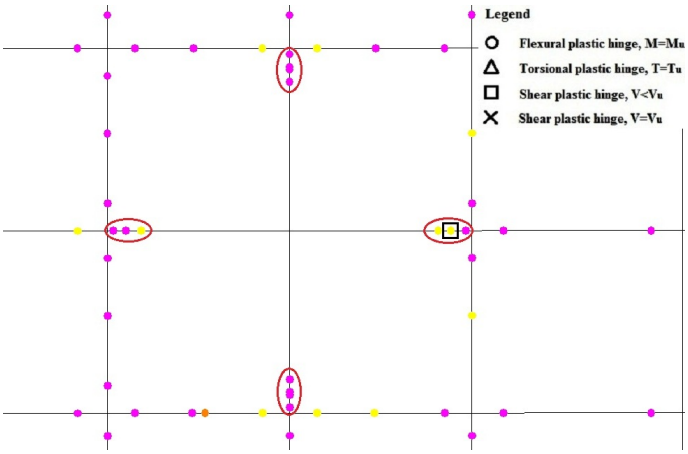

(a) State of hinges of connection B3 at 3% positive drift in East-West direction

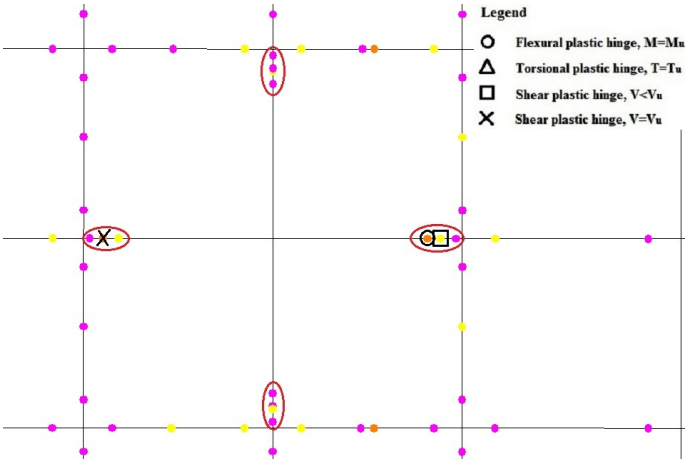

(b) State of hinges of connection B3 at 4.4% negative drift in East-West direction

Figure 4.40: State of hinges of connection B3 at the maximum numerical drift reached for positive and negative East-West directions of loading. Elements in critical sections are marked with a red circle

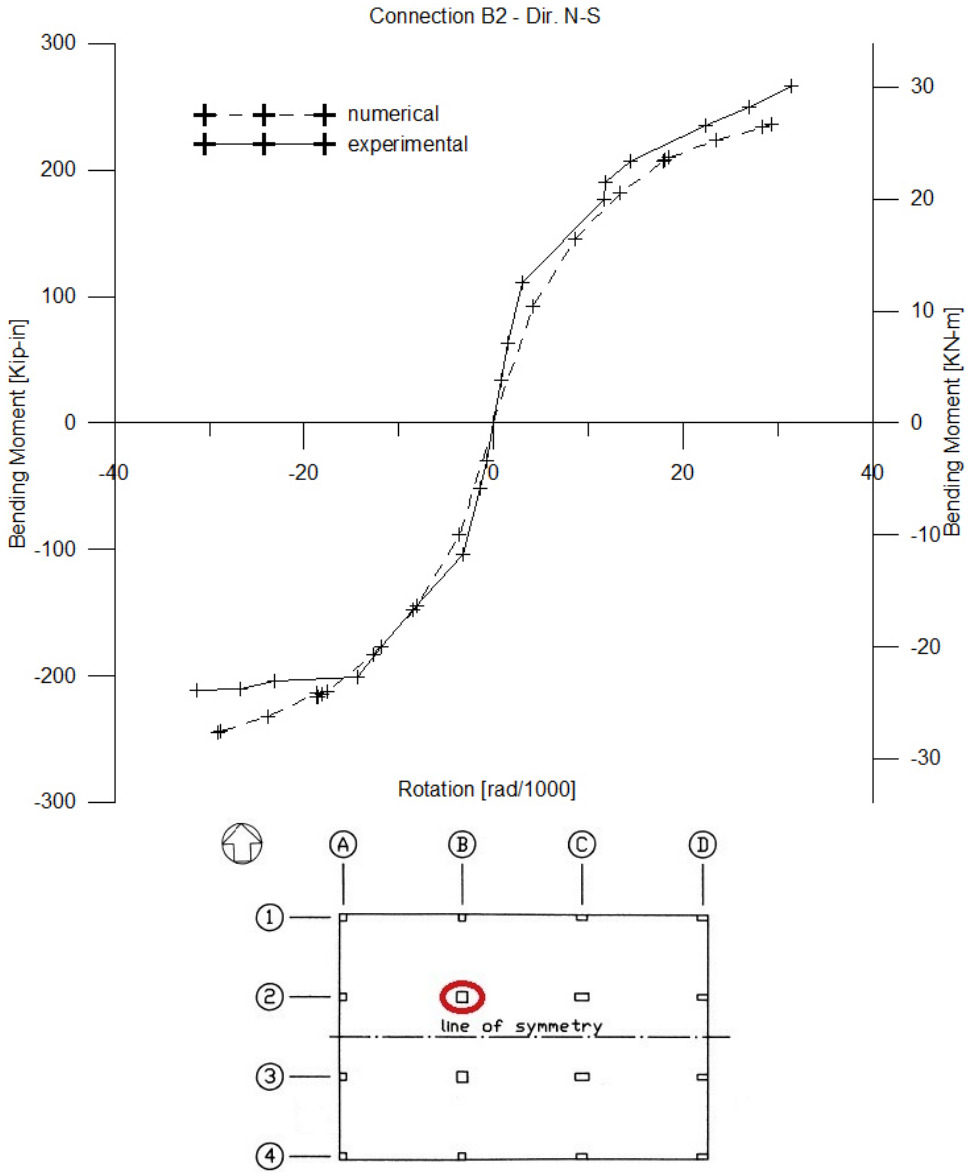

Figure 4.41: Comparison between the numerical moment-rotation curve and the experimental moment-rotation envelopes of joint B2 in North-South direction

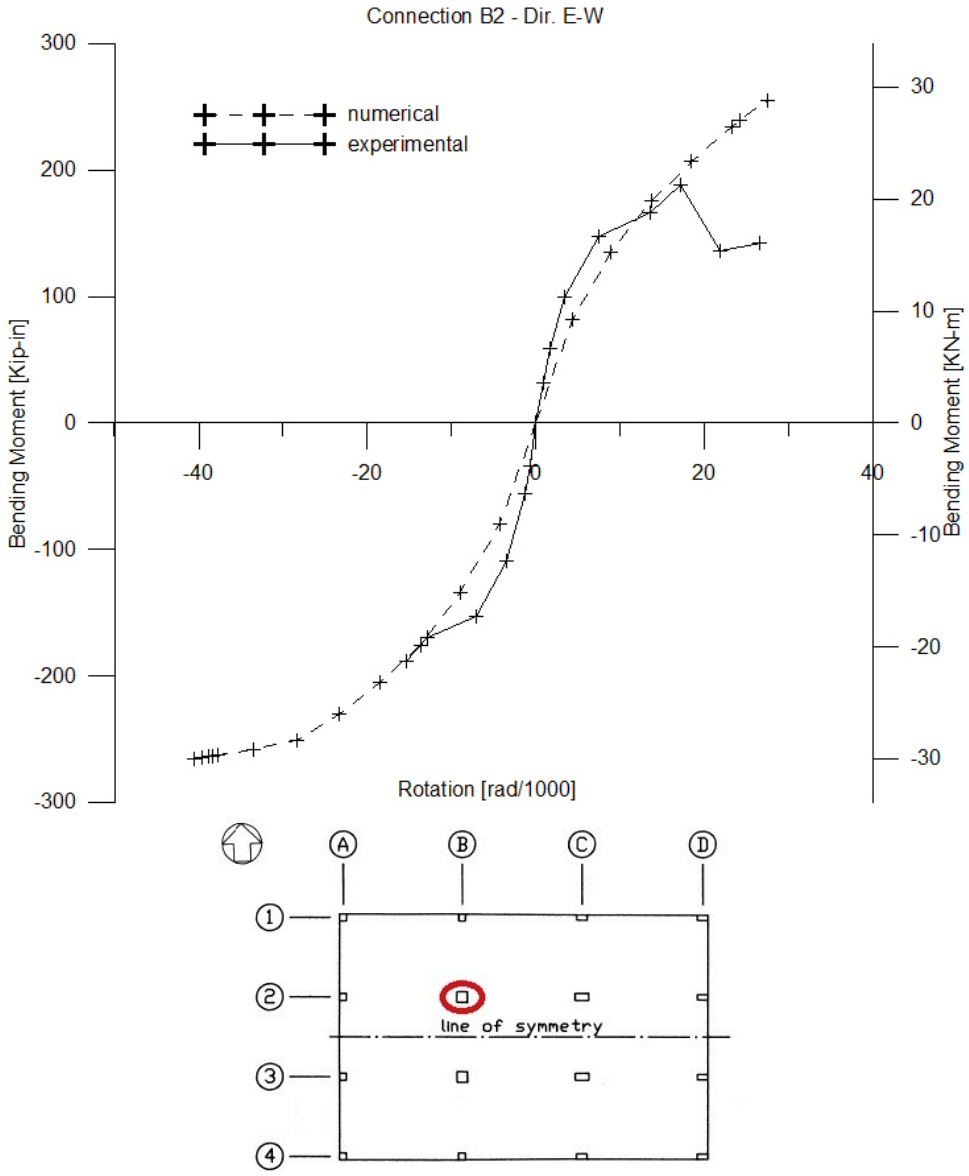

Figure 4.42: Comparison between the numerical moment-rotation curve and the experimental moment-rotation envelopes of joint B2 in East-West direction

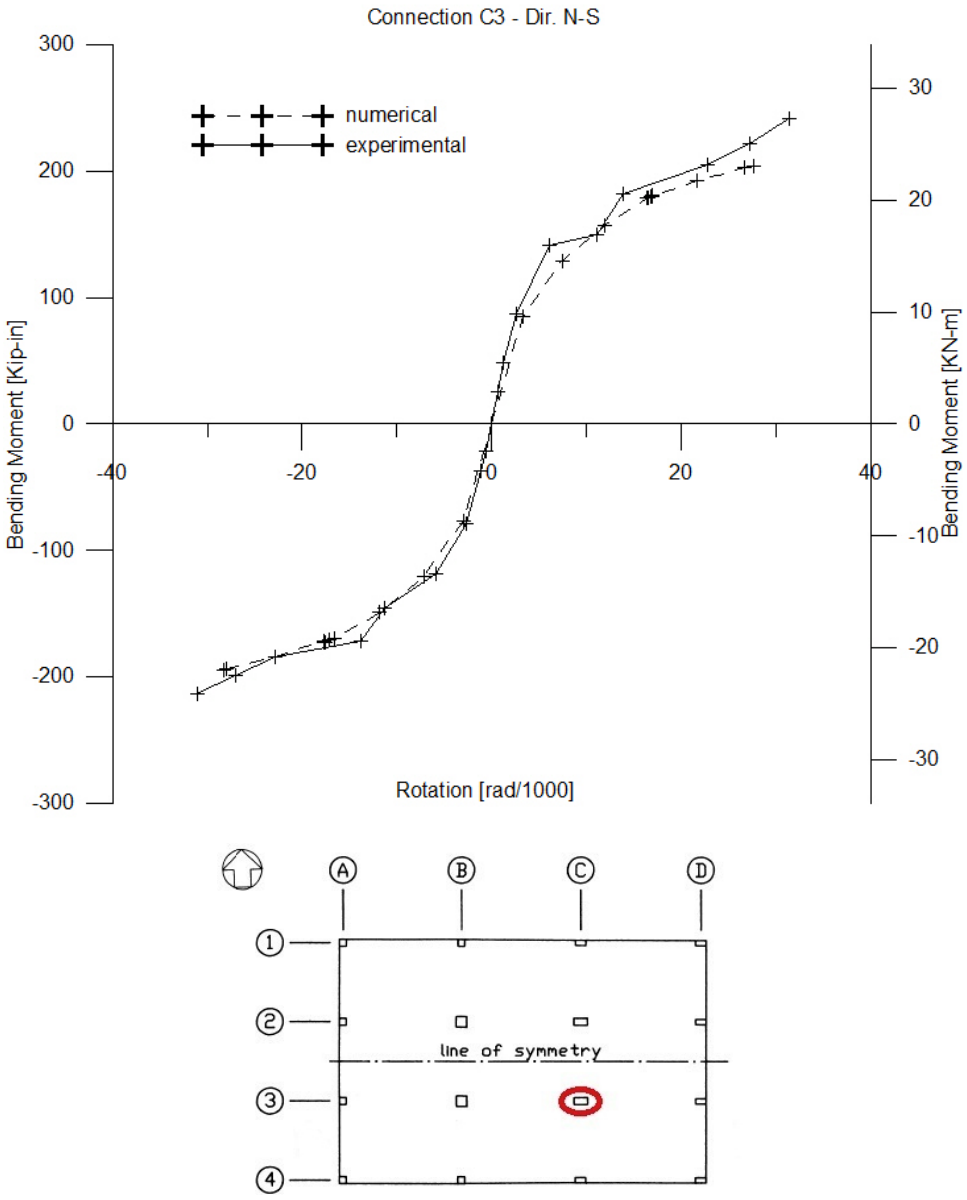

Figure 4.43: Comparison between the numerical moment-rotation curve and the experimental moment-rotation envelopes of joint C3 in North-South direction

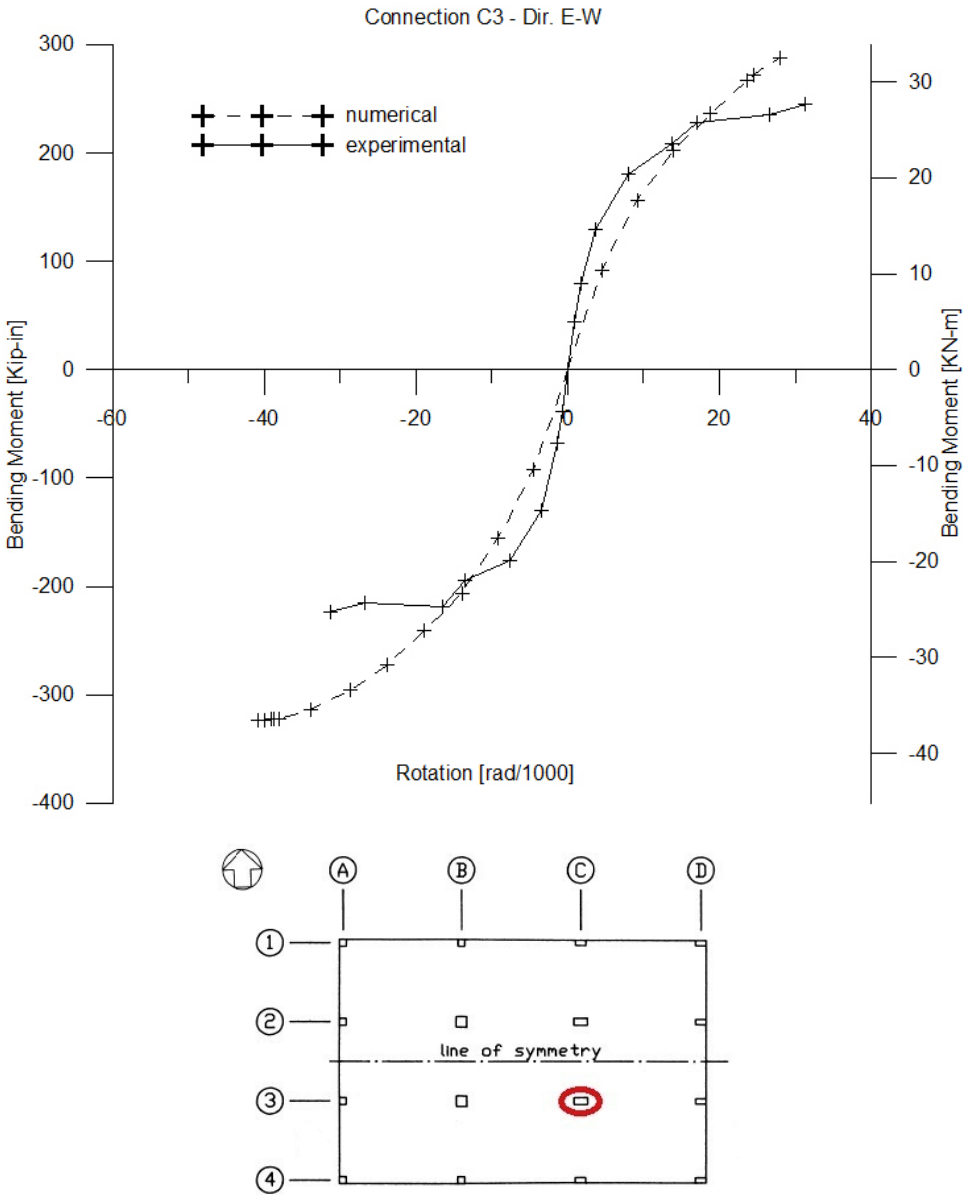

Figure 4.44: Comparison between the numerical moment-rotation curve and the experimental moment-rotation envelopes of joint C3 in East-West direction

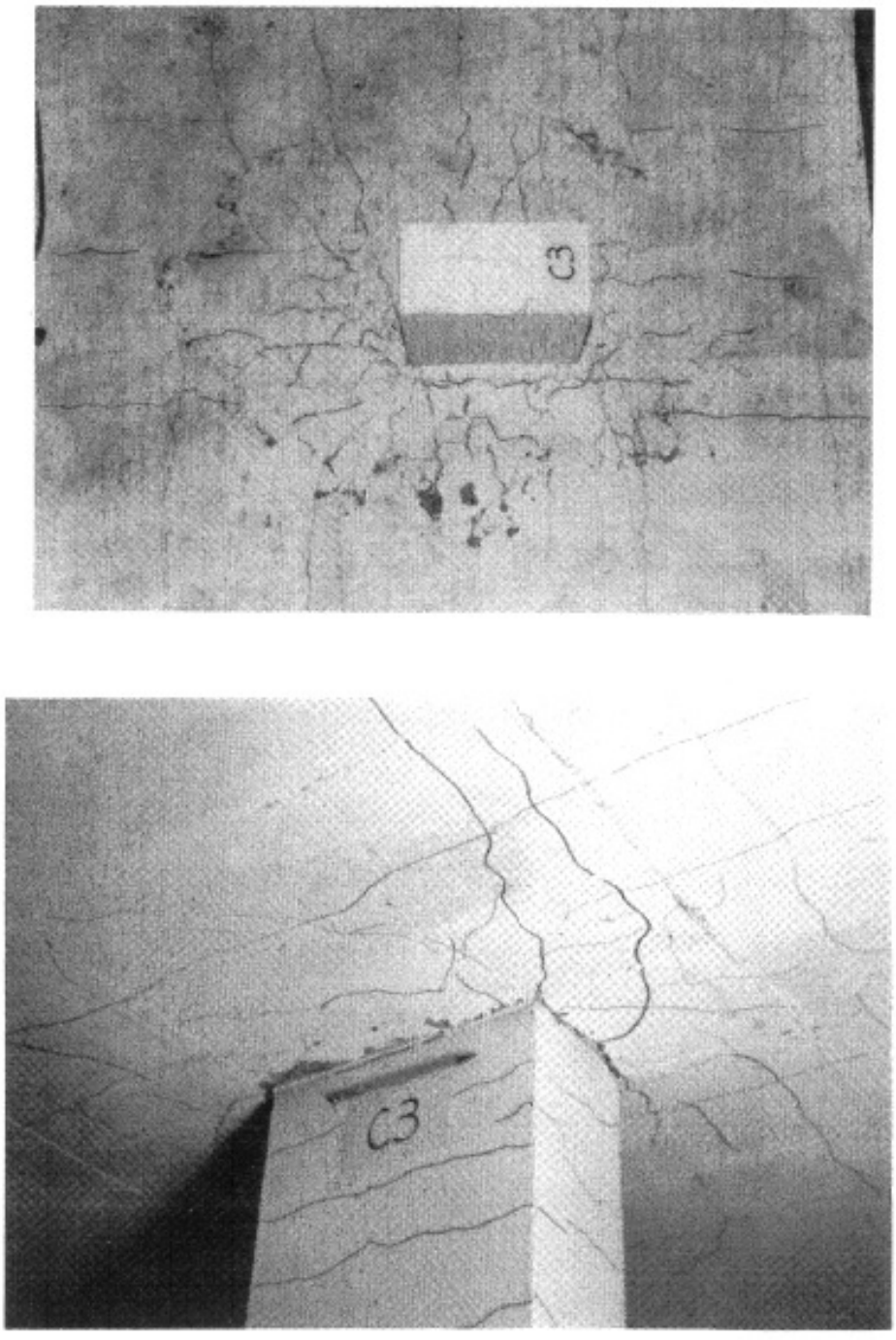

Figure 4.45: Photographs of damage of connection C3[13]

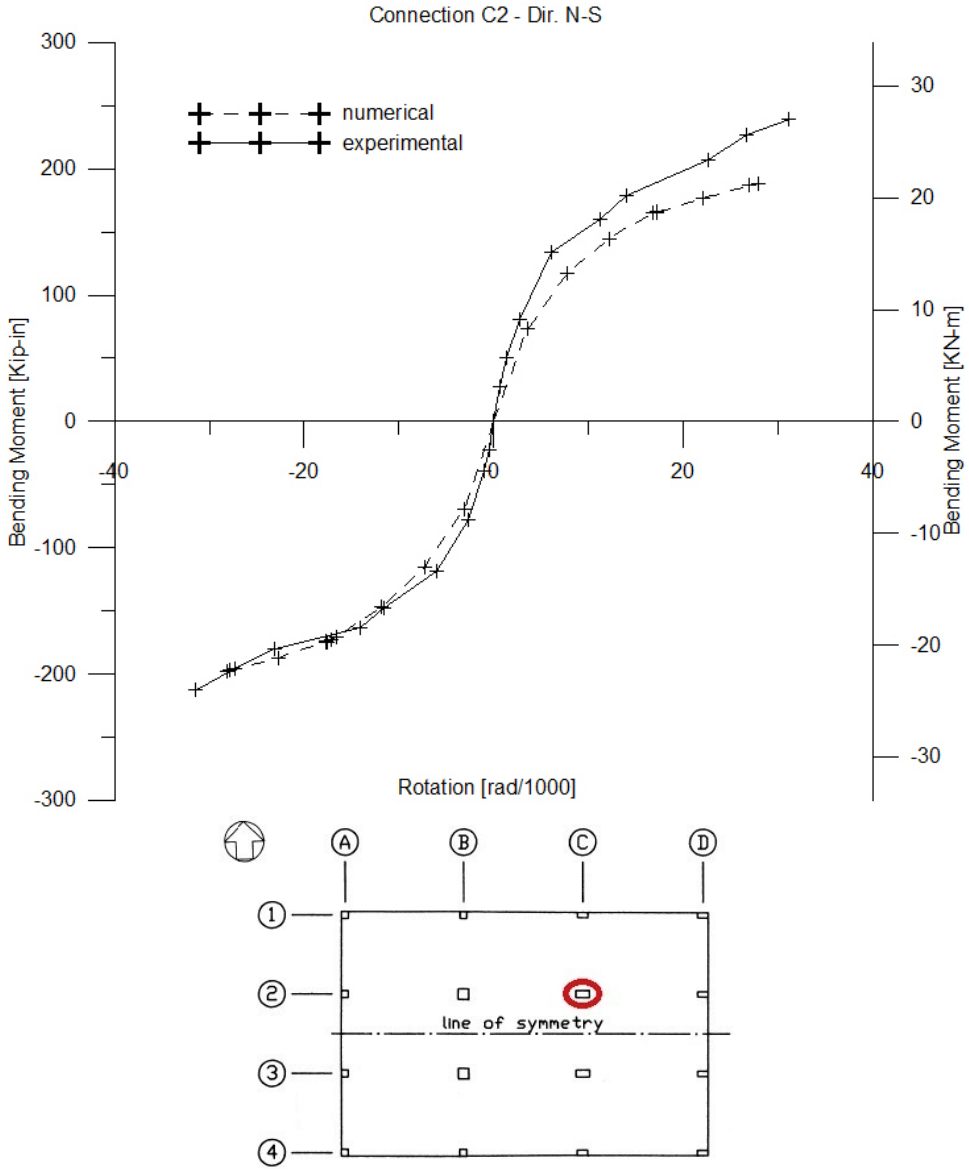

Figure 4.46: Comparison between the numerical moment-rotation curve and the experimental moment-rotation envelopes of joint C2 in North-South direction

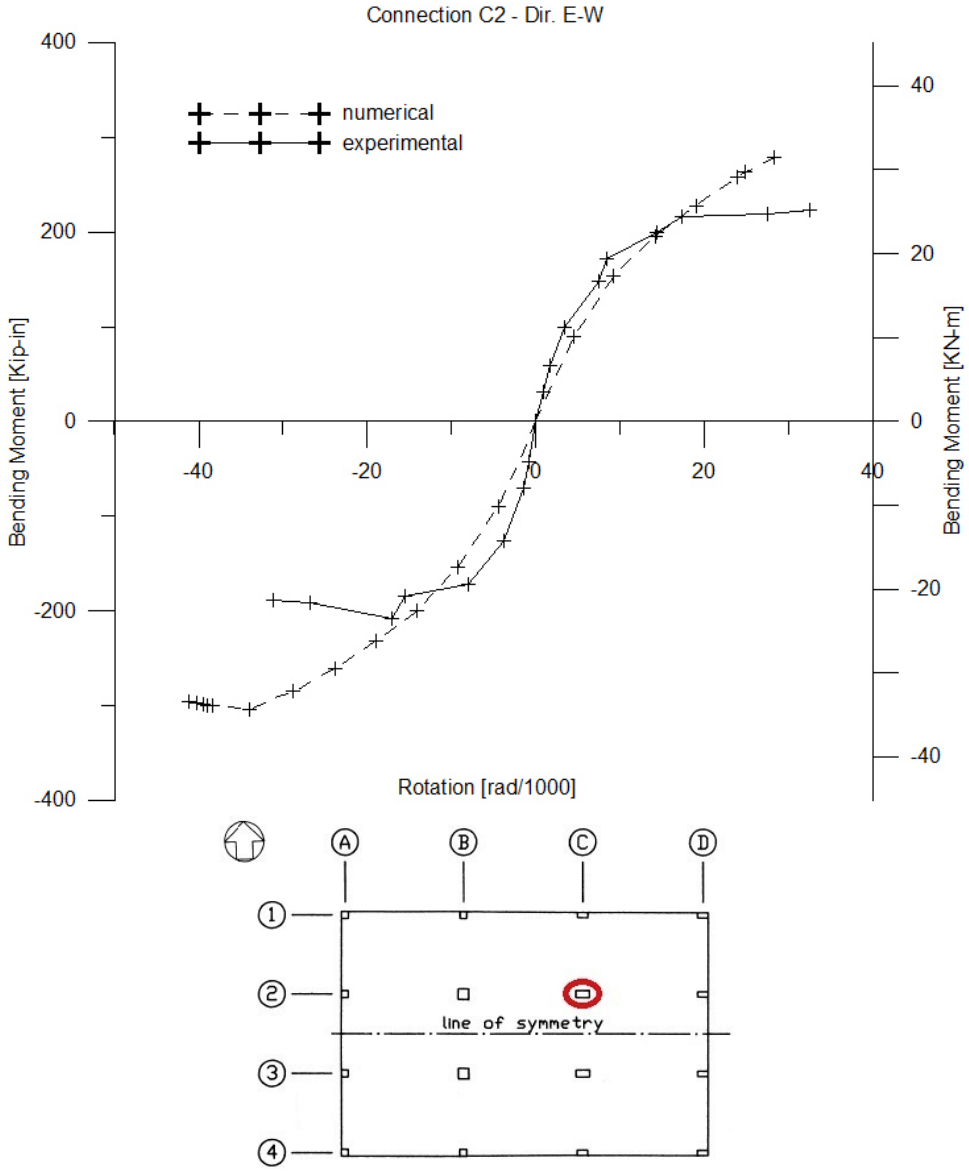

Figure 4.47: Comparison between the numerical moment-rotation curve and the experimental moment-rotation envelopes of joint C2 in East-West direction

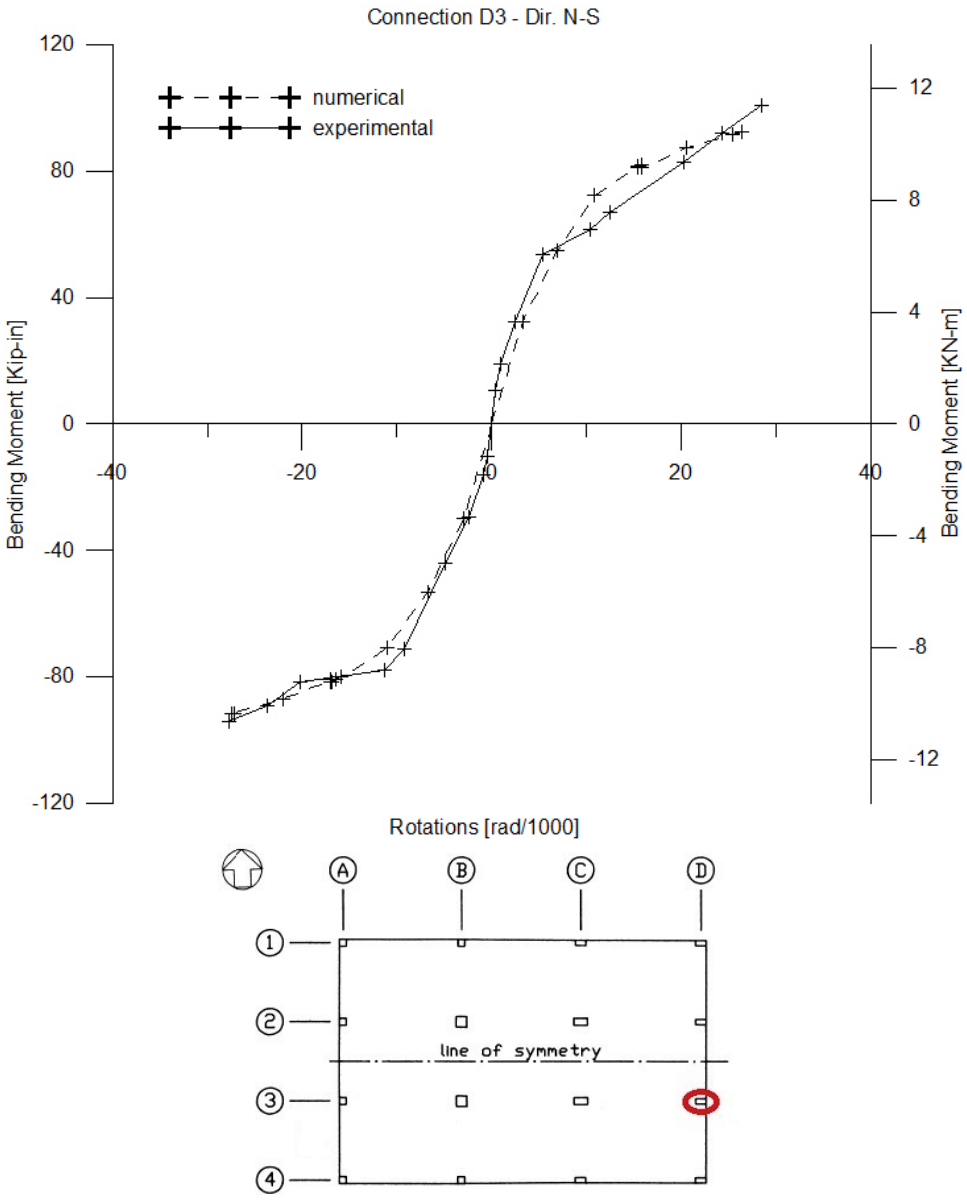

Figure 4.48: Comparison between the numerical moment-rotation curve and the experimental moment-rotation envelopes of joint D3 in North-South direction

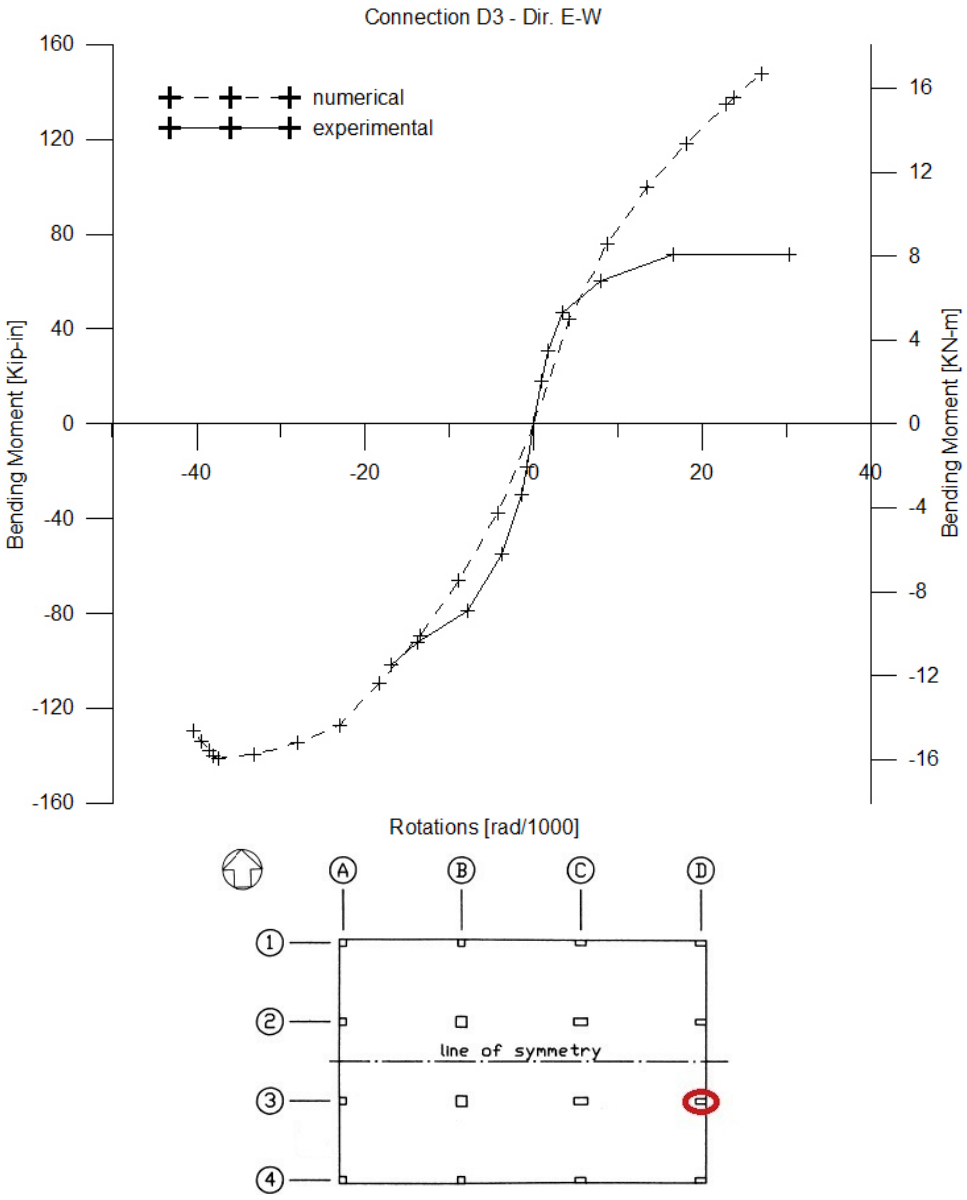

Figure 4.49: Comparison between the numerical moment-rotation curve and the experimental moment-rotation envelopes of joint D3 in East-West direction

The behavior of the whole structure in East-West direction, which is possible to appreciate in Fig. 4.21, shows an important deterioration, more severe than what observed in Fig. 4.20 for North-South direction. This is due to the fact that East-West tests at a certain drift have been done always after the reciprocal in North-South direction at the same drift. This phenomenon is also evident in the moment-rotation curves of the single connections, reported from Fig. 4.25 to Fig. 4.49. Thus, for this direction the model has more difficulties with respect to the previous case to fit well the experimental results. It is possible to notice that, from experimental results, external connections seems to be more damaged with respect to the internal ones; sudden drops in resistance appear which are not so evident in internal connections. For this reason, a first conclusion, could be that the model fits very well the behavior of internal connections, whereas it may be improved for edge and corner columns. In support of this consideration there is the fact that the grid model used[33] has been calibrated mostly on internal connection tests, thus the conclusion above is not surprising.

4.2.4 Effects of columns rectangularity on singular connections and on the whole structure

In this section the effects of column rectangularity on the response of the singular connections and on the whole structure will be investigated; in particular a comparison between effects on experimental tests[?] hwang-mohele) and ones on the numerical analyses will be carried out. Notice finally that only positive verses for both directions of loading will be taken into account for the comparison.
Some experimental studies[49, 48] carried out on edge column-slab connections and interior column-slab connections with rectangular column sections with an aspect ratio of 5, have already demonstrated that column rectangularity significantly enhances the ability of slab-column joint to transfer more unbalanced moment about the strong column axis at the expense of a lower ductility ratio or more brittle modes of failure due to higher shear stresses that develop along the column short side.
Let's consider connections C4 (edge), D4 (corner) and C3 (interior), thus one connection for each type present in the test slab, and let's start observing the numerical and experimental moment-rotation curves of edge column-slab connection C4 for both North-South and East-West directions (Fig. 4.50). The difference of behavior in the two orthogonal directions for both numerical and experimental curves is evident, at least in terms of strength, confirming the results of cited experimental studies for which an higher strength is expected about the strong column axis. It is also interesting to notice that the model connection is evidently more deformable in North-South direction than East-West direction, since for a certain bending moment the rotations

are higher in the first case than in the second; thus, the model is able to reproduce also this aspect of the test slab response.
According to experimental studies[49, 48] cited above, results of the analysis for loading along the weak column direction (North-South in this case) should also show higher connection ductilities; effectively this is verified both by the experimental test and by the model but with different magnitudes. In particular, according to the definition of connection ductility used in Anggadjaja and Teng report[49], the ductility μ for edge connection C4 for both the directions of loading are presented in table 4.1.
As it possible to notice from table 4.1, higher ductilities are shown, both for

Connection C4		
	numerical	**experimental**
μ_{N-S}	1.802	4.844
μ_{E-W}	1.595	2.327
difference	11.48%	51.96%

Table 4.1: Numerical and experimental ductilities of connection C4 for both directions of loading and their differences

numerical and experimental results, for direction North-South than for direction East-West; however, it is worth to observe that values of the numerical and experimental μ are very much different for both directions. In addiction, also the numerical and experimental differences between ductilities for North-South and East-West directions are strongly different in percentage; this means that the changing in ductility in the two orthogonal directions is not proportional for numerical and experimental results.
The same conclusions can be done for the comparison of the two direction of loading of corner slab-column connection D4 (Fig. 4.51), at least as regarding ductility (Table 4.2). On the contrary, a strange experimental strength behavior is observed in the positive quadrant, where the capacity in the North-South direction is higher than the one in East-West direction; this is probably due to the punching of several connections occurred during test EW25, has reported by authors of experimental tests[13], which caused the drop in resistance. Anyway, it's worth to notice that no studies exist, to writer's knowledge, on rectangular corner connections subjected to biaxial lateral loading; thus it is only an hypothesis of the writer that the moment-rotation curve of corner connection D4 should follow results obtained by Anggadjaja and Teng on edge connetions[49]. According to experimental results of Hwang and Moehle[13], this supposition is wrong; anyway tests on rectangular singular corner connections are maybe more suitable in order to carry out more reliable conclusions. Numerical results instead, well follow conclusions of experimental studies cited above (Fig. 4.51).

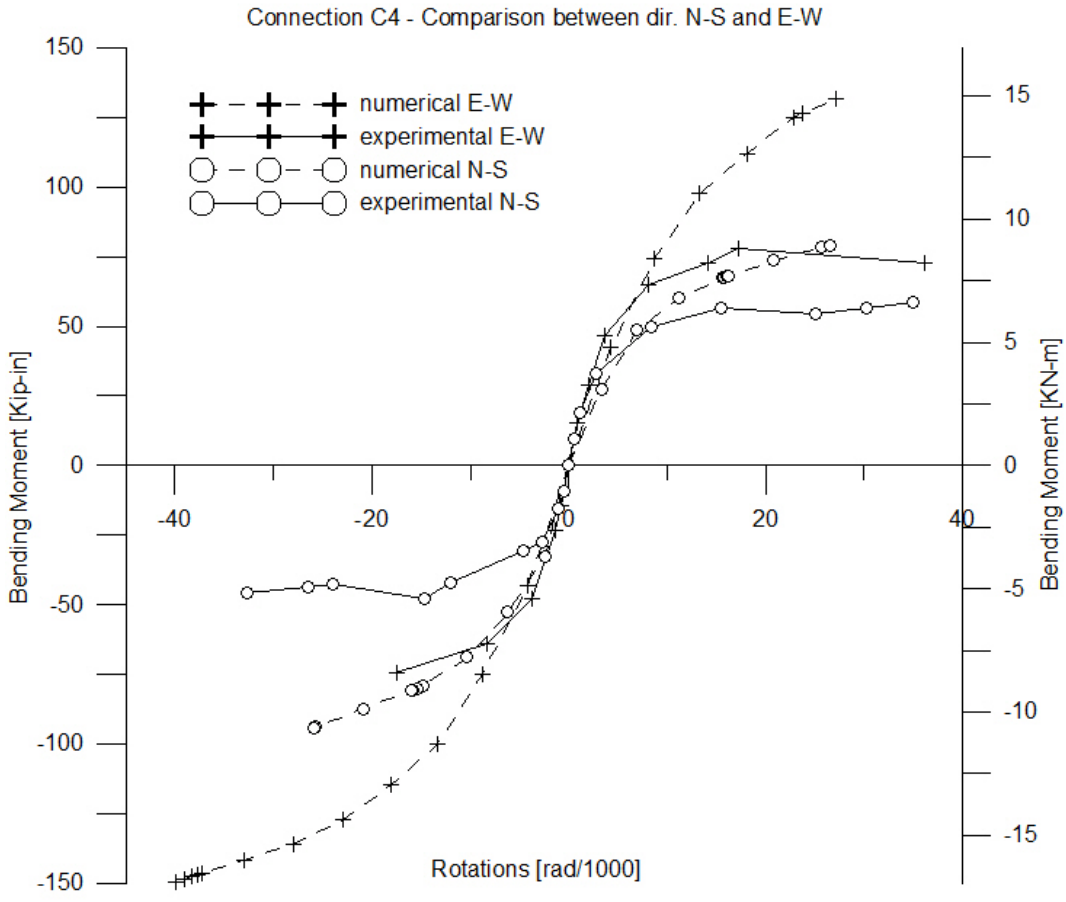

Figure 4.50: Comparison between the North-South and East-West behavior for both numerical and experimental moment-rotation curves of joint C4

As regard interior connection C3 (Fig. 4.52), the higher capacity of the response for direction North-South than direction East-West is confirmed both by test and model results (Fig. 4.52). In this case, ductility show instead a strange behavior, at least for experimental results. In fact for these an important and unexpected decrement of μ passing from direction East-West to North-South is computed, whereas numerical results show expected behavior with an increasing of the ductility for North-South direction (Table 4.3).

Connection D4		
	numerical	**experimental**
μ_{N-S}	1.860	3.409
μ_{E-W}	1.411	1.817
difference	24.11%	46.68%

Table 4.2: Numerical and experimental ductilities of connection D4 for both directions of loading and their differences

Connection C3		
	numerical	**experimental**
μ_{N-S}	2.146	1.727
μ_{E-W}	1.455	3.210
difference	32.21%	-85.81%

Table 4.3: Numerical and experimental ductilities of connection C3 for both directions of loading and their differences

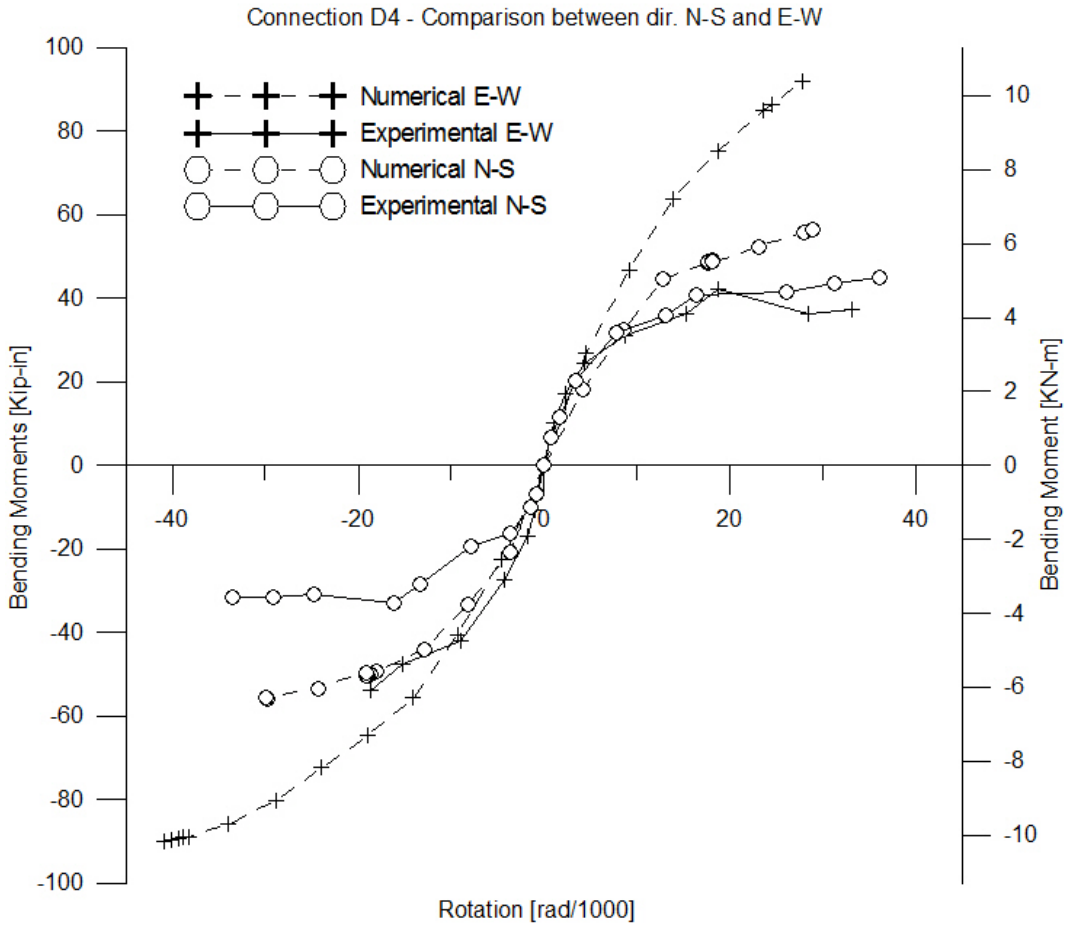

Figure 4.51: Comparison between the North-South and East-West behavior for both numerical and experimental moment-rotation curves of joint D4

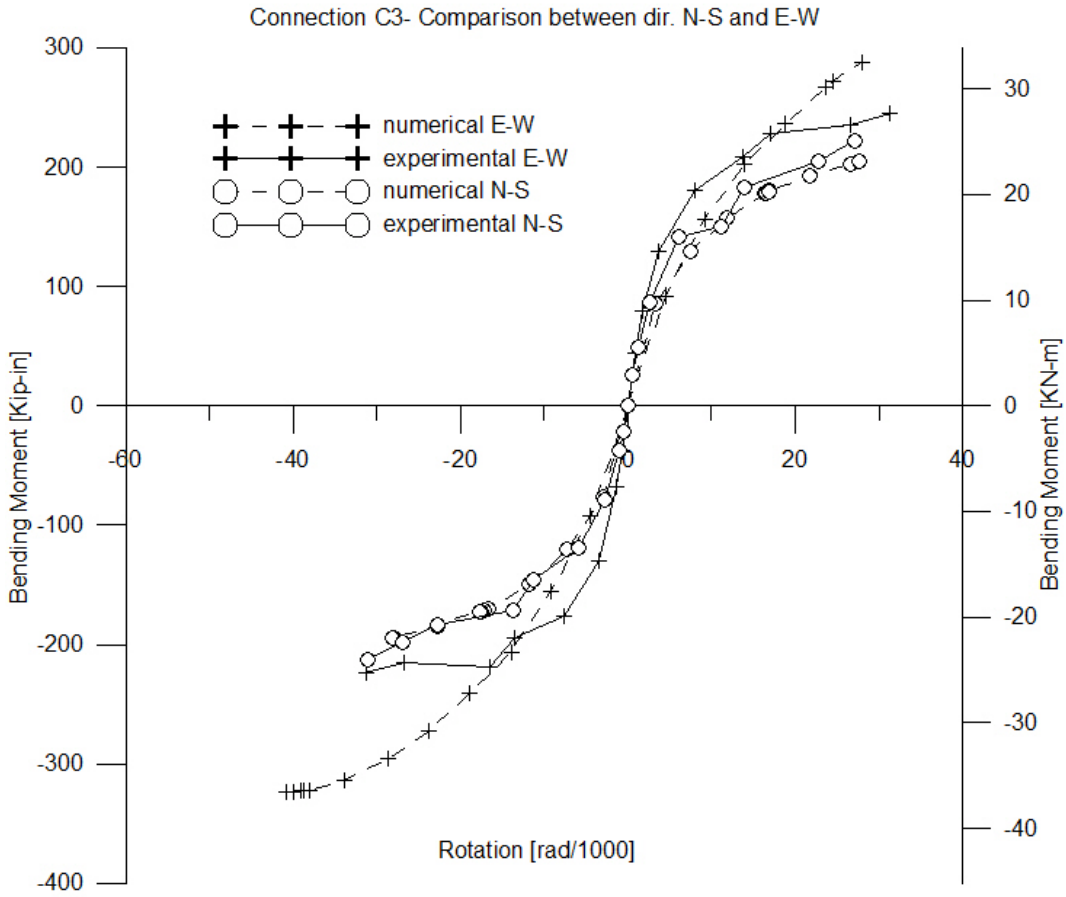

Figure 4.52: Comparison between the North-South and East-West behavior for both numerical and experimental moment-rotation curves of joint C3

It's interesting to notice how the effect of column rectangularities influences the global behavior of the structure, and this could be observed by the analysis of the pushover curves in the two principal directions. Observing Fig. 4.53, firstly it is possible to observe that, similarly to what happens for singular connections, the model is able to detect the decreasing of the maximum lateral load passing East-West to North-South direction. Anyway, tests results show this trend only up to 2% drift; after this experimental lateral load-drift curves (both in positive and negative directions) drop, because of punching of several connections, as referred by authors of experimental campaign[13] (reasons of this behavior already discussed in section 4.2.2).
In table 4.4 numerical and experimental ductilities of the whole structure, carried out from lateral load-drift curve as explained in Pan and Moehle article[5], are reported for both directions of loading.
It is possible to notice that also the global behavior of structure is influenced by rectangularity of some columns, in fact the ductility is higher for North-South direction than East-West direction; anyway, what is the most interesting to underline is that the numerical and experimental differences between ductilities in the two principal directions are absolutely similar in percentage and thus the model it's really able to fit this aspect of the experimental non-linear behavior, differently to what observed for connection C4.
It's finally important to notice that ductilities are computed only for the positive North-South and East-West directions of loading.

Global Structure		
	numerical	**experimental**
μ_{N-S}	1.774	2.349
μ_{E-W}	1.418	1.884
difference	20.11%	19.79%

Table 4.4: Numerical and experimental ductilities of the global structure for both directions of loading and their differences

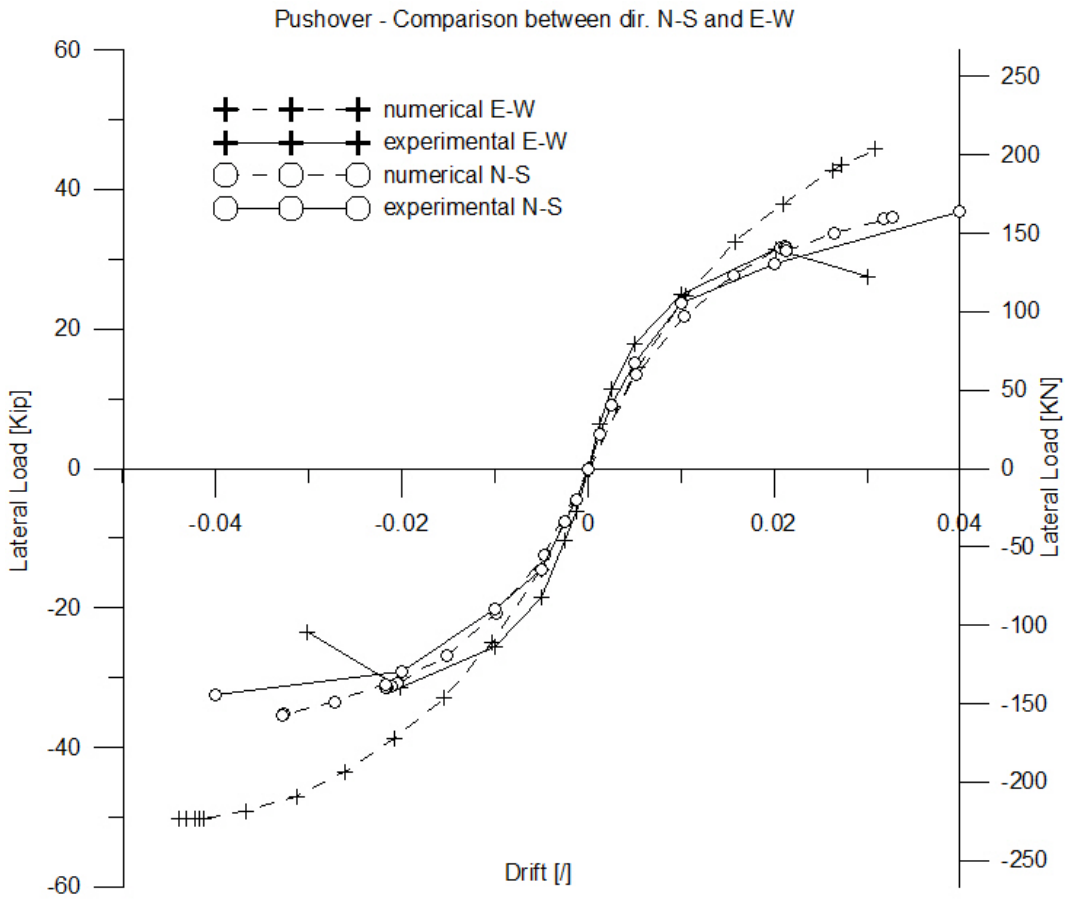

Figure 4.53: Comparison between the North-South and East-West lateral load-drift curve both numerical and experimental

4.2.5 Vertical load response

In this section a comparison between the experimental and numerical distribution of the base reactions for test LEAD (see Table 3.1) at the base of columns is presented.
As preliminary remark is necessary to specify that the horizontal reactions strongly depend on the stiffness of columns which depends in turn to the moment of inertia of the frame elements. As already specified in section 4.2.2, the choice used was to assume 50% of the uncracked moment of inertia of each section in order to take into account for cracking of concrete. According to this consideration and since gravity loads applied for test LEAD have not induced significant non-linear effects on the slab, it's reasonable to expect a certain gap between experimental and numerical reactions.
Fig. 4.54 represents the deformed shape and the activated hinges of the model slab. It is possible to observe, as already aforementioned, that the non-linear effects of self-weight and service loads are quite low, since only fuchsia hinges appear on the grid, meaning that no yielding of reinforcement has occurred but only concrete cracking. This is agree to what experimentally observed[13].
In Fig. 4.55, 4.56 and 4.57 the ratios of the numerical to the experimental reactions for each columns, are presented.
As it is possible to notice important differences exist between numerical and experimental results, taking into account that the reference value for the three graphs is one (one means that numerical and experimental results are exactly the same).
A good reference parameter for the comparison is the mean value of the ratios for each reaction's direction considered (Fig. 4.55, 4.56 and 4.57). Thank's to this it is possible to clearly notice that the model best fits vertical reactions, for which the mean error is equal to 11%; as regarding instead horizontal reactions the mean value is equal to 59% for North-South direction and 36% for East-West direction. Thus, an important scatter exists in the two latter cases.

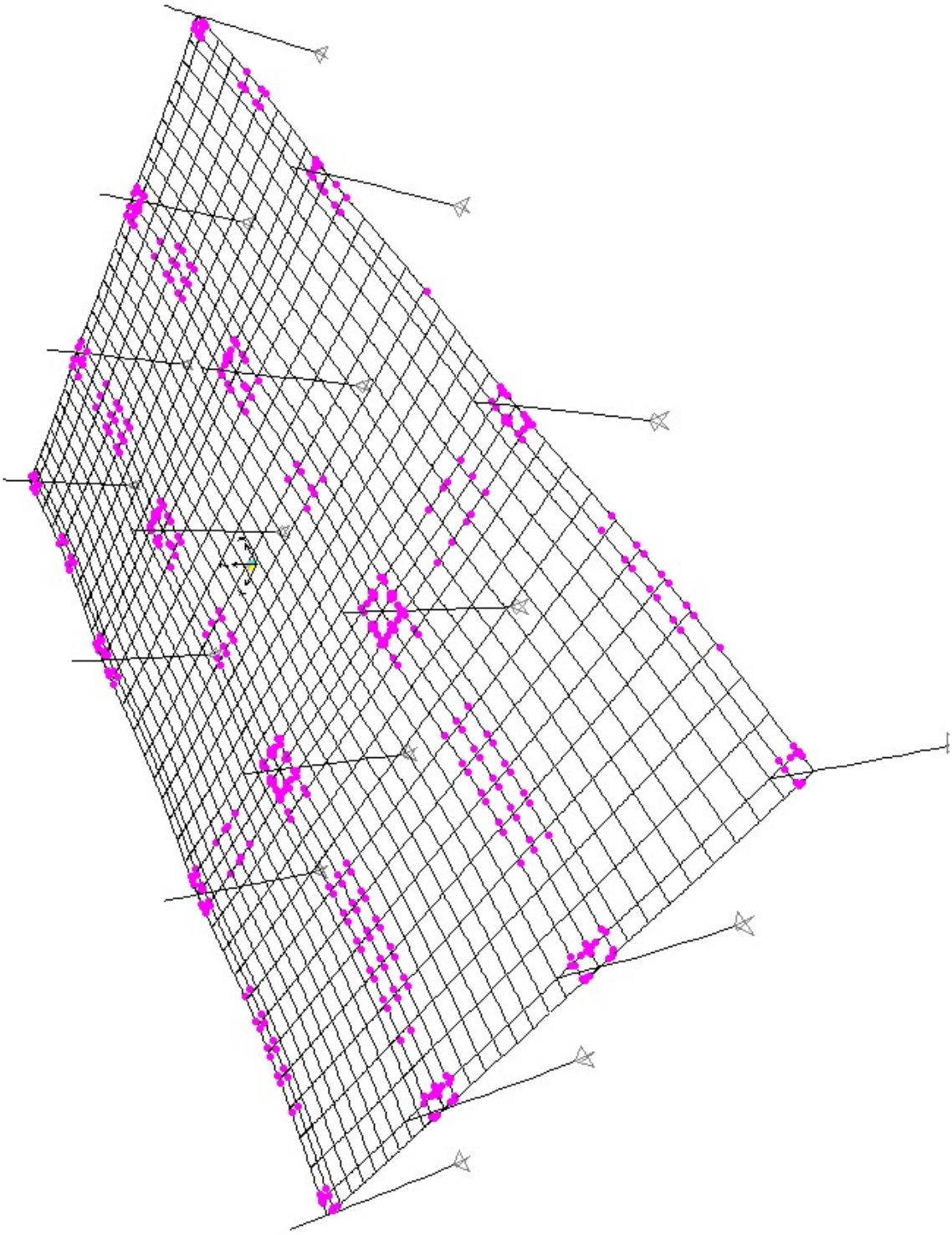

Figure 4.54: Representation of the deformed shape of slab and of the plastic hinges activated for gravity loads

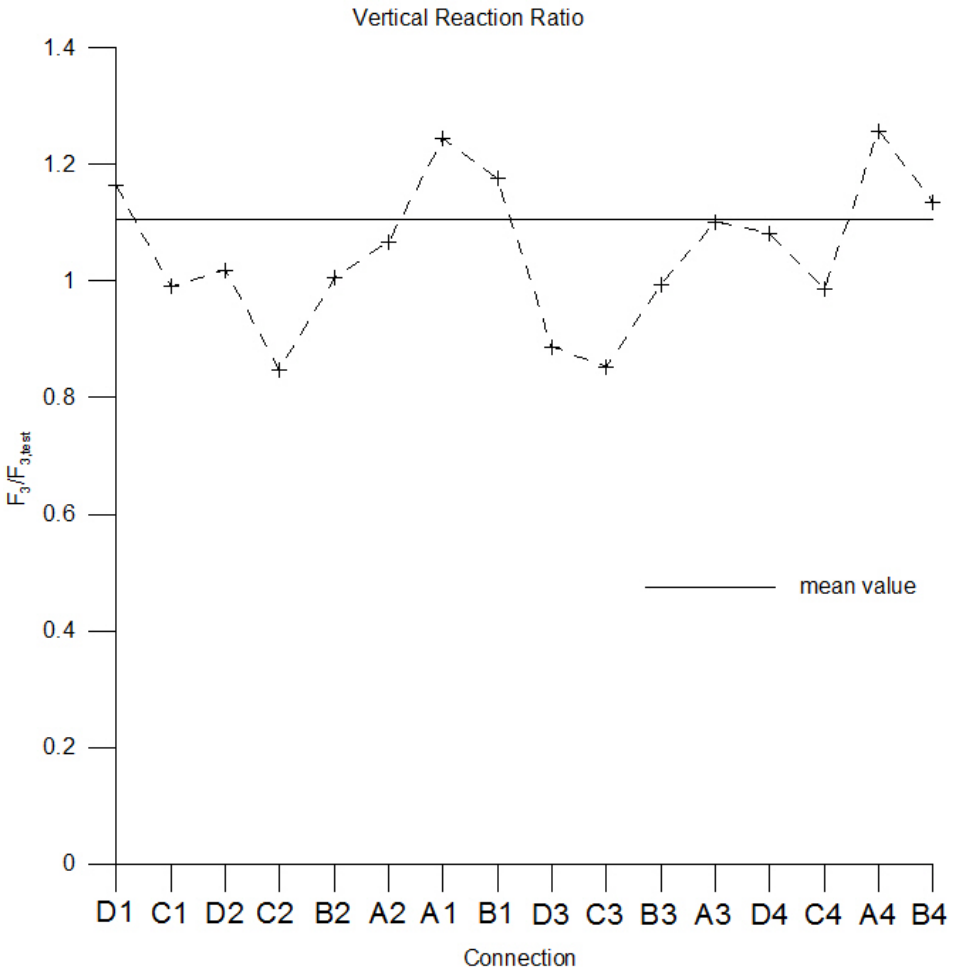

Figure 4.55: The ratios of the numerical to the experimental vertical reactions

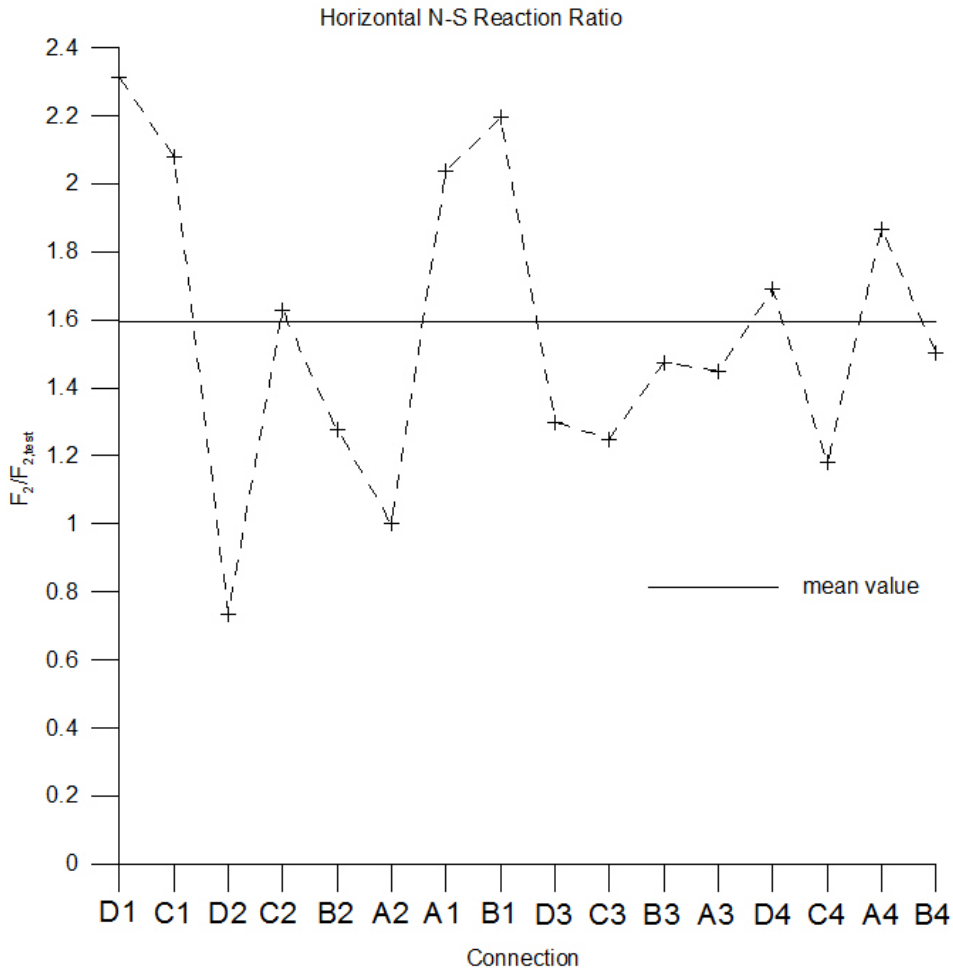

Figure 4.56: The ratios of the numerical to the experimental horizontal reactions in the North-South direction

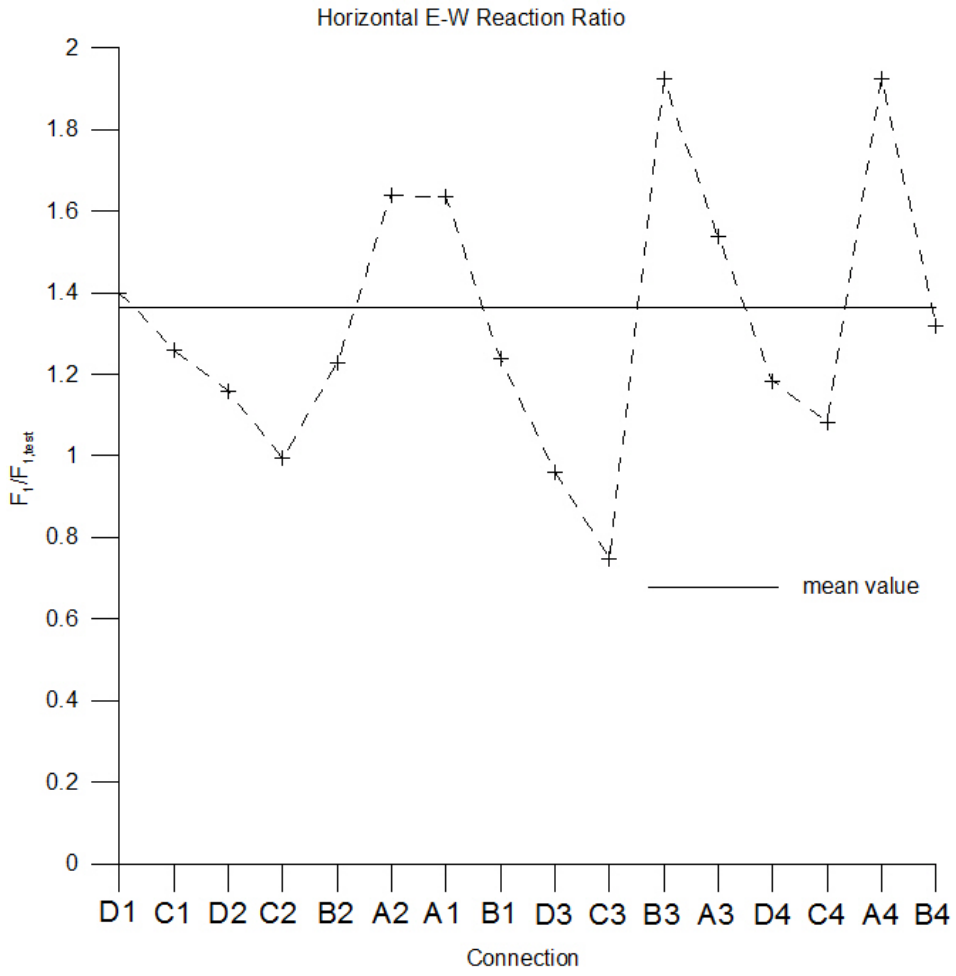

Figure 4.57: The ratios of the numerical to the experimental horizontal reactions in the East-West direction

Chapter 5

Conclusions

5.1 Summary

A model slab has been designed and assembled in order to represent the non-linear behavior and results obtained from an experimental test carried out on a flat slab structure subjected to gravity and lateral biaxial cyclic loads (Hwang and Moehle, 1993[13]).
The model slab has been based on a grid model (Coronelli, 2010[33]) able to represent the flexural, shear and torsional non-linear behavior of the slab thanks to the definition of point non-linear hinges.
The geometry of the grid has been chosen in order to second in the best way the irregularities of the structure, consisting on four different types of column cross-section.
The following types of analyses have been carried out on the model slab: a non-linear analysis under gravity loads (self-weight plus service loads) and a non-linear static (*pushover*) analysis under horizontal loads, which has results obtained from the gravity loads analysis as initial conditions. In totality, four different *pushover* analyses have been performed: one in the positive and one in the negative verse of both North-South and East-West directions of loadings.
Comparisons between numerical and experimental results regarding structural lateral load vs. horizontal displacement curves, moment vs. rotation curves of joints and reactions at the column bases have been performed. In addiction, an analysis and interpretation of the effects of columns rectangularity on ductility and strength of both the whole structure and singular connections has been executed, in the light of some experimental studies[49, 48].

5.2 Obtained results

This dissertation has been carried out in order to assess the performance of the grid model[33] on a complicate real study case consisting on a flat

slab structure composed by several slab-column connections with different column sections and subjected to a severe loading pattern. The aim is also to understand which are the principal factors and parameters influencing the numerical response, in order to better interpret the obtained results and their difference with respect to the experimental ones; this is particularly important for any future development of the model.
From the analysis and results obtained for the connections considered, the following conclusions have been reached:

1. The first important consideration carried out by the comparison of numerical and experimental results is the great influence that biaxial cyclic loading induces on the experimental structural response. In particular this type of loading produce an important mechanical deterioration of the structure, that induce an anticipation of the structural failure (punching of several connection) for East-West direction of loading. The grid model used has not the capacity to reproduce this phenomenon, because doing this means that the flexural, shear and torsional ultimate capacities with their relative deformations should be able to be influenced by the maximum values of internal actions reached during the previous orthogonal loading stage. This could be surely an important future development of the model, especially from the point of view of extending the use of this model for non-linear dynamic analyses.
   Hence, it is worth to interpret all the numerical results, and in particular their comparison with the experimental ones, in the light of these considerations.

2. For North-South direction of loading, the global behavior of the structure is well represented by the pushover curve, which fits very well the lateral load vs. horizontal displacement curve, furnished by authors of experimental test. The path and the maximum lateral load reached are very similar for both curves, maximum drift instead is different (experimental one is greater) since the numerical analysis stops too early because of numerical problems. A little bit larger difference starts to become evident for the negative verse of North-South direction of loading; in this case a little overestimation of the reached maximum lateral load is observed. This gap is due to the degradation of the real structure due to biaxial cyclic loading that become absolutely evident for experimental curve obtained for East-West direction of loading; in this case pushover curve cannot fit well experimental results.

3. The experimental interior connections (B2, B3, C2, C3) behavior is absolutely well numerically modeled for North-South direction of loading, whereas for the orthogonal direction numerical results leave experimental ones when the latter shows an important loss of strength or a

plateau because of punching of the connection.
Also in this case, the difference between numerical and experimental results are surely due to the deterioration of the flat slab thanks the biaxial cyclic loading.

4. For edge connections loaded perpendicularly to the edge (B4, C4 for North-South loading direction and D3 for East-West direction), numerical response does not fit well the experimental one; in particular experimental behaviors show plateaus which are sign of a ductile torsional behavior which evidently is not well modeled by the model.
   For edge connections loaded parallel to the edge (D3 for North-South direction of loading and B4, C4 for East-West direction), the precision of numerical response change according to the connection considered. In particular, joint D3 show a numerical behavior absolutely similar to the experimental one, due to the fact that in this case flexural and shear behavior prevail on the torsional one; as regard joints B4 and C4 instead, numerical results do not fit the real behaviors, showing plateaus probably due to flexural ductile behavior.
   The difference of model precision between joint D3 and joints B4 and C4, which are all loaded parallel to the slab edge, is in all probability due to the fact that the second are firstly loaded perpendicularly to their edge (North-South loading direction) and only secondly in their parallel direction. This means that B4 and C4 response in the long direction is strongly influenced (then worsened) by the previous loading stage in the short one.

5. Modeling of corner connections presents the same problems of edge connections loaded perpendicularly to their edges: experimental behavior show plateaus due to the mix of flexural and torsional ductile behavior which cannot be properly reproduced by the grid model.

6. According to the third, fourth and fifth considerations and to the discussion of obtained results in section 4.2.2 and 4.2.3, a proper modeling of torsional behavior for edge and corner connections seems to be fundamental in order to achieve better results in the global and localized numerical response.
   In particular it is noted that the value of the ultimate twist ψ_u is probably overestimated for edge and corner connections; theoretically, a lesser value of ψ_u leads torsional plastic hinges to reach before their capacity and thus delay the failure of shear plastic hinges, allowing in this way a more ductile behavior of the model.

7. Since model cannot consider biaxial degradation, it is possible to better observe the influence of column rectangularity on both the global and local structural response. According to experimental studies (Tan and

Teng, 2005[48]; Teng, 2008[49]) ductility should increase in the short side column direction whereas strength should increase in the long side column direction. These results are confirmed by numerical analysis both for global and connection response; experimental data do not show instead a unique trend for results, probably due to the deterioration given by biaxial cyclic loading.

8. The shown comparison between numerical and experimental reactions at the bases of columns under gravity loads only, shows an important scattering of results without a clear trend, particularly for horizontal reactions. This is due to the fact that, at this stage of loading, the elastic behavior of the structure is predominant to the non-linear one; thus, results are strongly dependent on the rigidity of structural elements (moments of inertia) which were not thoroughly investigated in this work, since it is outside the aim of this dissertation.
However, it is not hardy to suppose that, if the real structure was subjected to higher gravity loads, the numerical base reactions should be more similar than experimental one, since non-linear effects will become predominant.

5.3 Future developments and possible applications of the model

The application of the grid model in this work, shows its validity for the static non-linear analysis of flat-slab structures, even if some improvements are necessary.
From the results presented in Chapter 4 and conclusions of Chapter 5 it is possible to conclude that biaxial cyclic loading has greatly influenced the experimental results and thus their comparison with the numerical ones. For this reason, an important improvement of the grid model could be the definition, inside the procedure for carrying out the plastic hinge properties, of a method so that flexural, shear and torsional capacities are influenced by the bending moment, shear and torsion acting in the previous orthogonal loading stage. This improvement is important also in the view of using the grid model for verification and design of flat-slab structures subjected to seismic loading.
A further improvement, suggested by analyses of results obtained, is the better definition of torsional behavior of edge and corner connections; in particular studies on the definition of the ultimate twist are necessary, since this parameter has demonstrated to be fundamental in the torsional behavior of the outer connections.
Interesting are the possible future applications of the grid model in the usual engineering practice. The model is absolutely well suited for the evaluation

of the safety against seismic loading of existing structure designed only for gravity loads, without taking into account the unbalanced moments transferred in slab-column joints due to lateral loads.
Another very interesting application is the possibility to use the model for the design of slab with both regular and irregular columns configurations. In this case the procedure could be the following: firstly a pre-design of the elements, determining the system non-linear deformability and the internal actions. By this way, the model permits the computation of the bending moment (M_u) and shear (V_u) acting in the connections but also internal actions acting into the slab. Taking into account these, it is possible to design reinforcement, and after that, changing plastic hinges properties, the verification of the design and of the deformability of both the singular connections and of the whole structure, can be carried out.

Bibliography

1. Elstner R.C. and Hognestad E. Shearing strength of reinforced concrete slabs. *ACI Journal*, 28(2):29–57, 1956.

2. Dilger W. H. Flat Slab-Column Connections. In *Prog. Struct. Engng. Mater.*, volume 2, pages 386–399, 2000.

3. Sherif A. and Dilger W.H. Critical review of the punching shear provisions fo interior columns. *Canadian Journal of Civil Engineering*, (23):998–1011, 1996.

4. Stamencovic A. and Chapman J.C. Local Strength of Flat Slab at Column Heads. Technical Report Report 39, Construction Industry Research and Information Association, London, 1972.

5. Pan A. and Moehle J.P. Lateral Displacement Ductility of Reinforced Concrete Flat Plates. *ACI Structural Journal*, 86(3):250–258, May-June 1989.

6. Megally S. and Ghali A. Design Considerations for SLab-Column Connections in Seismic Zones. *ACI Structural Journal*, 97(5):303–314, September-October 1994.

7. Hueste M.B.D. and Wight J.K. Nonlinear Punching Shear Failure Model for Interior Slab-Column Connections. *Journal of Structural Engineering, ASCE*, 125(9):997–1008, 1999.

8. ACI Committee 421. *Seismic Design of Punching Shear Reinforcement in Flat Plates (ACI 421.2R-07)*. American Concrete Institute, Farmington Hills, Michigan, 2007. 26 pp.

9. ACI Committee 318. *Building Code Requirements for Structural Concrete (ACI 318-05) and Commentary (318R-05)*. American Concrete Institute, Farmington Hills, Michigan, 2005. 430 pp.

10. Collins M.P. and Mitchell D. Shear and Torsion Design of Prestressed and Non-Prestressed Concrete Beams. *PCI Journal*, September-October 1980. pp. 32-100.

11. Kanoh Y. and Yoshizaki. Strength of Slab-Column Connections Trasferring Shear and Moment. *ACI Journal Proceedings*, 76(3):461–468, March 1983.

12. Bentz E.C. *Sectional Analysis of RC Members*. PhD thesis, University of Toronto, 2000. 198 pp.

13. Hwang S.J. and Moehle J.P. An Experimental Study of Flat-Plate Structures under Vertical and Lateral Loads. Technical Report UCB/EERC-93/03, Earthquake Engineering Research Center, University of California at Berkeley, February 1993.

14. Cross H. The Column Analogy. *Bulletin 215*, 1930. University of Illinois Engineering Experiment Station, Urbana. 68 pp.

15. Portland Cement Association, Skokie. *Handbook of Frame Constants*, 1958. 33 pp.

16. Cross H. and Morgan N.D. *Continuous Frames of Reinforced Concrete*. Wiley, New York, 1932. 343 pp.

17. Hoffman E.S., Gustason D.P., and Gouwens A.J. *Stuctural Design Guide to the ACI Building Code*. Chapman & Hall, New York, 1998. 437 pp.

18. Rice P.F. Pratcical Approach to Two-Way Slab Design. *J. Struct. Div, ASCE*, 99:131–143, 1973.

19. Hawkins N.M. and Mitchell D. Progressive collapse of flat-plate structures. *ACI Journal*, 76(7):775–808, July 1979.

20. Sherif A. *Behavior of Reinforced Concrete Flat Slabs*. PhD thesis, University of Calgary, 1996.

21. Brown S. and Dilger W.H. Seismic Response of Flat Plate Column Connections. In *Proceedings of the Canadian Society for Civil Engineering-Annual Conference*, volume 2, pages 388–397, 1994.

22. Alexander S.D. and Simmonds s.H. Tests of column-flat plate connections in monolithic reinforced concrete structures. *ACI Structural Journal*, 89(5):495–502, 1992.

23. Hawkins N.M., Fallsen H.B., and Hinojosa R.C. Influence of column rectangularity on the behavior of flat plate structures. *ACI Special Publications*, (SP-30):127–146, 1971.

24. ACI Committee 318. *Building Code Requirements for Structural Concrete, ACI 318-95, and Commentary, ACI 318R-95*. American Concrete Institute, Farmington Hills, Michigan, 1995. 371 pp.

25. Kanoh Y. and Yoshizaki S. Experiments on Slab-Column and Slab-Wall Connections of Flat Plate Structures. *Concrete Journal*, 13:7–19, June 1975.

26. ACI-ASCE Committee 426. The Shear Strength of Reinforced Concrete Members-Slabs. volume 100 of *Proceedings*, pages 1543–1591. ASCE, August 1974.

27. Zee H.L. and Moehle J.P. Behavior of Interior and Exterior Flat Plate Connections Subjected to Inelastic Load Reversals. Technical Report UCB/EERC-84/07, Earthquake Engineering Research Center, University of California at Berkeley, August 1984. 130 pp.

28. Hirashi H., Nakata S., and Kaminosono T. Static tests on Shear Walls and Beam-Column Assemblies and Study on Correlation between Shaking Table Tests and Pseudo-Dynamic Tests. Technical Report SP-84, Earthquake Effects on Reinforced Concrete Structures - U.S.-Japan Research, American Concrete Institute, Detroit, 1985. pp. 11-48.

29. Sozen M.A. Review of Earthquake Response of Reinforced Concrete Buildings with a View to Drift Control. In *State-of-the-Art in earthquake Engineering*, Instanbul, 1980. 7th World Confrence on Earthquake Engineering. pp. 119-174.

30. ACI Committee 352. *Recommendations for Design of Slab-Column Connections in Monolithic Reinforced for Slabs (ACI 352.1R-89)*. American Concrete Institute, Farmington Hills, Michigan, 1989. 22 pp.

31. International Building Code. *IBC*, 2006.

32. Vanderbilt M.D. and Corley W.G. Frame Analysis of Concrete Buildings. *Concrete International*, 5(12):33–43, December 1983.

33. Coronelli D. A Grid Model for Flat Slab Structures. *ACI Structural Journal*, November-December 2010. Politecnico di Milano, Departement of Structural Engineering, Milano. 21 pp.

34. CSI. *CSI Analysis Reference Manual - SAP 2000 Advanced Research v.10*. Computers and Structures Inc., October 2005. 433 pp.

35. Whittle R.T. *Design of Reinforced Concrete Flat Slabs to BS 8110*. CIRIA, report 110 (revised edition) edition, 1994.

36. CEN, Brussels, Belgium. *Eurocode 2, Design of Concrete Structures - Part 1-1: General Rules and Rules for Buildings*, 2004. 225 pp.

37. Morrison D.G., Hirasawa I., and Sozen M.A. Lateral Load Tests of R/C Slab-Column Connections. *ASCEE, Journal of Structural Division*, 109(11):2699–2714, 1983.

38. Islam S. and Park R. Tests on Slab-Column Connections with Shear and Unbalanced Flexure. *ASCEE, Journal of Structural Division*, 102(ST3):549–568, 1976.

39. Sheu M.S. and Hawkins N.M. A Grid Model for Predicting the Monotonic and Hysteretic Behavior of Slab-Column Conenctions Trasferring Moments. In *Reinforced Concrete Structures Subjected to Wind and Earthquake Forces*. ACI, 1980. pp. 79-111.

40. Park H. and Choi K. Improved Strength Model for Interior Flat Plate-Column Connections Subjected to Unbalanced Moment. *ASCE, Journal of Structural Engineering*, 132(5):694–704, May 2006.

41. Park R. and Paulay T. *Reinforced Concrete Sructures*. John Wiley & Sons, New York, 1975. 769 pp.

42. Tian Y and Jirsa J.O. O.and Bayrak. Non-linear Modeling of Slab-Column Connections under Cyclic Loading. *ACI Structural Journal*, 106(1):30–38, January-February 2009.

43. Park R. and Gamble W.L. *Reinforced Concrete Slabs*. John Wiley & Sons, New York, 2000. 716 pp.

44. ACI-ASCE Committee 421. *Seismic Design of Punching Shear Reinforcement in Flat Plates*, 2007. Report ACI 421.2R-07, 24 pp.

45. Marti K.H. and Reineck. Punching of structural concrete slabs. Technical Report bulletin 12, Fib, 2001. pp. 211.

46. American Concrete Institute, Detroit. *Building Code Requirements for Reinforced Concrete (ACI 318-83)*, 1983. 111pp.

47. Pecknold D.A. Slab effective width for equivalent frame analysis. *ACI Journal*, 72(4):135–137, April 1975.

48. Tan Y. and Teng S. Interior Slab-Rectangular Column Conenctions Under Biaxial Lateral Loadings. *ACI Structural Journal*, 232:147–174, October 2005. Special Publication.

49. Anggadjaja E. and Teng S. Edge-Column Slab Connections under Gravity and Lateral Loading. *ACI Structural Journal*, 105(5):541–551, September-October 2008.

50. Gambarova P.G., Coronelli D., and Bamonte P. *Linee Guida per la Progettazione delle Piastre in C.A.* Pàtron Editore, Bologna, 2007. 118 pp.

51. Longoni A. Calcolo del punzonamento delle piastre in c.a. mediante un modello a graticcio. Master's thesis, Politecnico di Milano, 2009.